U.PORTO
FEUP FACULDADE DE ENGENHARIA
UNIVERSIDADE DO PORTO

Bioengineered nanocarriers for targeted drug delivery in glioblastoma multiforme therapy

Maria João Alves Ramalho

Dissertation for the degree
Doctor in Chemical and Biological Engineering

Porto, February 2019

Bioengineered nanocarriers for targeted drug delivery in glioblastoma multiforme therapy

Maria João Alves Ramalho
up200702633

Dissertation for the degree
Doctor in Chemical and Biological Engineering
Supervisor: Prof. Dr. Maria do Carmo Pereira
Co-supervisor: Prof. Dr. Manuel Coelho
Co-supervisor: Dr. Joana Angélica Loureiro

Porto, February 2019

Financial Support

This work was supported by national funding with a PhD fellowship (SFRH/PD/BD/105984/2014) from FCT – Fundação para a Ciência e a Tecnologia.

This work was also financially supported by: project UID/EQU/00511/2019 - Laboratory for Process Engineering, Environment, Biotechnology and Energy – LEPABE funded by national funds through FCT/MCTES (PIDDAC); Project POCI-01-0145-FEDER-006939, funded by FEDER funds through COMPETE2020 - Programa Operacional Competitividade e Internacionalização (POCI) and by national funds (PIDDAC) through FCT/MCTES; Project "LEPABE-2-ECO-INNOVATION" – NORTE-01-0145-FEDER-000005, funded by Norte Portugal Regional Operational Programme (NORTE 2020), under PORTUGAL 2020 Partnership Agreement, through the European Regional Development Fund (ERDF).

FCT
Fundação para a Ciência e a Tecnologia
MINISTÉRIO DA CIÊNCIA, TECNOLOGIA E ENSINO SUPERIOR

NORTE2020
PROGRAMA OPERACIONAL REGIONAL DO NORTE

COMPETE
2020

PORTUGAL
2020

UNIÃO EUROPEIA
Fundo Europeu
de Desenvolvimento Regional

"I have not failed.

I've successfully discovered

10,000 things that won't work."

Thomas Edison (1847 – 1931)

Acknowledgments

Several people contributed to this thesis and for that I am grateful to all of them. First of all, I wish to express my deepest gratitude to my supervisor Prof. Dr. Maria do Carmo Pereira for all scientific guidance and support though these years. I'm also grateful for her constant availability and encouragement. To my co-supervisors, Prof. Dr. Manuel Coelho and Dr. Joana Loureiro, I would also thank all the valuable scientific discussions, advices, corrections and suggestions.

To my all lab colleagues', (no one mentioned, no one forgotten!) thanks for their kind help and work discussions in group meetings, and in special thanks for all the companionship and good moments spent in the lab. You helped making the PhD student life easier.

I also acknowledge Dr. Paula Soares from the Cancer Signalling & Metabolism group for the possibility to use their facilities at the Institute for Research and Innovation in Health Sciences (i3S). I'm also sincerely grateful to Dr. Jorge Lima for all the scientific advices and pertinent suggestions for the cellular studies. I also thank to all the Cancer Signalling & Metabolism group members for their help in the lab, in special to Joana, Marcelo, Raquel e Helena for always being available to help. I'm also grateful to Rui Fernandes from i3S for the TEM morphologic analysis of nanoparticles and Dr. Paula Sampaio for the valuable help with confocal microscopy.

I must also gratefully acknowledge Dr. Fabien Gosselet and Dr. Emmanuel Sevin from the Blood-brain barrier laboratory at the University of Artois for their help in the blood-brain barrier toxicity experiments.

I am also thankful to all DEQ and LEPABE staff.

I would like to thank my friends and family for all the good moments and friendship.

Last but not least, I am grateful to my parents, for their continuous support, encouragement words and wise advices.

Thesis output

The research work for this thesis was developed at LEPABE - Laboratory for Process Engineering Environment, Biotechnology and Energy at the Faculty of Engineering of University of Porto. The *in vitro* cellular studies were performed by me at i3S – Institute for Research and Innovation in Health. The study of the toxicity of the nanocarriers on human brain-like endothelial cells was conducted in the Blood-brain barrier laboratory at the University of Artois by Dr. Fabien Gosselet and Dr. Emmanuel Sevin.

From this work, the following publications are published or submitted for publication.

- *Chapters in books*

Ramalho, M.J., Coelho, M.A.N. and Pereira, M.C. Nanocarriers for the delivery of temozolomide in the treatment of glioblastoma: a review (pp. 687-722). In: Grumezescu A, editor. Design and Development of New Nanocarriers. Elsevier. (2018) book ISBN: 978-953-51-4789-3 doi: 10.1016/B978-0-12-813627-0.00018-1

- *Papers in international scientific periodicals with referees*

Ramalho, M.J., Andrade, S., Coelho, M. A., Loureiro, J.A. and Pereira, M. C. Biophysical interaction of temozolomide and its active metabolite with biomembrane models: The relevance of drug-membrane interaction for Glioblastoma Multiform therapy. European Journal of Pharmaceutics and Biopharmaceutics. 136, 156-163, 2019. doi: 10.1016/j.ejpb.2019.01.015

Ramalho, M.J., Sevin, E., Gosselet, F., Lima, J., Coelho, M. A., Loureiro, J.A. and Pereira, M. C. Receptor-mediated PLGA nanoparticles for glioblastoma multiforme treatment. International Journal of Pharmaceutics. 545(1–2), 84–92, 2018. doi: 10.1016/j.ijpharm.2018.04.062

Ramalho, M.J., and Pereira, M.C. Preparation and Characterization of Polymeric Nanoparticles: An Interdisciplinary Experiment. Journal of Chemical Education, 93 (8), 1446–1451, 2016. doi: 10.1021/acs.jchemed.5b00837

- *Conference paper*

Ramalho, M.J., Loureiro, J.A, Lima, J., Coelho, M.A.N., and Pereira, M.C. Anti-transferrin receptor antibody conjugated PLGA nanoparticles for temozolomide delivery. Eur Biophys J (2017) 46 (Suppl 1): S92.

Also, from this work resulted the following presentations at international conferences:

Ramalho, M. J., Lima, J., Coelho, M. A., Loureiro, J. A. and Pereira, M.C. Conjugation with anti-transferrin receptor antibody increases PLGA nanoparticles uptake in Glioblastoma cells. NanoMedicine International Conference 2018, 23-25 October 2018, Venice, Italy. (*oral presentation*)

Ramalho, M. J., Andrade, S., Lima, J., Coelho, M. A., Loureiro, J.A. and Pereira, M. C. Solid Lipid Nanoparticles for Glioblastoma Multiforme therapy. 3rd ASPIC International Congress, 10-11 May 2018, Lisboa, Portugal *(poster presentation)*

Ramalho, M. J., Loureiro, J. A, Lima, J., Coelho, M. A., and Pereira, M.C. Anti-transferrin receptor antibody conjugated PLGA nanoparticles for temozolomide delivery. 19th International Union of Pure and Applied Biophysics (IUPAB) and 11th European Biophysical Societies' Association (EBSA) Congress, 16-20 July 2017, Edinburgh, Scotland (*oral and poster presentation*)

Ramalho, M. J., Loureiro, J. A., Coelho, M. A., and Pereira, M. C., Liposomes for temozolomide delivery., 2nd Doctoral Congress of Engineering (DCE17), 8-9 June 2017, Porto, Portugal (*oral presentation*)

Abstract

Glioblastoma multiforme (GBM) is the most lethal type of brain cancer, and its classical therapy fails to effectively cure the disease. Temozolomide (TMZ) is the first-line treatment for this type of tumours. As many other chemotherapeutic drugs, TMZ presents several limitations as high toxicity and low bioavailability, reducing its pharmacological activity. After administration, TMZ is rapidly converted into its active metabolite (MTIC). Since drug's permeability through the biological barriers and tumour cell membranes affects its bioavailability, the ability of the drug to interact with the biological membranes presents a major contribution on its pharmacological properties and activity.

Biomembrane models mimic the physiological conditions, allowing to predict the drugs' behaviour at biological membranes and its effects on the biodistribution profiles. In this work, a lipid bilayer model using liposomes was applied for the drug-membrane interaction studies. The zwitterionic phospholipid, 1,2-dimyristoyl-sn-glycero-3-phosphocholine (DMPC) and cholesterol were chosen for the model composition, since they represent the major components of the membranes of GBM cells and brain capillary endothelial cells. Thus, the molecular interactions between the drug and these models were studied by the evaluation of the partition of the drug into the phospholipid's membrane, its location within the bilayer and its effect on the fluidity of the membrane. The attained results suggest that the composition of membranes affects drugs partition, showing that drug biodistribution depends not only on its physicochemical features, but also depends on the characteristics of the membrane such as the packing of the lipid molecules. Also, MTIC exhibited low affinity to biological membranes, explaining its low bioavailability on the target cells. Therefore, new therapeutic approaches must be envisaged to increase the efficiency of this drug.

So, the delivery of TMZ using poly (lactic-co-glycolic acid) (PLGA) nanoparticles (NPs) is proposed in this work. Stable NPs functionalized with OX26 type monoclonal antibody (mAb) for transferrin receptor (TfR) were developed, targeting the GBM tumour cells, since these cells are known for overexpressing this receptor. The release profile of TMZ from the NPs was studied mimicking physiological conditions, and targeted cellular internalization was also investigated. Two GBM cell lines - U215 and U87 – were used to evaluate the i*n vitro* cytotoxicity of the drug, showing that the prepared nanocarriers enhance the anticancer activity of TMZ. The functionalization with OX26 mAb for TfR proved to be advantageous in enhancing the cellular internalization in GBM.

The developed NPs were then further optimized for the co-delivery of TMZ with O6-benzylguanine (O6BG). This molecule binds to the O6-methylguanine DNA methyltransferase (MGMT) protein leading to its inhibition. The MGMT protein is pointed as one of the main causes of therapeutic failure of TMZ. Therefore, O6BG decreases the resistance to TMZ's therapy by hindering the repair of the damaged DNA. However, systemic administration of two free drugs usually proves to be ineffective due to differences in the biodistribution profile of each drug. Therefore, the entrapment of both drugs in NPs is a suitable approach.

The mAb-modified PLGA NPs for the co-loading of both drugs were prepared and a design of experiment (Minitab Inc., USA) was used for the determination of the optimal experimental parameters. The developed NPs exhibited high encapsulation efficiencies (EE) for both drugs and showed a sustained drug release for several days. Two GBM cell lines - U215 and T98G – were used to evaluate the *in vitro* cytotoxicity of the prepared NPs. T98G cell line was used since it is a resistant line to TMZ's therapy due to its high expression of the MGMT protein. The attained results suggest that the developed NPs can enhance the anticancer activity of TMZ by decreasing the intrinsic resistance of cells. Thus, these NPs potentially offer a new effective strategy to overcome the limitations of the currently available therapies by the co-administration of TMZ and O6BG.

Keywords: Glioblastoma multiforme, Cancer therapy, Temozolomide, Poly (lactic-co-glycolic acid), Nanoparticles, Brain delivery, Experimental design, Fractional factorial design, Blood-brain barrier, Cell membrane, Monoclonal antibody, OX26, Transferrin, Transferrin receptor, Membrane biophysical models, Biomimetic models, Liposomes, Drug-membrane interaction, O6-benzylguanine

Resumo

O glioblastoma multiforme é o tipo de tumor cerebral com maior índice de mortalidade, e a terapia clinicamente disponível não permite curar a doença, apenas aumentar em cerca de 1 ano a esperança de vida do paciente. A temozolomida (TMZ) é o fármaco mais comummente usado para o tratamento deste tipo de tumores. Como muitos outros fármacos usados em quimioterapia, este medicamento apresenta várias limitações como alta toxicidade e baixa biodisponibilidade, reduzindo a sua atividade farmacológica. Após a administração, a TMZ é rapidamente convertida no seu metabolito ativo (MTIC). A capacidade de os fármacos penetrarem através das barreiras biológicas e das membranas das células tumorais afeta a sua biodisponibilidade. Deste modo, capacidade da molécula de interagir com as membranas biológicas apresenta uma contribuição importante para as suas propriedades e atividade farmacológicas.

Os modelos de membranas *in vitro* permitem simular as condições fisiológicas, de modo a prever o comportamento dos fármacos, e consequentemente prever a sua biodistribuição no organismo. Neste trabalho, foram aplicados modelos de bicamadas lipídicas, utilizando lipossomas, para estudar a interação entre o fármaco e a membrana. O fosfolípido 1,2-dimiristoil-sn-glicero-3-fosfocolina (DMPC) e o colesterol foram escolhidos para a composição do modelo, pois representam os principais componentes das membranas destas células tumorais GBM e das células encontradas na barreira hematoencefálica. Assim, as interações moleculares entre o fármaco e esses modelos foram estudadas, avaliando a partição do fármaco para a membrana fosfolipídica, sua localização na bicamada e seu efeito na fluidez da membrana. Os resultados obtidos sugerem que a composição das membranas afeta a distribuição dos fármacos na bicamada lipídica, mostrando que a biodistribuição do fármaco no organismo depende não apenas de suas características físico-químicas, mas também das características da membrana, como o empacotamento das moléculas lipídicas. Além disso, o MTIC exibiu baixa afinidade para as membranas biológicas, explicando a sua baixa biodisponibilidade nas células-alvo. Portanto, novas abordagens terapêuticas devem ser consideradas de modo a aumentar a eficiência deste fármaco.

Assim, a libertação controlada de TMZ utilizando nanopartículas de poli (ácido lático-co-ácido glicólico) (PLGA) foi proposta neste projeto. Foram desenvolvidas NPs funcionalizadas com o anticorpo monoclonal tipo OX26 que reconhece o recetor da transferrina (TfR). Como está bem descrito na literatura que as células tumorais de GBM possuem este recetor sobre expresso, a utilização deste anticorpo monoclonal permite direcionar as NPs para as células-alvo. O perfil de libertação de TMZ das NPs foi estudado simulando as condições fisiológicas, e a internalização celular foi avaliada. Duas linhas celulares de GBM - U215 e U87 - foram utilizadas para avaliar a citotoxicidade *in vitro* do fármaco, mostrando que as NPs desenvolvidas são capazes de melhorar o efeito anticancerígeno da TMZ. A funcionalização com o anticorpo OX26 provou ser vantajosa, aumentando internalização celular das NPs.

As NPs desenvolvidas foram depois otimizadas para a co-encapsulação de TMZ com a molécula O6-benzilguanina (O6BG). Este fármaco liga-se à proteína O6-Metilguanina-DNA metil-transferase (MGMT) levando à sua inibição. A proteína MGMT está identificada como uma das principais causas do insucesso da TMZ. Portanto, a O6BG diminui a resistência à terapia com TMZ, inibindo a reparação do DNA danificado. No entanto, a administração sistémica de dois fármacos livres geralmente mostra-se ineficaz devido às diferenças no perfil de biodistribuição de cada fármaco. Portanto, a encapsulação de ambas as moléculas em NPs de PLGA é uma abordagem adequada.

As NPs de PLGA modificadas com o anticorpo para a co-encapsulação de ambos os fármacos foram preparados e o desenho experimental foi implementado para a determinação dos parâmetros experimentais ótimos. As NPs desenvolvidos exibiram elevadas eficiências de encapsulação (EE) para ambos os fármacos e foram capazes de manter uma libertação controlada durante vários dias. Duas linhagens celulares de GBM - U215 e T98G - foram utilizadas para avaliar a citotoxicidade *in vitro* das NPs preparadas. A linha celular T98G foi utilizada por ser uma linha resistente à terapia com TMZ devido à sua alta expressão da proteína MGMT. Os resultados obtidos sugerem que as NPs desenvolvidas podem aumentar a atividade anticancerígena da TMZ, diminuindo a resistência intrínseca das células. Portanto, estas NPs podem ser uma estratégia efetiva para superar as limitações das terapias atualmente disponíveis com recurso à coadministração de TMZ e O6BG.

Palavras-chave: Glioblastoma multiforme, Tratamento de cancro, Temozolomida, Poli (ácido lático-co-ácido glicólico), Nanopartículas, Libertação controlada de fármacos para o cérebro, Desenho experimental, Desenho fatorial fracionado, Barreira hematoencefálica, Membrana celular, Anticorpo monoclonal, OX26, Transferrina, Recetor de transferrina, Modelos biofísicos de membranas, Modelos biomiméticos, Lipossomas, Interação fármaco-membrana, O6-benzilguanina

Contents

List of figures

Chapter 2 – State of the art

Chapter 3 – Interactions of temozolomide and its active metabolite with membrane biomimetic models

Chapter 4 -Design of PLGA nanoparticles for the delivery of temozolomide

Chapter 5 - PLGA nanoparticles for the co-delivery of temozolomide and O6-benzylguanine

Annex A

Annex B

List of tables

Chapter 2 – State of the art

Chapter 3 – Interactions of temozolomide and its active metabolite with membrane biomimetic models

Chapter 4 -Design of PLGA nanoparticles for the delivery of temozolomide

Chapter 5 - PLGA nanoparticles for the co-delivery of temozolomide and O6-benzylguanine

Annex A

List of Abbreviations

ABTS – 2,2′-azino-bis (3-ethylbenzothiazoline-6-sulfonic acid) diammonium salt
AIC – 5-amino-imidiazole-4-carboxoamide
BBB – Blood-brain barrier
BBTB – Blood-brain tumour barrier
BER – Base excision repair
C6 – Coumarin-6
CMC – Critical micellar concentration
CNS – Central nervous system
DDS - Drug delivery systems
DL -Drug loading
DLS - Dynamic light scattering
DMEM - Dulbecco's modified eagle medium
DMPC – 1,2-dimyristoyl-sn-glycero-3-phosphocholine
DMPC:chol – Vesicles composed of DMPC and cholesterol
DPH - 1,6-diphenyl-1,3,5-1,3,5-hexatriene
EDC - 1-Ethyl-3-(3-dimethylaminopropyl) carbodiimide
EDTA – Ethylenediaminetetraacetic acid
EE - Encapsulation efficiency
ELISA – Enzyme-linked immunosorbent assay
EPR effect - Enhanced permeability and retention effect
FBS - Fetal bovine serum
FDA - Food and Drug Administration
GBM – Glioblastoma multiforme
GI_{50} - Half maximal growth inhibitory concentration
HBLECs – Human brain-like endothelial cells
LSCM – Laser scanning confocal microscopy
LUVs - Large unilamellar vesicles
mAb – Monoclonal antibody
MC – Methyldiazonium cation
MDR - Multi-drug resistance

MGMT – O6-methylguanine DNA methyltransferase
MLVs - Multilamellar vesicles;
MMR – Mismatch repair
mPEG-Mal – Polyethylene glycol functionalized with maleimide
MTIC - 5-(3-methyltriazen-1-yl) imidazole-4-carboxamide;
MW – Molecular weight
NLC – Nanostructured lipid nanocarriers (NLC)
NP(s) – Nanoparticles(s)
O6BG – O-6 benzyl guanine
O6-meG – O6-methylgunanine
PBS - Phosphate buffered saline
PC – Phosphatidylcholine
PdI - Polydispersity index
Pe – Permeability coefficient
PEG - Polyethylene glycol
PGA – Poly glycolic acid
PLA - Poly lactic acid
PLGA - Poly (lactic-co-glycolic acid)
PVA – Poly (vinyl alcohol) (PVA)
RC – Regression coefficient
RES – Reticuloendothelial system
RGD -Tripeptide Arg-Gly-Asp
RH - Hydrodynamic radius
RT – Room temperature
SD – Standard deviation
SLN – Solid lipid nanoparticles
SRB - Sulforhodamine B
SUVs – Small unilamellar vesicles
TCA - Tricloroacetic acid
TEM - Transmission electron microscopy
Tf – Transferrin
TfR – Transferrin receptor
TMA-DPH – N, N, N-Trimethyl-4-(6-phenyl-1,3,5-hexatrien-1-yl) phenyl ammonium p toluenesulfonate
TMZ – Temozolomide

UV-Vis – Ultraviolet–Visible radiation

WHO – World Health Organization

List of Symbols

***[L]* -** Lipid molar concentration
μ - Electrophoretic mobility
A – Absorbance
B - Cooperativity
***D* -** Second or third derivative of the absorbance values
D - Translational diffusion coefficient
***E* -** Electric field
Ɛ - Dielectric constant
I - Light intensity
K - Boltzmann's constant
Kp – Partition coefficient
K_{SV} **-** Stern-Volmer constant
Ƞ - Viscosity
Q_m **-** Quencher concentration
T – Temperature
Tm – Main phase transition temperature
v – Velocity
V_m **-** Lipid molar volume
ζ - Zeta potential
α_m - Volume fraction of the membrane phase

Chapter 1 – Introduction

Glioblastoma multiforme (GBM) is the most common and invasive type of malignant brain tumour. This neoplasia presents high morbidity and mortality with an average survival rate of up to one year. Its classical treatment consists of combination of surgery, radio and chemotherapy (Morais et al., 2015).

Temozolomide (TMZ) is the main chemotherapeutic agent used for the treatment of GBM. TMZ is an alkylating agent, delivering a methyl group to purine bases of DNA, causing its degradation and consequent cell death (Wesolowski et al., 2010). However, as others chemotherapeutic agents, it presents some limitations owing to its high toxicity to healthy tissues and low bioavailability in the target tissues. This low bioavailability occurs due to the low permeability through the blood-brain barrier (BBB) (Pardridge, 2012) and tumour cell membranes (Ramalho et al., 2018). Several receptors and proteins are located at the cellular membranes, so these can act as a barrier or a target for a therapeutic drug (Alves et al., 2016). TMZ must interact with the biological membranes to cross them to reach the intracellular targets. Therefore, the ability of TMZ to interact with the biological membranes and barriers presents a major contribution on its pharmacological properties and activity. Thus, several drugs with great therapeutic potential fail to be effective *in vivo* due to their bioavailability. So, understanding TMZ interactions with biological membranes is essential.

The efficacy of TMZ is also decreased by the activity of the DNA repair enzyme O6-methylguanine DNA methyltransferase (MGMT), overexpressed in several tumour tissues (Jacinto and Esteller, 2007; McLendon et al., 2008). Multidrug resistance (MDR) is also a major limitation of GBM therapy due to the TMZ transport out of cells mediated by the cell membrane efflux pump, p-glycoprotein (Haar et al., 2012). Thus, this treatment is rarely successfully curative, only increasing modestly the survival time and total tumour remission is not achieved.

Despite the knowledge already obtained about GBM, most clinical trials of promising drugs or strategies for the treatment of this disease have failed. Therefore, is urgent to develop a suitable strategy to improve its therapy. Nanotechnology can be a promising approach for GBM chemotherapy with TMZ. Drug encapsulation in nano-sized carriers is able to decrease undesired side-effects in healthy tissues, and enhance drug bioavailability through increased accumulation in cancer cells due to the Enhanced Permeability and Retention effect (EPR effect) and circumvention of the MDR problem (Xin et al., 2016).

Regardless of the effort that has being applied to find novel and suitable nanotechnology-based approaches for GBM treatment with TMZ, to this date no nanosystem for TMZ delivery in GBM therapy is being studied on clinical trials.

The main aim of the present work was to design a suitable nanocarrier for TMZ and evaluate its ability to improve the therapeutic efficiency and reducing toxic effects of the drug. For that, TMZ was entrapped in PLGA NPs and the surface of these NPs was modified with a monoclonal antibody (mAb) for the transferrin receptor (TfR) for a dual-target purpose to simultaneously target the BBB and the GBM cells. The developed nanoformulation proved to be effective *in vitro* and was then optimized for the co-loading of TMZ and another agent, O6-benzylguanine (O6BG) to enhance TMZ's activity by MGMT protein inactivation.

This dissertation is organized into six chapters. This chapter, "Introduction", presents the subject and main goals of this research work. Chapter 2, "State of the art", presents an overview on the GBM tumour and TMZ pharmacological activity and limitations. In chapter 2, nanotechnology is also presented as a suitable therapeutic strategy and a review on the studies that have been developed so far on the TMZ delivery are presented. Chapter 3, "Interactions of temozolomide and its active metabolite with membrane biomimetic models", focus on the interaction studies of TMZ metabolites using a *in vitro* model for biological membranes. On chapter 4, "Design of PLGA nanoparticles for the delivery of temozolomide", the methodology and the attained results and respective discussion for the development of PLGA nanoparticles (NPs) for TMZ delivery are presented. Chapter 5, "PLGA nanoparticles for the co-delivery of temozolomide and O6-benzylguanine", presents the optimization and development of a dual-loading nanosystem to enhance TMZ therapeutic efficiency. Finally, an overall summary about this project, its main conclusions and some future work perspectives are presented on Chapter 6, "Concluding remarks and future perspectives".

Chapter 2 - State of the art

2.1 Glioblastoma multiforme

Cancer is one of the main causes of death worldwide. Despite the advances in medicine and technology fields, the aging and increase of the world's population has led to a raise in the incidence of this disease. In fact, the last statistic study carried out by the World Health Organization (WHO), in 2012, state that cancer corresponds to 27% of the causes of premature mortality (under the age of 70), accounting for 8.2 million deaths in the year of 2012 – being that 4.3 million of which were under the age of 70 (W.H.O, 2016).

Primary neoplasia of the central nervous system (CNS) represents 2% of all tumours and 20% of the tumours in children under the age of 15 years. These malignancies are the second leading cause of death from cancer. Intracranial tumours, glioblastomas, are one of the most common and invasive types of adult CNS neoplasia (Pourgholi et al., 2016). Tumours arising from glia cells are called gliomas and are named according to the specific type of cell from which they originate or share histological features. Astrocytomas are the main types of gliomas and originate from the astrocytes. Astrocytes, the main glial cells in the CNS, are responsible for providing structural and metabolic support to neurons such as supplying nutrients and modulating neurotransmitter function, maintenance and repair of the blood-brain barrier (Esiri and Oppenheimer, 1989). Astrocytomas are clinically divided into four grades (Grades I to IV) according to their level of malignancy. Grade IV gliomas, also known as glioblastoma multiforme (GBM), represent the most common, aggressive, and neurologically destructive primary brain tumours (Furnari et al., 2007). The WHO designation grade IV is attributed to malignant neoplasm with widespread infiltration in adjacent tissues, typically associated with rapid evolution and fatal prognosis (Louis et al., 2007).

GBM can also be classified into primary and secondary glioblastomas based on their clinical history, being that primary GBM accounts for approximately 90% of the glioblastoma tumours. GBM may develop from the beginning, in an acute *de novo* manner without previous symptoms, as primary glioblastoma or may also develop from the progression of a low-grade glioma (Grade I to III), being in these cases classified as secondary glioblastoma. These two types of glioblastoma are, morphological and histologically, indistinguishable and exhibit similar proliferation rates and invasiveness. However, in the last decades, it has been proved that these two tumour types display different signalling pathways and are associated with different responses to treatment (Furnari, et al., 2007). The carcinogenesis of glioblastomas is a complex and still largely unknown process. Only about 5% of patients with malignant glioblastomas have a family history of brain tumours and no environmental factors are associated with the development of the disease (Wen and Kesari, 2008).

GBM is the most common and malignant brain tumour, accounting for 77% of central nervous system tumours (Pourgholi, et al., 2016). Due to the finger-shaped tentacles of astrocyte cells (cells from which gliomas arise), GBM becomes a highly infiltrative tumour, rapidly growing in deep areas of the brain, making local accessibility difficult (Mujokoro et al., 2016). GBM is characterized by their cellular heterogeneity (Pourgholi, et al., 2016), and being a highly vascularized tumour tissue, where the blood vessels exhibit unique features, including aggressive proliferation of their endothelial cells. As result, GBM tissues exhibit higher microvessel density that is significantly correlated with the poor prognosis of the disease (Soda et al., 2013).

Tumour blood vessels in GBM are highly disorganized and permeable, resulting in the loss of the BBB integrity. The impaired BBB results in brain edema, which often causes serious symptoms in GBM patients (Soda, et al., 2013), such as increased intracranial pressure and haemorrhage, seizures, headaches, neurological deficits and mental impairment (Grossman and Batara, 2004). Patients presenting these neurological symptoms are submitted to imaging tests as magnetic resonance imaging and computerized tomography to detect the tumour existence, and further biopsy to confirm tumour grade malignance (Golla et al., 2014).

To date, despite the aggressive conventional treatment and evolving standard of care, average survival in most GBM patients is up 12 to 15 months. However, the elderly usually have a decreased life expectancy of about 40 to 50 weeks (Louis, et al., 2007; Pourgholi, et al., 2016; Soda, et al., 2013).

2.1.1 Current therapies for glioblastoma and their challenges

The first-line treatment of GBM is primarily through neurosurgery for tumour resection and subsequent combination of chemo- and radiotherapy. Despite intensive efforts to improve the efficacy of the classical therapy (Corsa et al., 2006; Vehlow and Cordes, 2013), treatment of GBM presents more than a few limitations such as damages in the brain tissue, drug resistance and insufficient delivery across the BBB. Among the current therapeutic approaches, all of them exhibit several limitations and disadvantages. Radiotherapy has several undesirable side effects such as damaging of the epithelial surfaces, infertility, hair loss, lymphedema, heart disease, radiation necrosis and tumour recurrence. Also, is well-reported that large size tumours respond poorly to radiotherapy (Mujokoro, et al., 2016). Chemotherapy also displays numerous undesired collateral effects since chemotherapeutic agents are not able to differentiate between healthy and tumour tissues and so will act on tissues without discrimination, resulting in devastating side-effects. Among these are nausea, hair loss, nerve damage, increased susceptibility to infections and fertility problems (Pourgholi, et al., 2016). Also, although chemotherapeutic agents could be effective in cancer treatment, their success is largely hindered as a result of the inadequate accessibility of antineoplastic agents to tumour tissue, lack of specificity, requiring high doses, rapid abolition, poor solubility, and inconsistent bioavailability (Brannon-Peppas and Blanchette, 2004; Steichen et al., 2013). As intracranial surgery is a highly invasive technique, it presents also a high risk of damage to the brain tissue. Additionally, the migration of tumour cells from the apparent tumour boundaries, and the infiltrative growth pattern of GBM hinders complete surgical resection allowing tumour recurrence and further invasion of surviving tumour cells in adjacent tissues (Vehlow and Cordes, 2013).

GBM exhibits several characteristics that contribute to its high resistance to the multimodal approach treatment resulting in the poor prognosis of the disease. Several determinant factors are associated to its resistance to therapy, such as: (1) several gene alterations and mutations, resulting in altered signalling pathways, (2) tumour tissue heterogeneity, (3) high proliferation rate and invasiveness, and (4) the anatomic location of the tumour (Bastiancich et al., 2016; Grossman and Batara, 2004; Vehlow and Cordes, 2013).

(1) Several gene alterations and mutations are frequently observed in GBM patients, resulting in alterations of the expression of several proteins and factors such as isocitrate dehydrogenase and phosphatidylinositide 3-kinase that can activate

oncogenes and inactivate tumour-suppressor genes. Also, epidermal growth factor receptor, involved in the uncontrolled cell division and vascular endothelial growth factor, responsible for angiogenesis stimulation, are both overexpressed in GBM patients. Also an unmethylated O6 -methylguanine methyltransferase promoter has been identified to play a major role in the resistance to chemotherapy of GBM patients (Grossman and Batara, 2004; Vehlow and Cordes, 2013). The role of MGMT will be further discussed in section 2.2.2.1.

(2) GBM tumours are characterized by a high heterogeneity at molecular and cellular levels (Bastiancich, et al., 2016). For example, most recently it has been established the existence of glioma stem-like cells that are very different from the rapidly-dividing cells that constitute the rest of the main tumour tissue. This high variability complicates the classification of the type of tumour and consequently the choice of the most appropriated therapy approach (Ahmed et al., 2013).

(3) Uncontrolled cellular proliferation and promoted angiogenesis contribute to the well-recognized infiltrative growth pattern of GBM tumours. Several studies also showed that the tumours cells can migrate into adjacent healthy tissues. All of these allow the invasion of neighbour tissues, hampering complete surgical resection allowing tumour regrowth (Ahmed, et al., 2013; Bao et al., 2006; Gilbertson and Rich, 2007; Lefranc et al., 2005).

(4) Anatomic location of the GBM tumours hampers its successful complete resection, exposing the adjacent tissues to the spreading of tumour cells or damaging neighbour tissues, which may compromise the motor and cognitive functions of the patient. Also, the use of imaging techniques for the assessment of the tumour grade and progression is hampered by its location, impeding to delineate the tumour margins and consequently its extension. Additionally, therapeutic agents to be successfully delivered in the tumour site have to cross several biological barriers such as the blood cerebrospinal, the blood-brain tumour (BBTB) and the BBB barriers (Bastiancich, et al., 2016; Vehlow and Cordes, 2013). The latter will be discussed in more detail further at section 2.2.2.2.

Although not yet curative, it has been established that combination of chemo- and radiotherapy provides the most effective approach for GBM treatment. The chemotherapeutic agent most used as firs-line treatment for GBM is TMZ, an alkylating agent that causes DNA degradation and consequent cell death (Pourgholi, et al., 2016).

2.2 Temozolomide as therapeutic agent

Alkylating agents were the first discovered antineoplastic agents used for cancer treatment. These antitumour pharmaceutical compounds are characterized by interaction with DNA, causing its irreparable damage and inhibiting cell replication. Until a decade ago, a class of alkylating agents named nitrosourea compounds, such as vincristine, were used as the standard treatment for GBM. However, a new class of alkylating agents, the triazene compounds, has been more recently explored for the treatment of several diseases since by altering their chemical structure, the derivatives can acquire different properties, as antimicrobial, antifungal, mutagenic, carcinogenic and teratogenic activity. The diazoamino group, an open chain with three nitrogen atoms in sequence, is responsible for the chemical, physical and antitumour properties of these molecules (Nifontov et al., 1994). TMZ is a monofunctional alkylating agent and was firstly synthesized in 1984 (Stevens et al., 1984). TMZ is now firmly established as the standard chemical treatment for GBM after being proved that the addition of TMZ to radiotherapy provided a 7.6-month overall survival benefit, in a clinical trial conducted in 2005 (Stupp et al., 2005). Thus, in the same year Food and Drug Administration (FDA) approved the use of TMZ for GBM treatment (Rønning et al., 2012; Stupp et al., 2005; Yang et al., 2014).

TMZ induces DNA alkylation and crosslinking, leading to its DNA degradation and subsequent cell death (Stupp, et al., 2005), and it is used in situations where surgery or radiotherapy are not possible or ineffective, or in combination therapy with surgery or radiotherapy as initial treatment. This drug is not successfully curative, only attenuating the symptoms or prolonging the survival of the patient (Stupp et al., 2001). However, TMZ can induce systemic toxicity including thrombocytopenia, lymphopenia and myelodysplasia. It was reported that 7% of patients who had to discontinue the treatment due to the presentation of these toxic side-effects (Stupp , et al., 2005).

2.2.1 Pharmacological activity of temozolomide and metabolites

TMZ is a low molecular weight molecule that can be administered orally and intravenously, and undergoes complete absorption after oral administration, and complete elimination after 8 hours of ingestion. It is spontaneously decomposed at physiologic pH to the active component 5-(3-methyltriazen-1-yl) imidazole-4-carboxamide (MTIC) (Andrasi et al., 2010). Since TMZ is stable in acidic environments it remains in a prodrug state while passing through the digestive system, allowing its oral administration. After being orally administered, the time necessary to reach peak plasma concentration is from 30 to 90 minutes, and its biological half-life is approximately 2 hours, being completely converted to MTIC at the end of this period. TMZ conversion into MTIC is irreversible and occurs mainly by pH-dependent hydrolysis and the hepatic metabolism does not show a significant contribution (Nagasawa et al., 2012).

Figure 2.1 shows the chemical structures of TMZ and its metabolites. The electropositive carbonyl C4 of the tetrazinone ring of TMZ undergoes a nucleophilic attack by water, causing the heterocyclic ring opening and producing an intermediate unstable carbamic acid that releases CO_2 and results in MTIC formation. Then, the MTIC rapidly degrades into 5-amino-imidiazole-4-carboxoamide (AIC) - an inactive derivative - and into the methyldiazonium cation (MC) - a highly reactive electrophilic ion. This highly reactive cation interacts with the DNA causing its methylation at the N7-guanine, O6-guanine and O3-adenine positions as it is shown in figure 2.2. Although being the least frequent target of TMZ, accounting for only 8%, the O6- position of guanine is the primarily responsible for the cytotoxic effects of the compound (Marchesi et al., 2007). The crosslinking of double-stranded DNA results in its damage, causing mismatch mechanisms unable to repair the glioblastoma's damaged DNA. A series of double-stranded breaks, calcium-dependent apoptosis, and autophagy after this mismatch ultimately result in cell death (Nagasawa, et al., 2012).

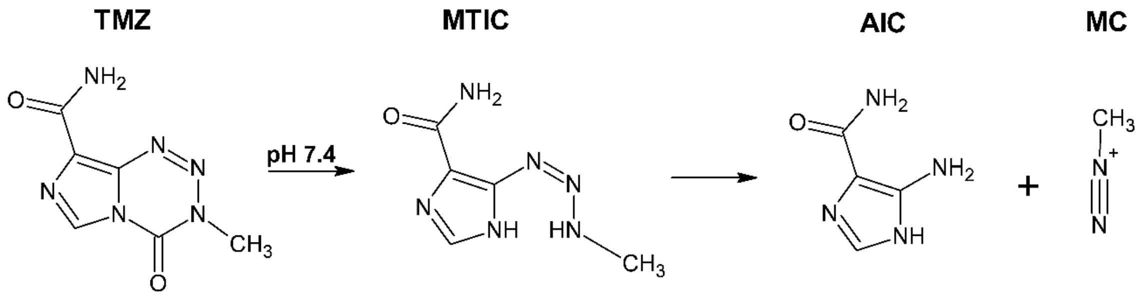

Figure 2.1 | Representation of the chemical structures of TMZ, MTIC, AIC, and methyldiazonium cation (MC). This scheme also represents the overall chemical reactions involved in TMZ activation (drawn in ACD/ChemSketch).

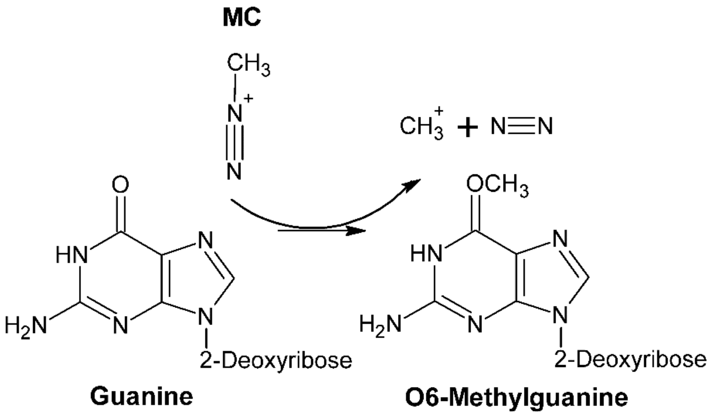

Figure 2. 2 | Image illustrating the DNA alkylation by MC (drawn in ACD/ChemSketch). TMZ's activity leads to the conversion of guanine into the O6-methylgunanine (O6-meG) nucleotide.

2.2.2 Challenges and limitations of temozolomide

TMZ, as other chemotherapeutic agents, exhibits several advantages over both neurosurgical resection of the tumour and radiotherapy since its administration is less invasive. However, its efficiency is limited by their non-specific toxicity causing harmful side effects in healthy tissues. Furthermore, the efficacy of TMZ is hampered by several resistance mechanisms and biological barriers as previously mentioned. Understanding the molecular pathways behind the resistance to TMZ chemotherapy is critical for the improvement of the treatment outcome and disease's prognosis.

Resistance to alkylating agent TMZ chemotherapy could be attributed either to both inherent and acquired tumour drug resistance mechanisms. Base excision repair (BER) and mismatch repair (MMR) mechanisms are involved in TMZ resistance (Johannessen and Bjerkvig, 2012). However, some other studies suggest that other major mechanisms may also be related to GBM resistance to TMZ (Yoshino et al., 2010).

2.2.2.1 MGMT protein

GBM patients usually show both intrinsic and acquired resistance, due to the overexpression of the DNA repair enzyme MGMT (Chamberlain, 2010; Hegi et al., 2005). MGMT protein is responsible for the removal of the methyl group from DNA, thus repairing the alkylating agent-induced DNA lesion (figure 3) (Yoshino, et al., 2010).

MGMT is a stable protein, with a half-life superior to 24 hours, known as a "suicide enzyme", since its repair mechanism leads to its irreversible inactivation (Christmann and Kaina, 2016). This protein repairs the DNA damage in a one-step reaction that does not involve excision of the alkylated base from DNA, instead the methyl group at the O6 position of guanine is transferred to the cysteine residue in the active centre of the MGMT molecule (figure 2.3). Although being the least frequent target of TMZ, the O-6 position of guanine is the primarily responsible for the cytotoxic effects of the compound (Marchesi, et al., 2007). Because the TMZ-induced O6-meG adducts leads to damage by mispairing with thymine during replication (Hansen and Kelley, 2000). After the DNA guanine being restored, the MGMT protein is irreversible inactivated (An et al., 2017). Since studies showed that MGMT protein is *de novo* synthetized after 1-2 cell cycles post TMZ treatment, sustained inactivation of MGMT is required for enhancing sensitivity (Kaina et al., 2010).

Molecules capable of inactivating the MGMT protein are a suitable strategy to enhance sensitivity to TMZ's therapy. Different low molecular weight pseudo substrates have been proposed, however the most studied molecules so far are O6-benzylgunanine (O6BG) and O6-4-bromothenylguanine. O6BG proved to be the most potent of those agents, and therefore is the most extensively studied for MGMT inactivation. This molecule is a guanine analogue that binds the MGMT enzyme, transferring the benzyl moiety to the active-site cysteine leading to its inactivation, and it is 2,000-fold more effective to inactivate the MGMT protein than the damage DNA (Kaina, et al., 2010). Co-administration of this agent potentiates the effects of other chemotherapeutic agents that damage DNA. Thus, O6BG has been showing promising *in vitro* and *in vivo* results by decreasing the resistance to TMZ enhancing its activity in TMZ-resistant tumour cells (Kanzawa et al., 2003; Ma et al., 2002). Combination therapy of TMZ and O6BG has also showed positive outcomes in clinical trials (Quinn et al., 2009; Warren et al., 2005; Warren et al., 2012). It has been proved that O6BG is able to cross the BBB showing potential for the treatment of brain tumours as GBM (Verbeek et al., 2008). However, O6BG, as other of these pseudo subtracts, exhibits high toxicity in healthy tissue, most particularly in bone marrow cells. Despite these agents not showing harmful side effects, inactivation of MGMT protein in healthy tissue also occurs, exacerbating the toxicity of the alkylating agents in these tissues (S. Srivenugopal et al., 2016). So, suitable strategies for targeted delivery to cancer tissues are required.

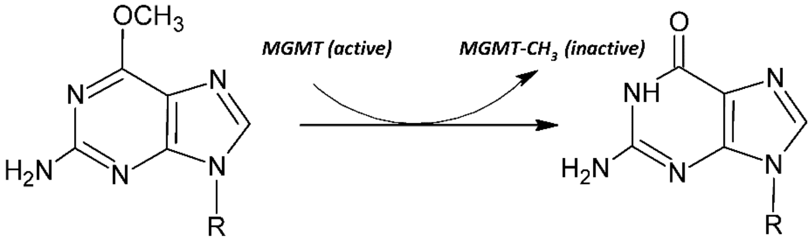

Figure 2. 3 | Image illustrating the DNA repair mechanism by the MGMT protein (drawn in ACD/ChemSketch).

Approximately 60% of the patients with newly diagnosed GBM show MGMT overexpression due to an intrinsic resistance to TMZ-based chemotherapy (Chamberlain, 2010). Beyond MGMT protein expression levels, also MGMT gene methylation status and quantitative MGMT mRNA levels are determining factors to the resistance to chemotherapy with TMZ (Yoshino, et al., 2010). The hyper-methylation of the MGMT gene causes the gene inactivation, suppressing the MGMT protein expression. Therefore, hypo-methylated MGMT gene leads to an overexpression of the MGMT enzyme and therefore a reduced TMZ therapy efficiency (Mujokoro, et al., 2016; Thon et al., 2013). As MGMT protein is rapidly degraded after receiving the alkyl groups from DNA, a mechanism of inhibition of the re-synthesis of the molecule could be suitable target to improve the therapeutic efficacy of TMZ (Grossman and Batara, 2004). Thus, co-treatment with miRNAs, small RNA molecules, proved to decrease resistance to TMZ by modulating gene transcription inhibiting the expression of the MGMT protein (Cipriani, 2016). Also, suppression of signalling pathways involved in MGMT gene expression, proved to increase TMZ toxicity (Wickström et al., 2015).

The MGMT protein also protects cells against the toxic effects of chloroethylating agents, transferring the chloroethyl group at the O6 position of the guanine of the damage DNA to the cysteine residue of the MGMT molecule (Cheng et al., 2017).

2.2.2.2 Biological barriers

The existent biological barriers, such as BBB and BBTB, also presents a major obstacle in the treatment of GBM, decreasing the efficiency of TMZ (Mujokoro, et al., 2016). BBTB can be characterized by three different microvessel populations found in GBM tumour surrounding environment. The first population consists in the continuous and non-fenestrated capillaries also found in healthy brain tissue. The second, continuous and fenestrated capillaries exhibit increased permeability, and finally the capillaries containing inter-endothelial gaps are not able to block the passage of large molecules (Groothuis, 2000). Hence, these major morphological alterations affect the normal vascular organization and function, resulting in this much more permeable barrier (van Tellingen et al., 2015). However, due to its high invasiveness, GBM tumour cells widespread into outer areas of the disrupted BBTB, where the function of the BBB is still intact. Thus, unlike as observed in the core of the tumour, the BBB is still intact in the tumour's margins, obstructing the delivery of drugs to the entire tumour extent (Groothuis, 2000; Soda, et al., 2013). Also, receptors for drug efflux are also expressed at the BBTB thereby ensuring the GBM chemo-resistance to TMZ (Groothuis, 2000).

The BBB prevents the delivery of most therapeutic agents, thus impeding an effective therapy. In fact, it is well-established that BBB blocks the passage of over 98% of small-molecule drugs and 100% of large-molecule (> 500 Da) (Cardoso et al., 2010). BBB is an organized interface between peripheral circulation and the CNS that can respond to local changes and requirements and has a dual function as a barrier and a carrier. It protects the microenvironment of the CNS by blocking the transport of potentially toxic or harmful substances from the bloodstream to the brain, but it allows the transport of nutrients. Thus, this interface maintains the CNS homeostasis through the regulation of the ion balance and metabolites influx/efflux (Groothuis, 2000; Liebner et al., 2011).

The BBB is composed by two membranes - luminal and abluminal - of capillary endothelium, composed by different cell types such as endothelial cells, pericytes, astrocytes and microglial cells (Soda, et al., 2013; Wohlfart et al., 2012). BBB function is maintained by tight junctions between the endothelial cells, physically restricting the diffusion of molecules into the brain (Abbott et al., 2010). The basal lamina is composed of type IV collagen, fibronectin, heparin sulphate and laminin. It regulates the permeability and cellular transport across the BBB. Pericytes are macrophage-like cells with smooth muscle properties that are embedded in the basal lamina around the blood vessels. They also regulate the permeability of BBB through the release of vasoactive substances. As they decrease with age, there is an increase in the BBB permeability (Rosenberg, 2012).

The BBB acts as dynamic system allowing limited diffusion of exogenous compounds into the brain (Abbott, 2013). The transport of these molecules through the BBB can occur through different influx pathways depending on their physicochemical properties. The transport of molecules can occur through two mechanisms: passive transport or active transport. Passive transport includes paracellular diffusion of water-soluble compounds and transcellular transport of small lipophilic molecules (less than 500

Da) to the cerebral parenchyma as schematized in figure 2.4. Active transport pathways include transcytosis mediated by membrane protein carriers of relatively small molecules; receptor-mediated transcytosis for macromolecules and transcytosis mediated by adsorption of positively charged peptides (figure 2.4). Since most of the polar molecules cannot diffuse through cell membranes, cells express in their membrane surface a large number of receptors and carriers. Receptor-mediated transcytosis requires the binding of macromolecules to a specific receptor on the cell, inducing endocytosis and subsequent transcytosis. Low-density lipoprotein, and transferrin (Tf) and insulin receptors are the most expressed in BBB membrane surface (Krol, 2012). Positively-charged proteins are able to cross the BBB due to the interaction with negatively charged glycocalyx and phospholipid head groups of the cellular membranes. Electrostatic interaction between the ligand and the surface of the endothelial cells triggers endocytosis followed by transcytosis (Abbott, et al., 2010).

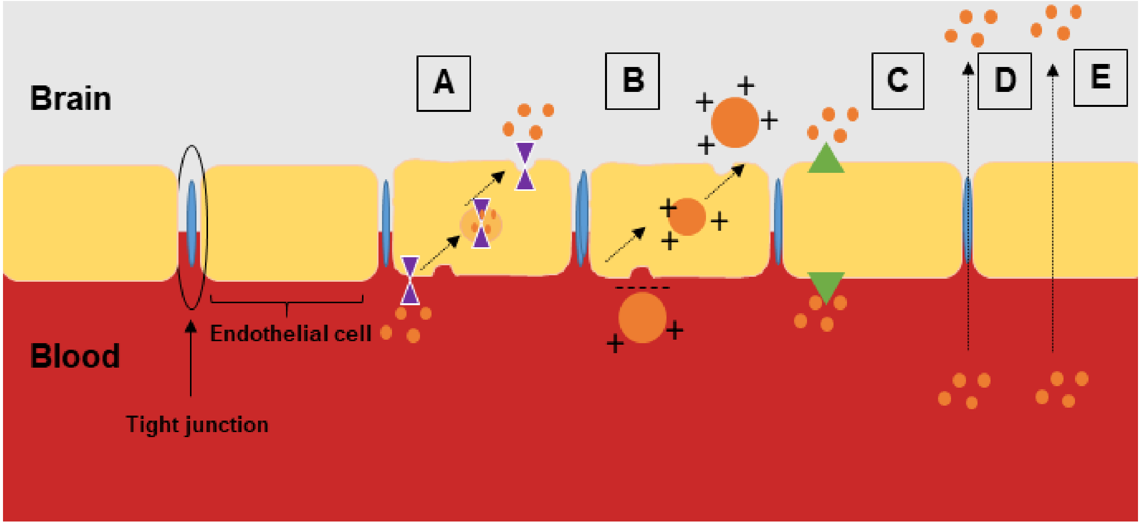

Figure 2. 4 | Transport pathways of molecules from blood to brain through the BBB. (A) Receptor-mediated transcytosis; (B) adsorptive-mediated transcytosis; (C) transport proteins-mediated transcytosis; (D) paracellular aqueous pathway and (E) transcellular lipophilic pathway.

The two most common approaches to circumvent BBB and increase chemotherapeutic efficacy are the local administration strategy associated with high neurotoxicity, and increasing of the drug delivery by using nanocarriers as discussed in the section 2.3 (Groothuis, 2000).

2.2.2.3 Cell membranes

Eukaryotic cell membranes are composed by three major classes of lipids molecules phospholipids, sphingolipids and sterols. Being phosphatidylcholine (PC), phosphatidylethanolamine (PE), phosphatidylserine (PS) the most commonly found phospholipids (Yeagle, 2016). Cholesterol is also a major component of cellular membranes accounting for up to 15-20% of lipid content in animal cells. This molecule provides mechanical strength and its interactions with membranal phospholipids affect the structural organization of the membranes, as well as their fluidity and packing. Cholesterol molecules also regulate the phase behaviour of membranes, promoting ordering and rigidity at the physiologically fluid state, while in the gel state exhibits opposite effects. Therefore, cholesterol displays a crucial role in many membrane processes, as drug transport (Bennett et al., 2018). It is reported that astrocytes and GBM cells have a PC content of approximately 40% and cholesterol content of about 15% (Toda et al., 2015).

Cellular membranes can be perceived as barrier or as a target for drugs, since several receptors and proteins crucial for the pharmacological activity are located at the cellular membrane (Alves, et al., 2016). TMZ must interact with the membranes of the GBM cells to reach the intracellular targets and a major mechanism related to its unsuccessful results in GBM chemotherapy is the MDR phenomenon. Glioblastoma cells become resistant to TMZ due to the overexpression of the p-glycoprotein pump in their membranes. This efflux pump is responsible for the transport of TMZ and other chemotherapeutic drugs out of cells as GBM cells (Binkhathlan and Lavasanifar, 2013).

2.3 Nanosystems for brain drug delivery

Nanomedicine has dictated trends in the last years, since nanomaterials exhibit unique physicochemical properties due to their small size and larger surface area. NPs are colloidal carriers with dimensions on the nano scale (10^{-9} m) with unique physicochemical properties as stability, varied composition, biocompatibility and biodegradability. Encapsulating molecules in a nanocarrier allows increasing their bioavailability and bioaccumulation in the target site and decreasing their toxicity. The fulfilment of these main goals allows maximizing therapeutic effects and minimizing side effects (Semete et al., 2010; Steichen, et al., 2013). Since the ability to cross the biological barriers and membranes is not dependent of the chemical structure of the nanoencapsulated drug, but of the physicochemical and biomimetic features of the NPs, nanocarriers must meet several requirements to be suitable for drug delivery to the brain. These properties include nontoxicity, capacity of interacting with receptors present at the BBB and membrane of the target cells, and ability to carry small molecules, proteins, peptides or nucleic acids (Chen and Liu, 2012; Masserini, 2013). Also, the NPs must effectively reach the target tissue without harmfully affecting other non-targeted tissues, must be able to cross the BBB and successfully deliver the drug at the specific target cells (Subas and Gurudutta, 2013).

As NPs can be internalized into the cells through a passive mechanism, by direct plasma membrane penetration (Krol, 2012), the surface and hydrophobicity characteristics of the NPs display a determining factor on the ability of the NP to cross the BBB and be internalized by the target cells. For example, several studies suggest that the MDR problem might be circumvented by the NP approach (Panyam and Labhasetwar, 2003; Vasir and Labhasetwar, 2007). It is also known that hydrophobic surfaces are rapidly opsonized followed by recognition by the reticuloendothelial system (RES). Although cationic NPs could undergo through adsorptive endocytosis mediated by charge–charge interaction with the negatively charged composition of the endothelial surface of the BBB (Fernandes et al., 2010), anionic NPs exhibit a higher cerebral uptake than cationic and neutral NPs. The mechanism behind anionic NPs transport across the BBB may be the NP-induced BBB opening. Additionally, negative charged NPs can achieve increased efficient uptake rates after the adsorption or covalently coupling of targeting ligands. Still, cationic NPs and NPs with high concentration of anionic charges may be toxic to the BBB, causing the swelling of endothelial cells leading to cell death (Lockman et al., 2004). Thus, the surface charges of NPs should be considered in the neurotoxicity and in the cerebral distribution profiles (Dikpati et al., 2012). However, the NP surface is not the only one to have influence on the successful brain delivery, but all the materials used in the NP formulation may influence their ability to deliver drugs to the brain (Wohlfart, et al., 2012). Thus, depending on the physicochemical characteristics of the drug to be encapsulated and the target tissue, different types of NPs can be envisaged. Some of the most used types of nanocarriers for several biomedical applications are represented in figure 2.5.

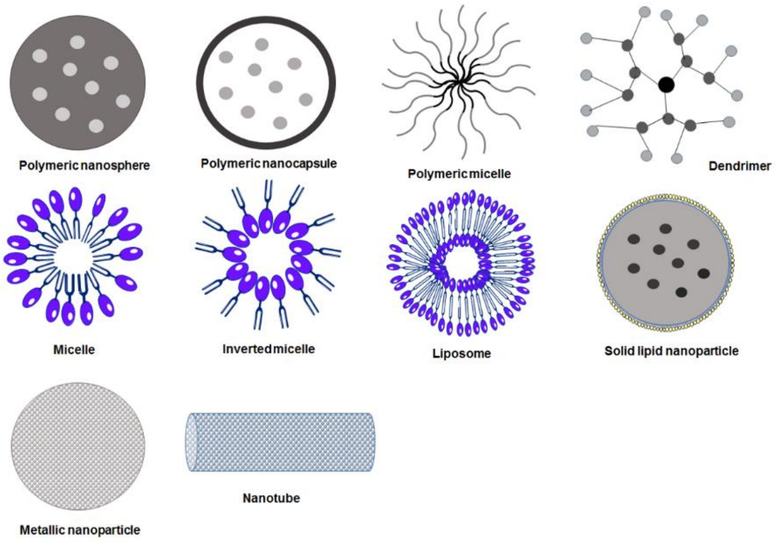

Figure 2. 5 | Schematic representation of the most used nanosystems (Ramalho et al., 2018).

Passive targeting strategies are also size-dependent due to the EPR effect verified in tumour microenvironment. Tumour tissues exhibit an increased permeability of blood vessels, while lymphatic drainage is decreased. This leads to an increase in the concentration of drug-loaded NPs in the tumour tissue (Parhi et al., 2012; Wang and Thanou, 2010). As this EPR effect is not verified in healthy tissues, NPs permeability is hampered (Steichen, et al., 2013). Furthermore, the NP size also is a determining factor on the cellular uptake mechanism. NPs smaller than 200 nm are up taken by clathrin-mediated endocytosis, whereas NPs with a size up to 500 nm are uptaken caveolae-mediated endocytosis (Wohlfart, et al., 2012). The size may also influence the NPs diffusion through the brain tissue. Recent studies have shown that NPs with very small dimensions may encounter diffusion problems in the brain tissue. In turn, PEGylated-NPs (Polyethylene glycol-NPs) with approximately 100 nm diffuse more freely into the human brain (Masserini, 2013).

Though, passive targeting mechanisms are specificity-limited and are the result of the overall physicochemical NPs features, presenting numerous limitations. Active targeting strategies could improve accumulation of NPs at the target site, through receptor-mediated endocytosis of the NPs by brain capillary endothelial cells and target cells. Different essential molecules for the normal cellular metabolism including Tf, folic acid, insulin, insulin-like growth factor and vasopressin have receptors at the luminal side of the endothelial cells of the BBB and several types of cancer cells and are transported via receptor-mediated endocytosis. Therefore, they have been extensively studied as potential targets for drug delivery (Boado et al., 2006; Coloma et al., 2000; Gu et al., 2017; Marchetti et al., 2014; Moriyama et al., 2018; Pardridge, 2015; Wu et al., 1997).

Another strategy used for the transport of nanocarriers across the BBB involve tight junction opening between endothelial cells, enabling the nanosystem to penetrate the BBB (Jain, 2012). Several modulators can be used to promote this opening, ranging from chemical as cell penetrating peptides and biological substances as virus and to physical stimuli such as high frequency focused ultrasound and electromagnetic fields (Chen and Liu, 2012).

2.4 Monoclonal antibodies for active targeting strategies

In addition to using different moieties as receptor ligands as mentioned above, the NPs' surface can be also modified with antibodies for the target of such receptors. The use of antibodies, most particularly monoclonal antibodies (mAbs), present some advantages due to of their high specificity, allowing to use a small amount and still achieving high levels of targeting (Loureiro et al., 2014). mAbs are monovalent antibodies that recognize the same epitope, the part of the antigen that is recognized, and are produced from a single clone. mAb molecules are being used for drug targeted delivery, due to their advantageous features over polyclonal antibodies, as exhibiting increased specificity, long half-life, homogeneous structure and their ability to be mass-produced (Yan et al., 2017).

So, mAb can be used as active targeting molecules to several membrane receptors, enhancing the transport across biological barriers as BBB and increasing the uptake in target cells by receptor-mediated endocytosis, avoiding the MDR problem (Haar, et al., 2012).

Different receptors for molecules essential for the normal cellular metabolism can be targeted. TfR is very concentrated in brain capillary endothelium, comparatively to other organs, making it a desirable target for enhanced drug delivery to the brain (Carroll et al., 2010). Also TfR is well-reported to be overexpressed in several tumour cells types (Frasco et al., 2015), including GBM cells (Calzolari et al., 2010). Tf is a plasma protein for the transport of iron, and its receptors are overexpressed due to the high iron requirement to maintain cellular intermediary metabolism (Pardridge et al., 1987). Therefore, TfR can be used as dual-targeting strategy, enhancing NPs efficiency. As mAb for TfR does not compete with the natural Tf molecules found in the bloodstream, its use allows avoiding saturation of the TfR and increasing specificity of the target (Lee et al., 2000). Thus, different clones of mAbs against the TfR have been investigated in a number of studies, such as RI7217, 8D3 and Ox-26 clones. For example, Salvati et al. (2013) used RI7217 mAb to functionalize liposomes for the transport across the BBB and target the amyloid-β peptide. The modification with RI7217 mAb proved to increase the permeability of the nanocarriers through the BBB *in vitro* model (Salvati et al., 2013). Cabezón and colleagues (2015) modified the surface of gold NPs using the 8D3 anti-TfR mAb. Animal studies using mice showed that the nanocarriers were efficiently internalized by the BBB cells, however the NPs did not dissociate from the TfR, concluding that although targeting of TfR is a suitable strategy, different mAb approaches should to be developed (Cabezón et al., 2015).

Vandelli et al. developed chitosan NPs modified with OX-26 mAb for brain delivery. Accumulation in brains of mice proved to be much higher for OX26-conjugated NPs than for unmodified NPs, showing that OX26 mAb is promising targeting strategy for brain drug delivery (Monsalve et al., 2015). Liu and colleagues also used OX26 mAb for brain targeting. The group functionalized SLN for the delivery of baicalin, a neuroprotective drug. Pharmacokinetics studies using rats showed that modification with OX-26 significantly improved the SLN accumulation in the brain tissue (Liu et al., 2015).

Despite that the application of mAbs considerably increases treatment costs (Lange et al., 2014), mAb type OX26 that has proven to efficiently bind cells that overexpress TfRs (Loureiro et al., 2017; Loureiro et al., 2016).

2.5 Nanosystems for the delivery of temozolomide

TMZ's low bioavailability in the brain tissue, high toxicity and cell resistance continue to be highlighted as major challenges in developing formulations for its clinical use. Therefore, several research groups have sought the development of new functional therapies using nanotechnologies for TMZ delivery without reducing its bioavailability or activity, in the last decades. Different types of approaches and nanomaterials have been proposed through the years. In this section, a summary of the developed nanosystems is presented: The nanocarriers were grouped in different tables (tables 2.1, 2.2, 2.3, 2.4 and 2.5) by their category.

In table 2.1 liposomes for the treatment of GBM are presented.

Table 2. 1 | Currently developed liposomes for TMZ delivery for GBM therapy. Note that n/a stands for not applicable.

NPs	Co-delivery	Ligand	Coating	Size (nm)	Surface charge	Development phase		Ref.
						Cell studies	Animal studies	
Liposome	n.a.	n.a.	n.a.	150	Neutral	n.a.	Biodistribution in mice and rabbits	(Gao et al., 2015)
Liposome	n.a.	n.a.	n.a.	100	Positive	Cytotoxicity, uptake studies	n.a.	(Patel, 2016)
Liposome	n.a.	Anti- TfR antibody	n.a.	40	Positive	Cytotoxicity, uptake studies	Biodistribution, survival and tumour growth in mice	(Kim et al., 2015)
Liposome	Quercetin	n.a.	PEG	100-300	Positive	Cytotoxicity, uptake studies	Biodistribution in rats	(Hu et al., 2016)
Liposome	n.a.	n.a.	n.a.	100-150	Positive	Cytotoxicity, uptake studies	n.a.	(Arcella et al., 2018)
Liposome	n.a.	n.a.	PEG	120	Neutral	Cytotoxicity studies	Tumour growth studies with rats	(Nordling-David et al., 2017)
Liposome	n.a.	n.a.	PEG	160	Neutral	Cytotoxicity studies	Biodistribution, survival and tumour growth studies with mice	(Lin et al., 2018)

Liposomes are probably the most popular among the lipid-based nanocarriers studied for nanomedicine applications (Yingchoncharoen et al., 2016). They are non-toxic and biocompatible, as they are very similar in structure and composition to the cell membrane phospholipids. Such nanocarriers are considered excellent systems for drug-controlled release due to their structural flexibility, size, composition and fluidity/permeability of the lipid bilayer versatility. Also, their surface is easily functionalized due to their polar headgroups (Torchilin, 2012).

Gao and co-workers (2015) developed liposomes for the delivery of TMZ. Although biodistribution studies using mice showed an increased accumulation of TMZ in brain tissue, the obtained nanoformulations exhibited low encapsulation efficiency and were not able to maintain a sustained and controlled release over time (Gao, et al., 2015). Simultaneous delivery of different chemotherapeutic drugs using liposomes has also been recently studied to potentiate chemotherapy efficacy for glioblastoma. In fact, Hu and colleagues (2016) developed PEGylated liposomes for the brain co-delivery of TMZ and another chemotherapeutic drug, quercetin. *In vivo* biodistribution studies using rats revealed a significant accumulation of the developed liposomes in the brain, enhancing drug delivery to brain tumours. However, the system failed to maintain a controlled and sustained release of TMZ for more than 24 hours (Hu, et al., 2016).

Patel and colleagues (2016) developed positively charged liposomes for the TMZ delivery that were able to enhance the TMZ cytotoxicity activity (Patel, 2016). Arcella et al. (2018) also developed cationic liposomes for the delivery of TMZ. The authors proposed that the positively charged liposomes would recruit several proteins *in vivo* that would confer natural targeting ability to the nanoformulation (Arcella, et al., 2018). To overcome some of the limitations of the passive targeting strategies already reported, Kim and partners (2015) developed cationic liposomes with anti-TfR antibody attached to their surface, to target both the BBB and cancer cells. Animal studies showed that tumour growth inhibition and animal survival was enhanced when TMZ was delivered by antibody-modified liposomes. Thus, the developed nanocarrier proved to be a promising strategy for the TMZ-based treatment for GBM tumours (Kim, et al., 2015). However, although positively charged liposomes could offer more stability than neutral liposomes, anionic liposomes would exhibit a higher cerebral uptake and stability (Patel, 2016). Also, it is proved that cationic liposomes and other nanocarriers can induce cytotoxicity by promoting the production of reactive oxygen species. The positive surface charge is related with disturbances in the energy metabolism, and in several other signalling pathways that eventually could lead to cell death (Knudsen et al., 2015; Yu et al., 2017).

Nordling-David and colleagues (2017) developed neutral liposomes for the convection-enhanced delivery of TMZ (Nordling-David, et al., 2017). In this delivery pathway, drugs are administered directly within the tumour tissue using a catheter, overcoming some biological barriers, such as the BBB (Mehta et al., 2017). However, animal studies using rats did not shown any advantages in using the liposomal formulation, since it did not enhance TMZ's therapeutic efficiency (Nordling-David, et al., 2017). One year later, another group also proposed neutral liposomes for the convection-enhanced delivery of TMZ. This group concluded that the developed nanosystem was able to enhance TMZ antitumour activity (Lin, et al., 2018). However, limitations in catheter technology have prevented this technique from being reliable and reproducible, and the clinical trials did not show a survival benefit for patients. Thus, further research to explore this technique is necessary to develop a more effective methodology (Vogelbaum and Aghi, 2015).

Despite, being a widely popular nanocarrier, liposomes present some disadvantages as well, as low solubility, short half-life and high production costs. Also, the phospholipids can undergo oxidation, and in several cases leakage of encapsulated molecules is verified, especially in low molecular weight molecules (Akbarzadeh et al., 2013). Also, some reports prove that liposomes can induce complement activation which can lead to hypersensitivity reactions (Szebeni et al., 2002).

Other lipid-based nanocarriers have also been proposed for the delivery of TMZ or its co-delivery with another chemotherapeutic agent, using passive and/or active targeting strategies as shown in table 2.2. As liposomes, these solid lipid nanoparticles (SLN) are biocompatible since most of the lipids are biodegradable, present a high drug entrapment of both lipophilic and hydrophilic drugs. However, these present some advantages over liposomes since their production is less expensive and uses water based technology, avoiding the use of organic solvents, and they are more easily scaled-up (Mukherjee et al., 2009). Huang and colleagues (2008) developed TMZ-loaded anionic SLN. *In vivo* biodistribution studies using rabbits showed an increased accumulation of intravenous injected NPs in the brain tissue. Thus, the developed nanosystem proved to be a promising nanoapproach for the sustained-release of TMZ and its delivery to brain tumours (Huang et al., 2008). However, no active targeting strategy to increase the specificity of the nanocarrier was used.

Table 2. 2 | Currently developed lipid-based nanosystems for TMZ delivery for GBM therapy. Note that n/a stands for not applicable.

NPs	**Co-delivery**	**Ligand**	**Coating**	**Size (nm)**	**Surface charge**	**Development phase**		**Ref.**
						Cell studies	**Animal studies**	
SLNs	n.a.	n.a.	Poloxamer 188	65	Negative	n.a.	Biodistribution, studies with rabbits	(Huang, et al., 2008)
SLNs	n.a.	Tf	Poloxamer 188	250	Positive	Cytotoxicity, uptake studies	Biodistribution in rats	(Jain et al., 2013)
SLNs	Vincristine	n.a.	n.a.	180	Positive	Cytotoxicity studies	Biodistribution and tumour growth in mice	(Wu et al., 2015)
NLCs	Vincristine	n.a.	n.a.	120	Positive	Cytotoxicity studies	Biodistribution and tumour growth in mice	(Wu, et al., 2015)
NLCs	n.a.	RGD	PEG	120	Positive	Cytotoxicity, uptake studies	Biodistribution and tumour growth studies with mice	(Song et al., 2016)

Some other authors developed SLN for the encapsulation and delivery of TMZ with (Jain, et al., 2013) and without active targeting strategies (Wu, et al., 2015). Although both prepared nanosystems proved to be efficient for TMZ delivery, both developed SLN exhibited a positive surface charge. Positively charged SLN are highly popular due to their interaction with biological membranes, being more likely to penetrate biological barriers. However cationic lipids show some toxicity to the cellular membrane associated with histological changes (Knudsen et al., 2014). In fact, it is reported that cationic SLN can induce cytotoxicity by promoting oxidative stress and disruption of the cellular membrane (Hwang et al., 2015). Also, cationic SLN are usually less stable than negatively charged SLN (Doktorovova et al., 2014).

Also, it was reported that nanostructured lipid nanocarriers (NLC) are more efficient in retaining encapsulated TMZ, allowing a slower and more controlled release of TMZ than SLN being more efficient for GBM therapy (Wu, et al., 2015). For this reason, some authors developed cationic NLC for the delivery of TMZ for GBM therapy. Song and colleagues (2016) used arginine-glycine-aspartic acid peptide (RGD) to modify the surface of the nanocarriers for the targeted delivery to tumour cells, since RGD binds to integrins highly overexpressed on the endothelial cells of tumour angiogenic vessels. Animal studies using GBM tumour bearing mice showed that TMZ-encapsulated in RGD-modified nanosystems inhibited tumour growth more efficiently than encapsulated in unmodified nanocarriers or in its free form, proving that these nanocarriers could be promising approach for GBM treatment (Song, et al., 2016). Chen and collaborators (2016) also developed cationic NLC for the simultaneous delivery of TMZ and a protein plasmid. Animal studies using malignant glioma tumour bearing mice showed that tumour growth inhibition was enhanced by the nanoformulations, proving that the nanocarrier is a suitable strategy for the dual delivery of genes and chemotherapeutic agents for GBM treatment (Chen et al., 2016).

Although the reported NLC systems proved to be efficient, all the authors proposed the use of cationic NLC. in addition to the toxicity problems associated with the use of positively charged lipids, it was also reported that cationic NLC accumulate more predominantly in lung, liver and kidney than in brain tissue (Poonia et al., 2016) and that anionic NLC exhibit higher drug targeting efficiency (Tapeinos et al., 2017).

Besides lipid-based nanosystems, also polymeric NPs have been studied for GBM therapy as shown in table 2.3.

Table 2. 3 | Currently developed polymeric nanosystems for TMZ delivery for GBM therapy. Note that n/a stands for not applicable.

Nanocarrier	Co-delivery	Ligand	Coating	Size (nm)	Surface charge	Development phase		Ref.
						Cellular studies	Animal studies	
PLA NPs	n.a.	n.a.	Sodium tauroglycolate	180-220	Negative	Cytotoxicity, cellular uptake and motility studies	n.a.	(Jain et al., 2013)
Chitosan NPS	5-fluorouracil	n.a.	Alginic and polygalacturonic acids	100-200	Positive and negative	n.a.	n.a.	(Di Martino et al., 2016)
Chitosan NPs	n.a.	Chlorotoxin	PEG	50	Negative	Cytotoxicity, uptake studies	Biodistribution studies with mice	(Fang et al., 2015)
Chitosan nanogels	microRNA and gold NPs	Folate	n.a.	100	Positive	Cytotoxicity, uptake studies	Tumour growth studies with mice	(Fan et al., 2015)
Chitosan hydrogel with solid lipids	n.a.	n.a.	Polysorbate 80	130	Positive	Cytotoxicity, nasal diffusion studies	Biodistribution studies with rats	(Khan et al., 2018)
Chitosan NPs entrapped in Poly(ε-caprolactonediol) and polyurethane nanofibers	n.a.	n.a.	Gold NPs	100	Positive	Cytotoxicity studies	n.a.	(Irani et al., 2017)
Poly(ε-caprolactonediol) and polyurethane nanofibers	n.a.	n.a.	Gold NPs	15-25	Data not shown	Cytotoxicity studies	n.a.	(Irani et al., 2017; Irani et al., 2017)

In fact, Patil and colleagues (2010) developed PEGylated poly (β-L-malic acid) nanocarriers with a modified surface using two different molecules for TMZ target delivery. A RVS10 clone mAb to the TfR was used to target the GBM tumour cells, and trileucine was used for pH-dependent endosomal membrane disruption to stimulate the NPs release into the cytoplasm. In this nanometric platform, instead of entrapped, the TMZ molecules were also covalently linked to the nanomaterial surface. The prepared NPs exhibited mean sizes of about 15 nm and low negative zeta potential values. *In vitro* cellular studies showed that cellular uptake was higher for mAb-modified NPs than for the unmodified NPs, suggesting that the developed nanocarriers were internalized by receptor-mediated endocytosis. Cellular studies also showed that cellular targeting with mAb for transferrin receptor and trileucine for endosomal membrane disruption, significantly enhanced the TMZ cytotoxicity effects, proving that the developed nanosystem is a suitable strategy for the specific targeted delivery of TMZ for GBM treatment (Patil et al., 2010). However, the small dimensions of the proposed nanosystems may induce cytotoxicity upon internalization, since a size dependent toxicity has been reported for polymeric NPs (Bhattacharjee et al., 2012). The NPs' *in vivo* toxicity is directly related to their biodistribution and blood-circulation times, which are both size-dependent. In fact, smaller NPs appear to be more toxic than larger ones due to the higher surface area relative to their total mass, which increases the chance to interact with surrounding biomolecules and, as a consequence, to trigger adverse responses (Shang et al., 2014).

Khan et al. (2018) also proposed a polymeric nanoformulation for the delivery of TMZ. The group prepared a nanohydrogel composed of chitosan and a solid lipid, gelucire, that exhibited mean sizes of approximately 130 nm. The attained encapsulation efficiency values were of almost 90%. *In vitro* nasal diffusion studies using excised goat nasal mucosa showed that the nanosystem improved diffusion comparatively to control due to the permeability enhancement properties of chitosan. The developed nanogel proved to be biocompatible and enhanced TMZ's toxicity towards glioma tumour cells. The authors proved that this nanosystem can target the brain through intranasal route due to the mucoadhesive properties of chitosan. The positive charge of chitosan interacts with the negative charged cell membranes leading to the transient opening of tight junctions, enhancing NPs' permeation across the mucosa. However, as mentioned already, positively charged NPs' are associated with increased toxicity (Khan, et al., 2018).

Other types of nanocarriers were also proposed for the delivery of TMZ in glioblastoma treatment as shown in table 2.4.

Table 2. 4 | Other developed nanosystems for TMZ delivery for GBM therapy. Note that n/a stands for not applicable.

Nanocarrier	Co-delivery	Ligand	Coating	Size (nm)	Surface charge	Development phase		Ref.
						Cellular studies	Animal studies	
Iron oxide NPs	n.a.	n.a.	PLGA and Polysorbate 80	220	Data not shown	Cytotoxicity studies	n.a.	(Ling et al., 2012)
Iron oxide NPs	Curcumin	n.a.	Glyceryl monooleate	200	Positive	Cytotoxicity, uptake studies	n.a.	(Dilnawaz and Sahoo, 2013)
Silica NPs	anti-miR221	n.a.	n.a.	100	Neutral	Cytotoxicity, uptake studies	n.a.	(Bertucci et al., 2015)
Micelles	HSVtk gene	n.a.	n.a.	110	Positive	Gene transfection efficiency, cytotoxicity studies	Biodistribution and tumour growth studies with rats	(Choi et al., 2017)
PAMAM dendrimers	n.a.	Tf	PEG	Data not shown	Data not shown	Cytotoxicity, uptake studies	Biodistribution and tumour growth studies with mice	(Sun et al., 2017)

2.5.1 PLGA nanoparticles for the delivery of temozolomide

As already mentioned in the last decades, polymeric NPs have been studied for GBM therapy. Among polymeric NPs, poly(D,L-lactic-co-glycolic) (PLGA) is probably the most popular (Ramalho and Pereira, 2016). PLGA has become one of the most attractive candidates for a range of applications due to being biocompatible, having adjustable biodegradation rate and tuneable mechanical properties, and being FDA-approved. PLGA NPs are able to maintain a controlled and sustained release for several days, allowing decreasing the drug doses and their administration frequency, minimizing the harmful side effects and presenting an economic advantage (Makadia and Siegel, 2011). Also, PLGA NPs are internalized by endocytosis, allowing drug accumulation in target cells and avoiding recognition by the glycoprotein-P complex. Also, PLGA is easily functionalized allowing the design of several NPs with different targeting moieties (Danhier et al., 2012). However, its use faces a few limitations as their poor loading capacity. The characteristic initial burst release can be another major pitfall since a large amount of drug is loss before reaching the target tissue. Also, the many required steps for NP production such as centrifugation and dialysis are expensive and difficult to scale-up. Another drawback of these polymeric NPs is the challenge of hydrophilic molecules entrapment, since those rapidly partition into the aqueous phase during NPs preparation. For that is necessary to use appropriate preparation methods as the double emulsion technique (Makadia and Siegel, 2011).

To date some pharmaceutical formulations using PLGA polymer are commercially available. In fact, since its FDA-approval in 1989, Lupron Depot® has been used for prostate cancer treatment. This formulation consists in PLGA microparticles containing leuprolide acetate. Another PLGA microparticles, with the commercial name Trelstar Depot®, are available for prostate cancer treatment since 2001, containing the active ingredient triptorelin pamoate (Byeon et al., 2015; Chaubal, 2002). Gliadel® is another PLGA-based formulation used for malignant gliomas. This microformulation is implanted in the patient, after tumour surgical resection releasing the chemotherapeutic agent, carmustine (Singh et al., 2014). However, there is no clinically approved PLGA micro/nanoformulations for the GBM treatment either using TMZ or another chemotherapeutic agent. Still, a great effort has been made by the scientific community to develop a suitable efficient nanosystem based on PLGA polymer for TMZ delivery, as shown in table 2.5.

Table 2. 5| Currently developed PLGA NPs for TMZ delivery for GBM therapy. Note that n/a stands for not applicable.

Nanocarrier	Co-delivery	Ligand	Coating	Size (nm)	Surface charge	Development phase		Ref.
						Cellular studies	Animal studies	
PLGA NPs	n.a.	n.a.	Poloxamer 188	150	Negative	Cytotoxicity, uptake studies	n.a.	(Jain et al., 2014)
PLGA NPs	n.a.	n.a.	Polyvinyl alcohol	200	Negative	Cytotoxicity studies	n.a.	(Ananta et al., 2016)
PLGA NPs	n.a.	Tf	PEG	120	Negative	Cytotoxicity studies	Biodistribution studies with rats	(Jain et al., 2011; Jain and Jain, 2013)
PLGA NPs	n.a.	Folate	PEG	400-600	Negative	n.a.	n.a.	(Maiti et al., 2016)
PLGA NPs	Paclitaxel	n.a.	PEG	200	Negative	Cytotoxicity studies	Biodistribution and tumour growth studies with mice	(Xu et al., 2016)

Jain and colleagues (2014) developed PLGA NPs for the delivery of TMZ. The authors proved that TMZ entrapment in these polymeric NPs enhanced its cellular uptake enabling a significant enhanced chemotherapeutic activity, also proving that the prepared system was a suitable nanocarrier for TMZ (Jain, et al., 2014). However, no active targeting strategy to increase the specificity of the nanocarrier was used.

Ananta and colleagues (2016) evaluated the effect of three different experimental procedures on the encapsulation of TMZ in PLGA NPs. The authors used a double-emulsion solvent evaporation method, and a single-emulsion with the aqueous phase TMZ-saturated and unsaturated aqueous phase. All the prepared PLGA NPs were not able to maintain a controlled and sustained release for several days, being that about 80% of the encapsulated TMZ was released in the first 6 hours. Cellular studies using a human GBM cell line showed no significant difference in cytotoxicity effects between free TMZ and encapsulated TMZ, probably due to the initial burst release of TMZ. Thus, the synthetized system didn't prove to be a suitable strategy for the GBM treatment (Ananta, et al., 2016).

Simultaneous delivery of different chemotherapeutic drugs using PLGA NPs has also been recently studied to potentiate chemotherapy efficacy for glioblastoma. In fact, Xu and co-workers (2016) intended the simultaneous delivery of TMZ with another chemotherapeutic agent. The group prepared PEGylated PLGA NPs for the entrapment of both TMZ and paclitaxel. Animal studies using mice showed an increased reduction in tumour size for the entrapped drugs, confirming that combined therapy using nanocarriers is an efficient method for the GBM treatment (Xu, et al., 2016). However, i*n vitro* release studies showed an initial burst release of about 80% of total TMZ in the first 24 hours, and almost 100% of the drug released after 3 days, proving that the system is not able to maintain a slow and controlled release for several days. Also, no active targeting strategy to increase the specificity of the nanocarrier was used.

As passive targeting strategies present some limitations, active targeting approaches have also been studied for the enhanced delivery of nanosystems. Different peripherally conjugated targeting moieties have been studied. For example, Lee and collaborators (2016) modified the surface of the PLGA NPs with folate molecules. Receptors for this molecule are overexpressed in tumour cells membrane. Although the authors tested several methods for the preparation of NPs, they failed in achieving acceptable encapsulation efficiency values that did not exceed 2%. Therefore, although the proposed system could be a suitable strategy for TMZ specific targeting to tumour cells expressing folate receptor, the system failed to be efficient for the delivery of TMZ (Maiti, et al., 2016).

Jain and co-workers (2011) also used an active targeting strategy. The authors modified the surface of the PLGA NPs with Tf molecules to enhance the transport across the BBB. Cytotoxicity studies on a neuroblastoma cell line showed an increased antiproliferative effect of TMZ when entrapped in the prepared NPs due to an increased intracellular uptake via TfR. Animal studies using albino rats showed an increased accumulation of TMZ in brain tissue for Tf-modified NPs than for unmodified NPs, proving that the developed nanocarrier was able to target the brain by receptor-mediated transcytosis across the BBB (Jain, et al., 2011). A few years later, the authors optimized the preparation of these NPs for TMZ encapsulation. The studied experimental variables were concentration of TMZ, concentration of PLGA/PEG-PLGA, stabilizer and sonication time, and their effect on particle mean dimensions and percentage of entrapped TMZ was assessed (Jain and Jain, 2013).

Despite the increased use of Tf as targeting ligand for brain delivery, its application *in vivo* is very limited (Chang et al., 2009). Endogenous levels of Tf are very high, leading to the saturation of the transferrin receptor (TfR) (van Rooy et al., 2011). Thus, the use of antibodies such as mAbs against the TfR are expected to present a better outcome (Loureiro et al., 2014).

The choice of the most appropriate nanosystem must consider the biological barriers that the nanocarrier will have to cross before reaching the target tissue, as well as the microenvironment in these tumour tissues. So, the psychochemical properties of the proposed nanosystems, as size and surface charge will influence its efficiency as its toxicity. Then, during the design of the NPs, it will be of outmost importance to evaluate all these issues to choose the most appropriate chemical features.

In addition to these desired physicochemical characteristics of the nanocarriers, also another feature plays a major role in the efficient activity of the designed nanosystems, the encapsulation efficiency. High encapsulation values are desired, making the nanosystem more efficient, minimizing the administration frequency and presenting an economic advantage. The development of an efficient system for TMZ is challenging, due to the physicochemical features of this drug.

Due to the TMZ properties and GBM microenvironment, none of the nanosystems presented here has reached the clinical trials stage. Thus, further studies are required to develop a practical and cost effective nanoformulation that can become commercially available for clinical use.

References

Abbott, N.J. 2013. Blood–brain barrier structure and function and the challenges for CNS drug delivery. Journal of Inherited Metabolic Disease. 36 (3), 437-449.
Abbott, N.J., Patabendige, A.A.K., Dolman, D.E.M., Yusof, S.R., Begley, D.J. 2010. Structure and function of the blood–brain barrier. Neurobiology of Disease. 37 (1), 13-25.
Ahmed, A.U., Auffinger, B., Lesniak, M.S. 2013. Understanding glioma stem cells: rationale, clinical relevance and therapeutic strategies. Expert review of neurotherapeutics. 13 (5), 545-555.
Akbarzadeh, A., Rezaei-Sadabady, R., Davaran, S., Joo, S.W., Zarghami, N., Hanifehpour, Y., Samiei, M., Kouhi, M., Nejati-Koshki, K. 2013. Liposome: classification, preparation, and applications. Nanoscale Research Letters. 8 (1), 102-102.
Alves, A.C., Ribeiro, D., Nunes, C., Reis, S. 2016. Biophysics in cancer: The relevance of drug-membrane interaction studies. Biochimica et Biophysica Acta (BBA) - Biomembranes. 1858 (9), 2231-2244.
An, N., Shi, Y., Ye, P., Pan, Z., Long, X. 2017. Association Between MGMT Promoter Methylation and Breast Cancer: a Meta-Analysis. Cellular Physiology and Biochemistry. 42 (6), 2430-2440.
Ananta, J.S., Paulmurugan, R., Massoud, T.F. 2016. Temozolomide-loaded PLGA nanoparticles to treat glioblastoma cells: a biophysical and cell culture evaluation. Neurological Research. 38 (1), 51-59.
Andrasi, M., Bustos, R., Gaspar, A., Gomez, F.A., Klekner, A. 2010. Analysis and stability study of temozolomide using capillary electrophoresis. Journal of Chromatography B. 878 (21), 1801-1808.
Arcella, A., Palchetti, S., Digiacomo, L., Pozzi, D., Capriotti, A.L., Frati, L., Oliva, M.A., Tsaouli, G., Rota, R., Screpanti, I., Mahmoudi, M., Caracciolo, G. 2018. Brain Targeting by Liposome–Biomolecular Corona Boosts Anticancer Efficacy of Temozolomide in Glioblastoma Cells. ACS Chemical Neuroscience.
Bao, S., Wu, Q., Sathornsumetee, S., Hao, Y., Li, Z., Hjelmeland, A.B., Shi, Q., McLendon, R.E., Bigner, D.D., Rich, J.N. 2006. Stem Cell–like Glioma Cells Promote Tumor Angiogenesis through Vascular Endothelial Growth Factor. Cancer Research. 66 (16), 7843-7848.

Bastiancich, C., Danhier, P., Préat, V., Danhier, F. 2016. Anticancer drug-loaded hydrogels as drug delivery systems for the local treatment of glioblastoma. Journal of Controlled Release. 243 29-42.

Bennett, W.F.D., Shea, J.E., Tieleman, D.P. 2018. Phospholipid Chain Interactions with Cholesterol Drive Domain Formation in Lipid Membranes. Biophysical journal. 114 (11), 2595-2605.

Bertucci, A., Prasetyanto, E.A., Septiadi, D., Manicardi, A., Brognara, E., Gambari, R., Corradini, R., De Cola, L. 2015. Combined Delivery of Temozolomide and Anti-miR221 PNA Using Mesoporous Silica Nanoparticles Induces Apoptosis in Resistant Glioma Cells. Small. 11 (42), 5687-5695.

Bhattacharjee, S., Ershov, D., Fytianos, K., van der Gucht, J., Alink, G.M., Rietjens, I.M.C.M., Marcelis, A.T.M., Zuilhof, H. 2012. Cytotoxicity and cellular uptake of tri-block copolymer nanoparticles with different size and surface characteristics. Particle and fibre toxicology. 9 11-11.

Binkhathlan, Z., Lavasanifar, A. 2013. P-glycoprotein Inhibition as a Therapeutic Approach for Overcoming Multidrug Resistance in Cancer: Current Status and Future Perspectives. Current Cancer Drug Targets. 13 (3), 326-346.

Boado, R.J., Zhang, Y., Zhang, Y., Pardridge, W.M. 2006. Humanization of anti-human insulin receptor antibody for drug targeting across the human blood–brain barrier. Biotechnology and Bioengineering. 96 (2), 381-391.

Brannon-Peppas, L., Blanchette, J.O. 2004. Nanoparticle and targeted systems for cancer therapy. Advanced drug delivery reviews. 56 (11), 1649-1659.

Byeon, H.J., Kim, I., Choi, J.S., Lee, E.S., Shin, B.S., Youn, Y.S. 2015. PEGylated apoptotic protein-loaded PLGA microspheres for cancer therapy. International Journal of Nanomedicine. 10 739-748.

Cabezón, I., Manich, G., Martín-Venegas, R., Camins, A., Pelegrí, C., Vilaplana, J. 2015. Trafficking of Gold Nanoparticles Coated with the 8D3 Anti-Transferrin Receptor Antibody at the Mouse Blood–Brain Barrier. Molecular Pharmaceutics. 12 (11), 4137-4145.

Calzolari, A., Larocca, L.M., Deaglio, S., Finisguerra, V., Boe, A., Raggi, C., Ricci-Vitani, L., Pierconti, F., Malavasi, F., De Maria, R., Testa, U., Pallini, R. 2010. Transferrin Receptor 2 Is Frequently and Highly Expressed in Glioblastomas. Translational Oncology. 3 (2), 123-134.

Cardoso, F.L., Brites, D., Brito, M.A. 2010. Looking at the blood–brain barrier: Molecular anatomy and possible investigation approaches. Brain Research Reviews. 64 (2), 328-363.

Carroll, R.T., Bhatia, D., Geldenhuys, W., Bhatia, R., Miladore, N., Bishayee, A., Sutariya, V. 2010. Brain-targeted delivery of Tempol-loaded nanoparticles for neurological disorders. Journal of Drug Targeting. 18 (9), 665-674.

Chamberlain, M.C. 2010. Temozolomide: therapeutic limitations in the treatment of adult high-grade gliomas. Expert Review of Neurotherapeutics. 10 (10), 1537-1544.

Chang, J., Jallouli, Y., Kroubi, M., Yuan, X.-b., Feng, W., Kang, C.-s., Pu, P.-y., Betbeder, D. 2009. Characterization of endocytosis of transferrin-coated PLGA nanoparticles by the blood–brain barrier. International Journal of Pharmaceutics. 379 (2), 285-292.

Chaubal, M. 2002. Polylactides/glycolides-excipients for injectable drug delivery and beyond. Drug Deliv Technol. 2 34-36.

Chen, Y., Liu, L. 2012. Modern methods for delivery of drugs across the blood–brain barrier. Advanced drug delivery reviews. 64 (7), 640-665.

Chen, Z., Lai, X., Song, S., Zhu, X., Zhu, J. 2016. Nanostructured lipid carriers based temozolomide and gene co-encapsulated nanomedicine for gliomatosis cerebri combination therapy. Drug Delivery. 23 (4), 1369-1373.

Cheng, J., Ye, F., Dan, G., Zhao, Y., Zhao, J., Zou, Z. 2017. Formation and degradation of nitrogen mustard-induced MGMT-DNA crosslinking in 16HBE cells. Toxicology. 389 67-73.

Choi, E., Han, J., Tan, X., Oh, J., Lee, D., Rhim, T., Lee, M. 2017. Combined delivery of temozolomide and the thymidine kinase gene for treatment of glioblastoma. Journal of Drug Targeting. 25 (2), 156-162.

Christmann, M., Kaina, B. 2016. Chapter 2 - MGMT—a critical DNA repair gene target for chemotherapy resistance, in: M.R. Kelley, M.L. Fishel (Eds.), DNA Repair in Cancer Therapy (Second Edition), Academic Press, Boston, pp. 55-82.

Cipriani, D. 2016. P06.12 miRNA expression, MGMT protein expression and response to temozolomide-based chemotherapy in glioblastoma. Neuro-Oncology. 18 (Suppl 4), iv30-iv30.

Coloma, M.J., Lee, H.J., Kurihara, A., Landaw, E.M., Boado, R.J., Morrison, S.L., Pardridge, W.M. 2000. Transport Across the Primate Blood-Brain Barrier of a Genetically Engineered Chimeric Monoclonal Antibody to the Human Insulin Receptor. Pharmaceutical Research. 17 (3), 266-274.

Corsa, P., Parisi, S., Raguso, A., Troiano, M., Perrone, A., Cossa, S., Munafò, T., Piombino, M., Spagnoletti, G., Borgia, F. 2006. Temozolomide and radiotherapy as first-line treatment of high-grade gliomas. Tumori. 92 (4), 299.

Danhier, F., Ansorena, E., Silva, J.M., Coco, R., Le Breton, A., Preat, V. 2012. PLGA-based nanoparticles: an overview of biomedical applications. Journal of controlled release : official journal of the Controlled Release Society. 161 (2), 505-522.

Di Martino, A., Pavelkova, A., Maciulyte, S., Budriene, S., Sedlarik, V. 2016. Polysaccharide-based nanocomplexes for co-encapsulation and controlled release of 5-Fluorouracil and Temozolomide. European Journal of Pharmaceutical Sciences. 92 276-286.

Dikpati, A., Madgulkar, A., Kshirsagar, S.J., Bhalekar, M., Chahal, A.S. 2012. Targeted drug delivery to CNS using nanoparticles. JAPS J. 2 (1), 179-191.

Dilnawaz, F., Sahoo, S.K. 2013. Enhanced accumulation of curcumin and temozolomide loaded magnetic nanoparticles executes profound cytotoxic effect in glioblastoma spheroid model. European Journal of Pharmaceutics and Biopharmaceutics. 85 (3, Part A), 452-462.

Doktorovova, S., Souto, E.B., Silva, A.M. 2014. Nanotoxicology applied to solid lipid nanoparticles and nanostructured lipid carriers – A systematic review of in vitro data. European Journal of Pharmaceutics and Biopharmaceutics. 87 (1), 1-18.

Esiri, M.M., Oppenheimer, D.R. 1989. Diagnostic neuropathology: A practical manual, 1st ed ed., Blackwell Scientific Publications, Oxford - London.

Fan, L., Yang, Q., Tan, J., Qiao, Y., Wang, Q., He, J., Wu, H., Zhang, Y. 2015. Dual loading miR-218 mimics and Temozolomide using AuCOOH@FA-CS drug delivery system: promising targeted anti-tumor drug delivery system with sequential release functions. Journal of Experimental & Clinical Cancer Research : CR. 34 106.

Fang, C., Wang, K., Stephen, Z.R., Mu, Q., Kievit, F.M., Chiu, D.T., Press, O.W., Zhang, M. 2015. Temozolomide Nanoparticles for Targeted Glioblastoma Therapy. ACS Applied Materials & Interfaces. 7 (12), 6674-6682.

Fernandes, C., Soni, U., Patravale, V. 2010. Nano-interventions for neurodegenerative disorders. Pharmacological Research. 62 (2), 166-178.

Frasco, M.F., Almeida, G.M., Santos-Silva, F., Pereira, M.d.C., Coelho, M.A. 2015. Transferrin surface-modified PLGA nanoparticles-mediated delivery of a proteasome inhibitor to human pancreatic cancer cells. Journal of Biomedical Materials Research Part A. 103 (4), 1476-1484.

Furnari, F.B., Fenton, T., Bachoo, R.M., Mukasa, A., Stommel, J.M., Stegh, A., Hahn, W.C., Ligon, K.L., Louis, D.N., Brennan, C. 2007. Malignant astrocytic glioma: genetics, biology, and paths to treatment. Genes & development. 21 (21), 2683-2710.

Gao, J., Wang, Z., Liu, H., Wang, L., Huang, G. 2015. Liposome encapsulated of temozolomide for the treatment of glioma tumor: preparation, characterization and evaluation. Drug Discoveries & Therapeutics. 9 (3), 205-212.

Gilbertson, R.J., Rich, J.N. 2007. Making a tumour's bed: glioblastoma stem cells and the vascular niche. Nat Rev Cancer. 7 (10), 733-736.

Golla, H., Ale Ahmad, M., Galushko, M., Hampl, J., Maarouf, M., Schroeter, M., Herrlinger, U., Hellmich, M., Voltz, R. 2014. Glioblastoma multiforme from diagnosis to death: a prospective, hospital-based, cohort, pilot feasibility study of patient reported symptoms and needs. Supportive Care in Cancer. 22 (12), 3341-3352.

Groothuis, D.R. 2000. The blood-brain and blood-tumor barriers: a review of strategies for increasing drug delivery. Neuro-oncology. 2 (1), 45-59.

Grossman, S.A., Batara, J.F. 2004. Current management of glioblastoma multiforme. Seminars in Oncology. 31 (5), 635-644.

Gu, J., Al-Bayati, K., Ho, E.A. 2017. Development of antibody-modified chitosan nanoparticles for the targeted delivery of siRNA across the blood-brain barrier as a strategy for inhibiting HIV replication in astrocytes. Drug Delivery and Translational Research. 7 (4), 497-506.

Haar, C.P., Hebbar, P., Wallace, G.C., Das, A., Vandergrift, W.A., Smith, J.A., Giglio, P., Patel, S.J., Ray, S.K., Banik, N.L. 2012. Drug Resistance in Glioblastoma: A Mini Review. Neurochemical Research. 37 (6), 1192-1200.

Hansen, W.K., Kelley, M.R. 2000. Review of Mammalian DNA Repair and Translational Implications. Journal of Pharmacology and Experimental Therapeutics. 295 (1), 1-9.

Hegi , M.E., Diserens , A.-C., Gorlia , T., Hamou , M.-F., de Tribolet , N., Weller , M., Kros , J.M., Hainfellner , J.A., Mason , W., Mariani , L., Bromberg , J.E.C., Hau , P., Mirimanoff , R.O., Cairncross , J.G., Janzer , R.C., Stupp , R. 2005. MGMT Gene Silencing and Benefit from Temozolomide in Glioblastoma. New England Journal of Medicine. 352 (10), 997-1003.

Hu, J.U.N., Wang, J., Wang, G., Yao, Z., Dang, X. 2016. Pharmacokinetics and antitumor efficacy of DSPE-PEG2000 polymeric liposomes loaded with quercetin and temozolomide: Analysis of their effectiveness in enhancing the chemosensitization of drug-resistant glioma cells. International Journal of Molecular Medicine. 37 (3), 690-702.

Huang, G., Zhang, N., Bi, X., Dou, M. 2008. Solid lipid nanoparticles of temozolomide: potential reduction of cardial and nephric toxicity. Int J Pharm. 355 (1-2), 314-320.

Hwang, T.-L., Aljuffali, I.A., Hung, C.-F., Chen, C.-H., Fang, J.-Y. 2015. The impact of cationic solid lipid nanoparticles on human neutrophil activation and formation of neutrophil extracellular traps (NETs). Chemico-Biological Interactions. 235 106-114.

Irani, M., Mir Mohamad Sadeghi, G., Haririan, I. 2017. Gold coated poly (ε-caprolactonediol) based polyurethane nanofibers for controlled release of temozolomide. Biomedicine & Pharmacotherapy. 88 667-676.

Irani, M., Mir Mohamad Sadeghi, G., Haririan, I. 2017. A novel biocompatible drug delivery system of chitosan/temozolomide nanoparticles loaded PCL-PU nanofibers for sustained delivery of temozolomide. International Journal of Biological Macromolecules. 97 744-751.

Irani, M., Sadeghi, G.M.M., Haririan, I. 2017. The sustained delivery of temozolomide from electrospun PCL-Diol-b-PU/gold nanocompsite nanofibers to treat glioblastoma tumors. Materials Science and Engineering: C. 75 165-174.

Jacinto, F.V., Esteller, M. 2007. MGMT hypermethylation: A prognostic foe, a predictive friend. DNA Repair. 6 (8), 1155-1160.

Jain, A., Chasoo, G., Singh, S.K., Saxena, A.K., Jain, S.K. 2011. Transferrin-appended PEGylated nanoparticles for temozolomide delivery to brain: in vitro characterisation. Journal of Microencapsulation. 28 (1), 21-28.

Jain, A., Jain, S.K. 2013. Formulation and optimization of temozolomide nanoparticles by 3 factor 2 level factorial design. Biomatter. 3 (2), e25102.

Jain, A., Singhai, P., Gurnany, E., Updhayay, S., Mody, N. 2013. Transferrin-tailored solid lipid nanoparticles as vectors for site-specific delivery of temozolomide to brain. Journal of Nanoparticle Research. 15 (3), 1-9.

Jain, D.S., Athawale, R.B., Bajaj, A.N., Shrikhande, S.S., Goel, P.N., Nikam, Y., Gude, R.P. 2013. Poly lactic acid (PLA) nanoparticles sustain the cytotoxic action of temozolomide in C6 Glioma cells. Biomedicine & Aging Pathology. 3 (4), 201-208.

Jain, D.S., Athawale, R.B., Bajaj, A.N., Shrikhande, S.S., Goel, P.N., Nikam, Y., Gude, R.P. 2014. Unraveling the cytotoxic potential of Temozolomide loaded into PLGA nanoparticles. DARU Journal of Pharmaceutical Sciences. 22 (1), 18-18.

Jain, K.K. 2012. Nanobiotechnology-based strategies for crossing the blood-brain barrier. Nanomedicine. 7 (8), 1225-1233.

Johannessen, T.-C.A., Bjerkvig, R. 2012. Molecular mechanisms of temozolomide resistance in glioblastoma multiforme. Expert Review of Anticancer Therapy. 12 (5), 635-642.

Kaina, B., Margison, G.P., Christmann, M. 2010. Targeting O6-methylguanine-DNA methyltransferase with specific inhibitors as a strategy in cancer therapy. Cellular and Molecular Life Sciences. 67 (21), 3663-3681.

Kanzawa, T., Bedwell, J., Kondo, Y., Kondo, S., Germano, I.M. 2003. Inhibition of DNA repair for sensitizing resistant glioma cells to temozolomide. Journal of neurosurgery. 99 (6), 1047-1052.

Khan, A., Aqil, M., Imam, S.S., Ahad, A., Sultana, Y., Ali, A., Khan, K. 2018. Temozolomide loaded nano lipid based chitosan hydrogel for nose to brain delivery: Characterization, nasal absorption, histopathology and cell line study. International Journal of Biological Macromolecules. 116 1260-1267.

Kim, S.-S., Rait, A., Kim, E., DeMarco, J., Pirollo, K.F., Chang, E.H. 2015. Encapsulation of temozolomide in a tumor-targeting nanocomplex enhances anti-cancer efficacy and reduces toxicity in a mouse model of glioblastoma. Cancer Letters. 369 (1), 250-258.

Knudsen, K.B., Northeved, H., Ek, P.K., Permin, A., Andresen, T.L., Larsen, S., Wegener, K.M., Lam, H.R., Lykkesfeldt, J. 2014. Differential toxicological response to positively and negatively charged nanoparticles in the rat brain. Nanotoxicology. 8 (7), 764-774.

Knudsen, K.B., Northeved, H., Kumar Ek, P., Permin, A., Gjetting, T., Andresen, T.L., Larsen, S., Wegener, K.M., Lykkesfeldt, J., Jantzen, K., Loft, S., Møller, P., Roursgaard, M. 2015. In vivo toxicity of cationic micelles and liposomes. Nanomedicine: Nanotechnology, Biology and Medicine. 11 (2), 467-477.

Krol, S. 2012. Challenges in drug delivery to the brain: Nature is against us. Journal of Controlled Release. 164 (2), 145-155.

Lange, A., Prenzler, A., Frank, M., Kirstein, M., Vogel, A., von der Schulenburg, J.M. 2014. A systematic review of cost-effectiveness of monoclonal antibodies for metastatic colorectal cancer. European Journal of Cancer. 50 (1), 40-49.

Lee, H.J., Engelhardt, B., Lesley, J., Bickel, U., Pardridge, W.M. 2000. Targeting Rat Anti-Mouse Transferrin Receptor Monoclonal Antibodies through Blood-Brain Barrier in Mouse. Journal of Pharmacology and Experimental Therapeutics. 292 (3), 1048.

Lefranc, F., Brotchi, J., Kiss, R. 2005. Possible Future Issues in the Treatment of Glioblastomas: Special Emphasis on Cell Migration and the Resistance of Migrating Glioblastoma Cells to Apoptosis. Journal of Clinical Oncology. 23 (10), 2411-2422.

Liebner, S., Czupalla, C.J., Wolburg, H. 2011. Current concepts of blood-brain barrier development. International Journal of Developmental Biology. 55 (4-5), 467-476.

Lin, C.-Y., Li, R.-J., Huang, C.-Y., Wei, K.-C., Chen, P.-Y. 2018. Controlled release of liposome-encapsulated temozolomide for brain tumour treatment by convection-enhanced delivery. Journal of Drug Targeting. 26 (4), 325-332.

Ling, Y., Wei, K., Zou, F., Zhong, S. 2012. Temozolomide loaded PLGA-based superparamagnetic nanoparticles for magnetic resonance imaging and treatment of malignant glioma. International Journal of Pharmaceutics. 430 (1), 266-275.

Liu, Z., Zhao, H., Shu, L., Zhang, Y., Okeke, C., Zhang, L., Li, J., Li, N. 2015. Preparation and evaluation of Baicalin-loaded cationic solid lipid nanoparticles conjugated with OX26 for improved delivery across the BBB. Drug Development and Industrial Pharmacy. 41 (3), 353-361.

Lockman, P.R., Koziara, J.M., Mumper, R.J., Allen, D.D. 2004. Nanoparticle Surface Charges Alter Blood–Brain Barrier Integrity and Permeability. Journal of Drug Targeting. 12 (9-10), 635-641.

Louis, D.N., Ohgaki, H., Wiestler, O.D., Cavenee, W.K., Burger, P.C., Jouvet, A., Scheithauer, B.W., Kleihues, P. 2007. The 2007 WHO Classification of Tumours of the Central Nervous System. Acta Neuropathologica. 114 (2), 97-109.

Loureiro, J., Andrade, S., Duarte, A., Neves, A., Queiroz, J., Nunes, C., Sevin, E., Fenart, L., Gosselet, F., Coelho, M., Pereira, M. 2017. Resveratrol and Grape Extract-loaded Solid Lipid Nanoparticles for the Treatment of Alzheimer's Disease. Molecules. 22 (2), 277.

Loureiro, J.A., Gomes, B., Coelho, M.A., Carmo Pereira, M.d., Rocha, S. 2014. Targeting nanoparticles across the blood-brain barrier with monoclonal antibodies. Nanomedicine. 9 (5), 709-722.

Loureiro, Joana A., Gomes, B., Coelho, M.A.N., Carmo Pereira, M.d., Rocha, S. 2014. Targeting nanoparticles across the blood–brain barrier with monoclonal antibodies. Nanomedicine. 9 (5), 709-722.

Loureiro, J.A., Gomes, B., Fricker, G., Coelho, M.A.N., Rocha, S., Pereira, M.C. 2016. Cellular uptake of PLGA nanoparticles targeted with anti-amyloid and anti-transferrin receptor antibodies for Alzheimer's disease treatment. Colloids and Surfaces B: Biointerfaces. 145 8-13.

Ma, J., Murphy, M., O'Dwyer, P.J., Berman, E., Reed, K., Gallo, J.M. 2002. Biochemical changes associated with a multidrug-resistant phenotype of a human glioma cell line with temozolomide-acquired resistance. Biochemical Pharmacology. 63 (7), 1219-1228.

Maiti, P., Hall, T.C., Paladugu, L., Kolli, N., Learman, C., Rossignol, J., Dunbar, G.L. 2016. A comparative study of dietary curcumin, nanocurcumin, and other classical amyloid-binding dyes for labeling and imaging of amyloid plaques in brain tissue of 5×-familial Alzheimer's disease mice. Histochemistry and Cell Biology. 146 (5), 609-625.

Makadia, H.K., Siegel, S.J. 2011. Poly Lactic-co-Glycolic Acid (PLGA) as Biodegradable Controlled Drug Delivery Carrier. Polymers. 3 (3), 1377-1397.

Marchesi, F., Turriziani, M., Tortorelli, G., Avvisati, G., Torino, F., De Vecchis, L. 2007. Triazene compounds: Mechanism of action and related DNA repair systems. Pharmacological Research. 56 (4), 275-287.

Marchetti, C., Palaia, I., Giorgini, M., De Medici, C., Iadarola, R., Vertechy, L., Domenici, L., Di Donato, V., Tomao, F., Muzii, L., Benedetti Panici, P. 2014. Targeted drug delivery via folate receptors in recurrent ovarian cancer: a review. OncoTargets and therapy. 7 1223-1236.

Masserini, M. 2013. Nanoparticles for Brain Drug Delivery. ISRN Biochemistry. 2013 18.

McLendon, R., Friedman, A., Bigner, D., Van Meir, E.G., Brat, D.J., Mastrogianakis, G.M., Olson, J.J., Mikkelsen, T., Lehman, N., Aldape, K. 2008. Comprehensive genomic characterization defines human glioblastoma genes and core pathways. Nature. 455 (7216), 1061-1068.

Mehta, A.M., Sonabend, A.M., Bruce, J.N. 2017. Convection-Enhanced Delivery. Neurotherapeutics. 14 (2), 358-371.

Monsalve, Y., Tosi, G., Ruozi, B., Belletti, D., Vilella, A., Zoli, M., Vandelli, M.A., Forni, F., López, B.L., Sierra, L. 2015. PEG-g-chitosan nanoparticles functionalized with the monoclonal antibody OX26 for brain drug targeting. Nanomedicine. 10 (11), 1735-1750.

Morais, L.C., Queiroz, V.C.J., Cavalcante, J.E.S., Matozinho, H.H.S., Silva, F.H.R., Costa, M.G.P., Pereira I, F.Y., Tavares, L.C.P., Guimarães, G.M. 2015. Treatment and prognosis of glioblastoma multiforme: a literature review. Journal of the Neurological Sciences. 357 e183.

Moriyama, T., Kakiuchi, D., Grasso, L., Hutto, D.L., Fernando, D., Schweizer, C. 2018. Farletuzumab, a monoclonal antibody directed against folate receptor alpha, shows no evidence of teratogenicity in cynomolgus monkeys. Reproductive Toxicology. 79 89-95.

Mujokoro, B., Adabi, M., Sadroddiny, E., Adabi, M., Khosravani, M. 2016. Nano-structures mediated co-delivery of therapeutic agents for glioblastoma treatment: A review. Materials Science and Engineering: C. 69 1092-1102.

Mukherjee, S., Ray, S., Thakur, R.S. 2009. Solid Lipid Nanoparticles: A Modern Formulation Approach in Drug Delivery System. Indian Journal of Pharmaceutical Sciences. 71 (4), 349-358.

Nagasawa, D.T., Chow, F., Yew, A., Kim, W., Cremer, N., Yang, I. 2012. Temozolomide and Other Potential Agents for the Treatment of Glioblastoma Multiforme. Neurosurgery Clinics of North America. 23 (2), 307-322.

Nifontov, V.I., Bel'skaya, N.P., Shtokareva, E.A. 1994. The reactivity and mechanism of action of triazenes (review). Pharmaceutical Chemistry Journal. 28 (10), 687-706.

Nordling-David, M.M., Yaffe, R., Guez, D., Meirow, H., Last, D., Grad, E., Salomon, S., Sharabi, S., Levi-Kalisman, Y., Golomb, G., Mardor, Y. 2017. Liposomal temozolomide drug delivery using convection enhanced delivery. Journal of Controlled Release. 261 138-146.

Panyam, J., Labhasetwar, V. 2003. Biodegradable nanoparticles for drug and gene delivery to cells and tissue. Advanced drug delivery reviews. 55 (3), 329-347.

Pardridge, W.M. 2015. Blood–brain barrier drug delivery of IgG fusion proteins with a transferrin receptor monoclonal antibody. Expert Opinion on Drug Delivery. 12 (2), 207-222.

Pardridge, W.M. 2012. Drug transport across the blood–brain barrier. Journal of Cerebral Blood Flow & Metabolism. 32 (11), 1959-1972.

Pardridge, W.M., Eisenberg, J., Yang, J. 1987. Human blood-brain barrier transferrin receptor. Metabolism. 36 (9), 892-895.

Parhi, P., Mohanty, C., Sahoo, S.K. 2012. Nanotechnology-based combinational drug delivery: an emerging approach for cancer therapy. Drug discovery today. 17 (17-18), 1044-1052.

Patel, B.K.P.R.H. 2016. Formulation development and evaluation of temozolomide loaded hydrogenated soya phosphatidylcholine liposomes for the treatment of brain cancer. Asian Journal of Pharmaceutical and Clinical Research. 9 (3), -5.

Patil, R., Portilla-Arias, J., Ding, H., Inoue, S., Konda, B., Hu, J., Wawrowsky, K.A., Shin, P.K., Black, K.L., Holler, E., Ljubimova, J.Y. 2010. Temozolomide delivery to tumor cells by a multifunctional nano vehicle based on poly(beta-L-malic acid). Pharmaceutical research. 27 (11), 2317-2329.

Poonia, N., Kharb, R., Lather, V., Pandita, D. 2016. Nanostructured lipid carriers: versatile oral delivery vehicle. Future Science OA. 2 (3), FSO135.

Pourgholi, F., hajivalili, M., Farhad, J.-N., Kafil, H.S., Yousefi, M. 2016. Nanoparticles: Novel vehicles in treatment of Glioblastoma. Biomedicine & Pharmacotherapy. 77 98-107.

Quinn, J.A., Jiang, S.X., Reardon, D.A., Desjardins, A., Vredenburgh, J.J., Rich, J.N., Gururangan, S., Friedman, A.H., Bigner, D.D., Sampson, J.H., McLendon, R.E., Herndon, J.E., 2nd, Walker, A., Friedman, H.S. 2009. Phase II trial of temozolomide plus o6-benzylguanine in adults with recurrent, temozolomide-resistant malignant glioma. Journal of clinical oncology : official journal of the American Society of Clinical Oncology. 27 (8), 1262-1267.

Ramalho, M.J., Coelho, M.A.N., Pereira, M.C. 2018. Chapter 18 - Nanocarriers for the delivery of temozolomide in the treatment of glioblastoma: A review, in: A.M. Grumezescu (Ed.) Design and Development of New Nanocarriers, William Andrew Publishing, pp. 687-722.

Ramalho, M.J., Pereira, M.C. 2016. Preparation and Characterization of Polymeric Nanoparticles: An Interdisciplinary Experiment. Journal of Chemical Education. 93 (8), 1446-1451.

Ramalho, M.J., Sevin, E., Gosselet, F., Lima, J., Coelho, M.A.N., Loureiro, J.A., Pereira, M.C. 2018. Receptor-mediated PLGA nanoparticles for glioblastoma multiforme treatment. International Journal of Pharmaceutics. 545 (1), 84-92.

Rønning, P.A., Helseth, E., Meling, T.R., Johannesen, T.B. 2012. A population-based study on the effect of temozolomide in the treatment of glioblastoma multiforme. Neuro-Oncology.

Rosenberg, G.A. 2012. Neurological diseases in relation to the blood–brain barrier. Journal of Cerebral Blood Flow & Metabolism. 32 (7), 1139-1151.

S. Srivenugopal, K., Rawat, A., K. Niture, S., Paranjpe, A., Velu, C., N. Venugopal, S., Rao Madala, H., Basak, D., R. Punganuru, S. 2016. Posttranslational Regulation of O6-Methylguanine-DNA Methyltransferase (MGMT) and New Opportunities for Treatment of Brain Cancers. Mini Reviews in Medicinal Chemistry. 16 (6), 455-464.

Salvati, E., Re, F., Sesana, S., Cambianica, I., Sancini, G., Masserini, M., Gregori, M. 2013. Liposomes functionalized to overcome the blood-brain barrier and to target amyloid-β peptide: the chemical design affects the permeability across an in vitro model. International journal of nanomedicine. 8 1749-1758.

Semete, B., Booysen, L., Lemmer, Y., Kalombo, L., Katata, L., Verschoor, J., Swai, H.S. 2010. In vivo evaluation of the biodistribution and safety of PLGA nanoparticles as drug delivery systems. Nanomedicine : nanotechnology, biology, and medicine. 6 (5), 662-671.
Shang, L., Nienhaus, K., Nienhaus, G.U. 2014. Engineered nanoparticles interacting with cells: size matters. Journal of Nanobiotechnology. 12 (1), 5.
Singh, G., Kaur, T., Kaur, R., Kaur, A. 2014. Recent biomedical applications and patents on biodegradable polymer-PLGA. International Journal of Pharmacology and Pharmaceutical Sciences. 1 30-42.
Soda, Y., Myskiw, C., Rommel, A., Verma, I.M. 2013. Mechanisms of neovascularization and resistance to anti-angiogenic therapies in glioblastoma multiforme. Journal of Molecular Medicine. 91 (4), 439-448.
Song, S., Mao, G., Du, J., Zhu, X. 2016. Novel RGD containing, temozolomide-loading nanostructured lipid carriers for glioblastoma multiforme chemotherapy. Drug Delivery. 23 (4), 1404-1408.
Steichen, S.D., Caldorera-Moore, M., Peppas, N.A. 2013. A review of current nanoparticle and targeting moieties for the delivery of cancer therapeutics. European Journal of Pharmaceutical Sciences. 48 (3), 416-427.
Stevens, M.F.G., Hickman, J.A., Stone, R., Gibson, N.W., Baig, G.U., Lunt, E., Newton, C.G. 1984. Antitumour imidazotetrazines. 1. Synthesis and chemistry of 8-carbamoyl-3-(2-chloroethyl)imidazo[5,1-d]-1,2,3,5-tetrazin-4(3H)-one, a novel broad-spectrum antitumor agent. Journal of Medicinal Chemistry. 27 (2), 196-201.
Stupp, R., Gander, M., Leyvraz, S., Newlands, E. 2001. Current and future developments in the use of temozolomide for the treatment of brain tumours. The Lancet Oncology. 2 (9), 552-560.
Stupp , R., Mason , W.P., van den Bent , M.J., Weller , M., Fisher , B., Taphoorn , M.J.B., Belanger , K., Brandes , A.A., Marosi , C., Bogdahn , U., Curschmann , J., Janzer , R.C., Ludwin , S.K., Gorlia , T., Allgeier , A., Lacombe , D., Cairncross , J.G., Eisenhauer , E., Mirimanoff , R.O. 2005. Radiotherapy plus Concomitant and Adjuvant Temozolomide for Glioblastoma. New England Journal of Medicine. 352 (10), 987-996.
Stupp, R., van den Bent, M.J., Hegi, M.E. 2005. Optimal role of temozolomide in the treatment of malignant gliomas. Current Neurology and Neuroscience Reports. 5 (3), 198-206.
Subas, C.D., Gurudutta, P. 2013. Nanobiotechnology-based Drug Delivery in Brain Targeting. Current Pharmaceutical Biotechnology. 14 (15), 1264-1274.
Sun, T., Wu, H., Li, Y., Huang, Y., Yao, L., Chen, X., Han, X., Zhou, Y., Du, Z. 2017. Targeting transferrin receptor delivery of temozolomide for a potential glioma stem cell-mediated therapy. Oncotarget. 8 (43), 74451-74465.
Szebeni, J., Baranyi, L., Savay, S., Milosevits, J., Bunger, R., Laverman, P., Metselaar, J.M., Storm, G., Chanan-Khan, A., Liebes, L., Muggia, F.M., Cohen, R., Barenholz, Y., Alving, C.R. 2002. ROLE OF COMPLEMENT ACTIVATION IN HYPERSENSITIVITY REACTIONS TO DOXIL AND HYNIC PEG LIPOSOMES: EXPERIMENTAL AND CLINICAL STUDIES. Journal of Liposome Research. 12 (1-2), 165-172.
Tapeinos, C., Battaglini, M., Ciofani, G. 2017. Advances in the design of solid lipid nanoparticles and nanostructured lipid carriers for targeting brain diseases. Journal of Controlled Release. 264 306-332.
Thon, N., Kreth, S., Kreth, F.-W. 2013. Personalized treatment strategies in glioblastoma: MGMT promoter methylation status. OncoTargets and therapy. 6 1363-1372.

Toda, Y., Takata, K., Nakagawa, Y., Kawakami, H., Fujioka, S., Kobayashi, K., Hattori, Y., Kitamura, Y., Akaji, K., Ashihara, E. 2015. Effective internalization of U251-MG-secreted exosomes into cancer cells and characterization of their lipid components. Biochemical and Biophysical Research Communications. 456 (3), 768-773.

Torchilin, V. 2012. Liposomes in Drug Delivery, in: J. Siepmann, R.A. Siegel, M.J. Rathbone (Eds.), Fundamentals and Applications of Controlled Release Drug Delivery, Springer US, pp. 289-328.

van Rooy, I., Mastrobattista, E., Storm, G., Hennink, W.E., Schiffelers, R.M. 2011. Comparison of five different targeting ligands to enhance accumulation of liposomes into the brain. Journal of Controlled Release. 150 (1), 30-36.

van Tellingen, O., Yetkin-Arik, B., de Gooijer, M.C., Wesseling, P., Wurdinger, T., de Vries, H.E. 2015. Overcoming the blood–brain tumor barrier for effective glioblastoma treatment. Drug Resistance Updates. 19 1-12.

Vasir, J.K., Labhasetwar, V. 2007. Biodegradable nanoparticles for cytosolic delivery of therapeutics. Advanced drug delivery reviews. 59 (8), 718-728.

Vehlow, A., Cordes, N. 2013. Invasion as target for therapy of glioblastoma multiforme. Biochimica et Biophysica Acta (BBA) - Reviews on Cancer. 1836 (2), 236-244.

Verbeek, B., Southgate, T.D., Gilham, D.E., Margison, G.P. 2008. O6-Methylguanine-DNA methyltransferase inactivation and chemotherapy. British Medical Bulletin. 85 (1), 17-33.

Vogelbaum, M.A., Aghi, M.K. 2015. Convection-enhanced delivery for the treatment of glioblastoma. Neuro-Oncology. 17 (suppl_2), ii3-ii8.

W.H.O. 2016. World health statistics 2016: Monitoring health for the SDGs, sustainable development goals, WHO Press: World Health Organization, Geneva.

Wang, M., Thanou, M. 2010. Targeting nanoparticles to cancer. Pharmacological research : the official journal of the Italian Pharmacological Society. 62 (2), 90-99.

Warren, K.E., Aikin, A.A., Libucha, M., Widemann, B.C., Fox, E., Packer, R.J., Balis, F.M. 2005. Phase I Study of O6-Benzylguanine and Temozolomide Administered Daily for 5 Days to Pediatric Patients With Solid Tumors. Journal of Clinical Oncology. 23 (30), 7646-7653.

Warren, K.E., Gururangan, S., Geyer, J.R., McLendon, R.E., Poussaint, T.Y., Wallace, D., Balis, F.M., Berg, S.L., Packer, R.J., Goldman, S., Minturn, J.E., Pollack, I.F., Boyett, J.M., Kun, L.E. 2012. A phase II study of O6-benzylguanine and temozolomide in pediatric patients with recurrent or progressive high-grade gliomas and brainstem gliomas: a Pediatric Brain Tumor Consortium study. Journal of Neuro-Oncology. 106 (3), 643-649.

Wen, P.Y., Kesari, S. 2008. Malignant Gliomas in Adults. New England Journal of Medicine. 359 (5), 492-507.

Wesolowski, J.R., Rajdev, P., Mukherji, S.K. 2010. Temozolomide (Temodar). American Journal of Neuroradiology. 31 (8), 1383-1384.

Wickström, M., Dyberg, C., Milosevic, J., Einvik, C., Calero, R., Sveinbjörnsson, B., Sandén, E., Darabi, A., Siesjö, P., Kool, M., Kogner, P., Baryawno, N., Johnsen, J.I. 2015. Wnt/β-catenin pathway regulates MGMT gene expression in cancer and inhibition of Wnt signalling prevents chemoresistance. Nature Communications. 6 8904.

Wohlfart, S., Gelperina, S., Kreuter, J. 2012. Transport of drugs across the blood–brain barrier by nanoparticles. Journal of Controlled Release. 161 (2), 264-273.

Wu, D., Yang, J., Pardridge, W.M. 1997. Drug targeting of a peptide radiopharmaceutical through the primate blood-brain barrier in vivo with a monoclonal antibody to the human insulin receptor. The Journal of Clinical Investigation. 100 (7), 1804-1812.

Wu, M., Fan, Y., Lv, S., Xiao, B., Ye, M., Zhu, X. 2015. Vincristine and temozolomide combined chemotherapy for the treatment of glioma: a comparison of solid lipid nanoparticles and nanostructured lipid carriers for dual drugs delivery. Drug Delivery. 1-6.

Xin, Y., Huang, Q., Tang, J.-Q., Hou, X.-Y., Zhang, P., Zhang, L.Z., Jiang, G. 2016. Nanoscale drug delivery for targeted chemotherapy. Cancer Letters. 379 (1), 24-31.

Xu, Y., Shen, M., Li, Y., Sun, Y., Teng, Y., Wang, Y., Duan, Y. 2016. The synergic antitumor effects of paclitaxel and temozolomide co-loaded in mPEG-PLGA nanoparticles on glioblastoma cells. Oncotarget. 7 (15), 20890-20901.

Yan, X., Zhao, Y., Zhang, Y., Qu, H. 2017. Monoclonal Antibodies and Immunoassay for Medical Plant-Derived Natural Products: A Review. Molecules. 22 (3).

Yang, L.-J., Zhou, C.-F.U., Lin, Z.-X. 2014. Temozolomide and Radiotherapy for Newly Diagnosed Glioblastoma Multiforme: A Systematic Review. Cancer Investigation. 32 (2), 31-36.

Yeagle, P.L. 2016. The membranes of cells, Academic Press.

Yingchoncharoen, P., Kalinowski, D.S., Richardson, D.R. 2016. Lipid-Based Drug Delivery Systems in Cancer Therapy: What Is Available and What Is Yet to Come. Pharmacological Reviews. 68 (3), 701-787.

Yoshino, A., Ogino, A., Yachi, K., Ohta, T., Fukushima, T., Watanabe, T., Katayama, Y., Okamoto, Y., Naruse, N., Sano, E. 2010. Gene expression profiling predicts response to temozolomide in malignant gliomas. International journal of oncology. 36 (6), 1367.

Yu, J., Zhang, H., Li, Y., Sun, S., Gao, J., Zhong, Y., Sun, D., Zhang, G. 2017. Metabolomics revealed the toxicity of cationic liposomes in HepG2 cells using UHPLC-Q-TOF/MS and multivariate data analysis. Biomedical Chromatography. 31 (12), e4036.

Chapter 3 - Interactions of temozolomide and its active metabolite with membrane biomimetic models

3.1 Introduction

The ability of drugs to interact with the biological barriers and membranes influences their pharmacological activity. The bioavailability of a drug in the target tissue depends on these interactions that regulate transport across biological barriers and uptake in the target cells. In fact, TMZ like also several other drugs with great therapeutic potential fail to be effective *in vivo* due to their low bioavailability in the target tissues (Lucio et al., 2010). So, understanding the interaction of TMZ with biological membranes is essential. Since complete and irreversible conversion of TMZ into MTIC occurs after 2 hours of administration (Lopes et al., 2013), it is crucial to evaluate the interactions with membranes of the active metabolite. However, no studies concerning the interaction of TMZ metabolites with biological membranes have been reported so far.

Since lipids are the major components of cellular membranes, is essential to study the interaction of a drug with the lipid component of the membranes. Also, cellular membranes exhibit combinations of phospholipids, cholesterol and proteins organised in relatively ordered microdomains known as lipid rafts. These lipid rafts regulate several cellular processes and signalling and trafficking pathways by acting as assembly centres of signalling molecules. Lipid rafts are exhibit a more ordered and tightly packing than the surrounding bilayer (Sezgin et al., 2017). Although drugs bind to the proteins of the membranes, the lipid phase plays also a major role. When drugs cross or bind to lipid membranes, they can modify the physical properties of membranes as the lipid conformation, viscosity and surface charge. Some drugs can induce structural modifications in the lipid phase causing structural defects and consequently, disturbing the membrane functions. On the other hand, membranes can induce changes in the properties of the drugs and also several intrinsic physicochemical properties of a drug can hamper their penetration into the cell membranes (Lucio et al., 2010). Despite that, drug-membrane interactions are frequently neglected.

Therefore, the study of cellular lipids and their interaction with drugs is essential to assess therapeutic efficiency. Lipidic biomimetic models are a suitable tool to study the membrane properties and its interaction with drugs. These models can mimic the cell membranes in physiological conditions. Different biomimetic models can be used such as lipid monolayers, lipid vesicles and lipid bilayers. Lipid bilayers, such as liposomes, are the ones that best mimic the entire lipidic assembly of cellular membranes (Lucio, et al., 2010).

Liposomes as biomembrane models present some advantages over classical computational methods, mainly in the determination of the drug partition coefficient (*Kp*). The interaction between a drug and a lipid membrane is mainly regulated by the lipophilic/hydrophilic properties of the drug. *Kp* is an important indicator of lipophilicity and is essential to understand the pharmacokinetic and pharmacodynamic characteristics of a drug. This parameter allows predicting and understand the passive diffusion processes that occur in biological membranes that affect the absorption, distribution, metabolism, and elimination of drugs and can be associated with their toxic and/or therapeutic activity (Nunes et al., 2011). Some computational methods can be used predict this coefficient (Bannan et al., 2016; Kujawski et al., 2012). However, using liposomes as *in vitro* membrane models allows to evaluate the lipophilicity of a drug, in a more efficient manner than the existent computational models and the classic two-phase octanol/water system, since it acknowledges the electrostatic interactions and ion-dipole forces between the drug and the membrane phospholipids that regulate several phenomena such the transport of macromolecules across membranes and barriers. Other different biophysical parameters can also be evaluated using liposomes as biomimetic models such as the drug's location within the membrane model, and its effect on the fluidity of the membrane (Loureiro et al., 2018). Depending on the physicochemical properties of the drugs, they can interact with phospholipids more closely to the polar head groups or align between the hydrophobic tails.

In this study liposomes were used as membrane models. The design of the chosen model was based on the composition of the biological cell membranes. The 1,2-dimyristoyl-sn-glycero-3-phosphocholine (DMPC) is a zwitterionic phospholipid and was chosen for this work, since neutral phosphatidylcholine (PC) was identified as the lipid component in higher amount in eukaryotic cell membranes, as the membrane of GBM cells (Toda et al., 2015) and in brain capillary endothelial cells (Benistant et al., 1995). Thus, a system of liposomes composed of DMPC phospholipids is proposed. The influence of the addition of cholesterol molecules to the model was studies, since this is reported as a major component of cellular membranes accounting for up to 20% of lipid content in healthy and GBM cells (Benistant, et al., 1995; Toda, et al., 2015). For that, DMPC:chol vesicles were also prepared.

Thus, the main goal of this chapter was to study the molecular interactions between the active metabolite – MTIC - and mimetic biomembrane model composed of DMPC and cholesterol, focusing in the lipidic components of the membrane. Since TMZ is a pro-drug and at physiologic pH is rapidly and irreversible hydrolysed into its the active form MTIC, MTIC-membrane interactions were studied. Thus, this chapter describes the implementation of a membrane model and the study of its interactions with MTIC. TMZ was used for comparison. Different biophysical parameters were evaluated such as the partition of the drug metabolites into the lipid bilayers, their location within the membrane model and its effect on the fluidity of the membrane.

3.2 Materials and Methods

3.2.1 Materials

1,2-dimyristoyl-sn-glycero-3-phosphocholine (DMPC, MW 677.9) and cholesterol (MW 386.65) were acquired from Avanti polar lipids (Alabama, USA). 1,6-diphenyl-1,3,5-1,3,5-hexatriene (DPH, MW 232.32) and N, N, N-Trimethyl-4-(6-

phenyl-1,3,5-hexatrien-1-yl) phenyl ammonium p-toluenesulfonate (TMA-DPH, MW 461.60), phosphate buffered saline (PBS), chloroform and methanol were acquired from Sigma-Aldrich (Germany).

TMZ (MW 194.15, purity ≥ 99%) was obtained from Selleck Chemicals (Munich, Germany). TMZ was dissolved in PBS (0.01 M, pH 7.4) for total conversion to MTIC (MW 182.18) and stored at room temperature. For the preparation of TMZ solution, the drug was dissolved in PBS (0.01 M, pH 5.5) and stored at room temperature. Acidic PBS was used to ensure that TMZ does not undergoes hydrolysis into conversion to MTIC.

All PBS solutions were prepared using filtered and deionized ultrapure water (Milli-Q Academic, Millipore, France).

3.2.2 Preparation of *in vitro* membrane models

Phospholipid vesicles, also known as liposomes, were used as *in vitro* models for biological membranes and were prepared using the lipid film hydration method. This is one of most commonly used methods for liposome preparation and it is the simplest method of vesicle formation. Vesicles can be classified based on their size and number of bilayers. Regarding the later, vesicles can be unilamellar when exhibiting only a single phospholipid bilayer sphere enclosing the aqueous solution; or multilamellar (MLV), displaying several concentric bilayers. Unilamellar vesicles can be further classified into small unilamellar vesicles (SUV) or large unilamellar vesicles (LUV). Lipid film hydration yields MLVs, and the vesicles can be downsized by a variety of techniques, including sonication or extrusion (Akbarzadeh et al., 2013).

LUVs were prepared, one containing solely DMPC in its composition, and DMPC and cholesterol (molar ratio of 85:15), at a final lipid concentration of 5 mM. Briefly, a chloroform solution composed of DMPC or DMPC and cholesterol was poured into a test-tube, and a lipid film was formed by evaporating the chloroform through manual rotation under a nitrogen atmosphere. The dried lipid film was then hydrated with PBS buffer (0.01 M, pH 7.4). When hydrated, phospholipids spontaneously assemble into vesicles due to their amphiphilic nature, above a certain concentration, known as the critical micelle concentration (CMC). Phospholipids tend to assemble in vesicles in order to decrease the system free energy, by decreasing the water-contact of phospholipids hydrophobic tails (Lopes, 2013).

After hydration, the lipid film was peeled off completely through vigorous shaking in a vortex (Genius 3, ika®vortex, Germany) and ultrasounds in a sonicator bath (ultrasonic frequency of 45 kHz, Ultrasonic cleaner, VWRTM, Malasya) for 15 min, to produce MLVS. To obtain LUVs, MLVs were submitted to an extrusion procedure using different Nuclepore™ track-etched polycarbonate membranes (Maidstone, UK) with a specific pore size through an extruder pressurized with nitrogen gas (Thermobarrel Extruder, Lipex Biomembrane, B.C., Canada). All steps were performed above the lipids phase transition temperature, at 37 ^{o}C (Koynova and Caffrey, 1998), to ensure maximal membrane fluidity.

For fluorescence measurements, DPH and TMA-DPH were previously dissolved in a chloroform/methanol (volume ratio of 3:1) and added to the lipid mixture at a lipid/probe molar ratio of 100:1.

The LUVs prepared at pH 7.4 and 5.5 were stored at room temperature (RT).

3.2.3 Physicochemical characterization of the prepared biomembrane models

3.2.3.1 Dynamic light scattering for size determination

The mean diameter and size distribution of the prepared vesicles were evaluated by Dynamic Light Scattering (DLS). When a light irradiates a NPs' suspension, part of the incident light is scattered by the NP. If the NP isn't moving, the amount of scattered light is constant. However, in colloidal suspensions, the NPs are in constant movement due to Brownian motions. This leads to variations in the intensity of the scattered light. Thus, DLS technique allows to determine the average dimensions and size distribution of the NPs, by measuring the fluctuations of scattered light intensity as a function of time. The rate of variation of the scattered light is directly proportional to the movement of the NPs and can be related to their diffusion coefficient. As the diffusion of the NPs depends on the temperature, viscosity and NP size, and since the solvent and temperature are known and constant, it is possible to determine the NP size, using the Stokes-Einstein equation (Stetefeld et al., 2016):

$$R_H = \frac{kT}{6\pi\eta D} \tag{3.1}$$

where, R_H is the hydrodynamic radius; k, the Boltzmann constant; T, the temperature; η, the viscosity of the solvent; D, the diffusion coefficient.

The obtained size value is the hydrodynamic radius (HR). HR represents the size of a hypothetical sphere that moves the same way as the NP that is being measured, i.e. HR represents the NP and its solvation shell. Therefore, the determined HR values are slightly higher than the real radius of the NP (Hassan et al., 2015).

In addition to the size, DLS also allows the determination of the Polydispersity Index (PdI). PdI is an indicative of the heterogeneity of sizes of NPs in a suspension. For a near-monodisperse sample, a PDI of 0.1 or lower is expected. The presence of aggregates can distort the results, since the equipment analyse them as single particle of bigger size, resulting in higher PdIs. As these aggregates also scatter more light than the NP, these aggregates may mask the NP (Langevin et al., 2018).

The measurements were performed in a ZetaSizer Nano ZS (Malvern Instruments, UK). The attained data is given in intensity distribution. At least three independent measurements were performed.

3.2.3.2 Laser doppler velocimetry method for zeta potential determination

The zeta potential values of the prepared vesicles were determined by laser doppler velocimetry method. Zeta potential is a key indicator of the colloidal dispersion stability since it controls the electrostatic interactions between the NPs. While, NPs with high absolute zeta potential values will repel each other, preventing aggregation; in NPs with low absolute zeta potential values aggregation usually is observed (Kaszuba et al., 2010).

NPs in a colloidal suspension attract ions to their surface, originating a layer covering the surface of the NP, known as the Stern layer. A second layer outside the Stern layer is also formed, where ions diffuse more freely. This diffuse layer terminates the boundary of the particle as a single charged entity. Zeta potential is the electric potential that exists at this hypothetical boundary (Bhattacharjee, 2016).

When an electric field is applied to the NPs' suspension, electrophoresis occurs since charged particles of the sample are attracted to the electrode of opposite charge. While the sample undergoes electrophoresis, an emitting a beam hits the NPs, and the scattered light is detected by a photodetector. The light frequency shift is proportional to the velocity of the NPs, allowing the determination of the electrophoretic mobility (μ) using the following equation:

$$\mu = \frac{v}{E} \tag{3.2}$$

where, v is the velocity; and E, the applied electric field.

Then, the mobility the zeta potential values are obtained using the Smoluchowski equation (Wiersema et al., 1966):

$$\mu = \frac{\varepsilon\zeta}{4\pi\eta} \tag{3.3}$$

where, ζ, the zeta-potential; ε, the dielectric constant; and η, the viscosity coefficient.

The measurements were performed also using a ZetaSizer Nano ZS (Malvern Instruments, UK). The analysis was performed using the dielectric constant of water. At least three independent measurements were performed.

3.2.4 Determination of partition coefficient of TMZ and MTIC by derivative spectrophotometry

UV-Vis spectrophotometry is a largely used technique in analytical chemistry for the determination of the concentration of some substance in solution in an easy, practical and fast way. The radiation source focuses a light beam which travels through a path reaching the sample. In the sample part of the radiation is absorbed, and only some of it is transmitted through the sample reaching the detector. Thus, the amount of absorbed radiation is determined by the difference between the incident light and the light which effectively reaches the detector. This relationship is translated by the following equation (Siddiqui et al., 2017):

$$A = -log\left(\frac{I}{I_0}\right) \tag{3.4}$$

where A is the absorbance; I, the light that was through the sample and reached the detector; and I_0, the incident light.

In this experiment, derivative UV-Vis spectrophotometry was used to assess the K_p values of TMZ and MTIC between lipid vesicles and the aqueous medium avoiding phase separation. Changes in the absorbance properties of the drugs due to their partition from the aqueous medium to the lipid membrane were evaluated, and the second- or third-derivative was used to reduce background noise.

Several methodologies have been proposed for the determination of *Kp* values involving physical separation of the different phases. After drug partition and the equilibrium is reached, the phases are separated and the amount of drug in each phase is determined. Physical separation can be achieved by centrifugation, dialysis, chromatography or filtration. Besides being time-consuming, these separative methods yield results with low reproducibility. Therefore, methods that allow to measure drug partition without physical phase separation of the different phases offer an advantage. UV-vis spectrophotometry has gained relevance for *Kp* values determination, but derivative spectrophotometry offers an extra advantage since it allows to remove the background originated by the scattered light from the DMPC liposomes by the use of the second or third derivative, improving the signal resolution (Magalhães et al., 2010).

Both prepared models, DMPC and DMPC:chol LUvs were applied. TMZ and MTIC were dissolved in PBS with different pH values, 5.5 and 7.4 respectively, at a final concentration of 150 μM. Acidic PBS (pH 5.5) was used to prevent TMZ conversion into MTIC, and pH 7.4 to mimic physiological conditions for the active metabolite. The prepared solutions were then added to liposomes suspensions with lipidic concentrations ranging from 0 to 4000 μM, in a 96-well plate. Controls were prepared without addition of drugs. The samples were incubated at 37°C for 30 min with agitation, to allow the drugs to reach the partition equilibrium between the lipid and the water phases. The absorption spectra (200–360 nm range) of samples and control solutions were obtained at 37 ^{0}C to mimic physiological conditions (HT Microplate Spectrophotometer, BioTek). The attained data were treated as previously described (Magalhães, et al., 2010). Briefly, (i) the correspondent control spectrum is subtracted to each absorption spectrum to yield the corrected spectrum; (ii) the spectra of second and third derivative are obtained to improve the method's resolution since it allows to remove the interferences originated due to the light scattered by the LUVs; (iii) the most suitable wavelength value, where scattering is negligible, is chosen and its second or third derivative spectra versus LUVs concentration graph is obtained; and (iv) finally the K_p value is determined fitting a non-linear regression curve using the following equation:

$$D_T = D_W + \frac{(D_m - D_W)\, K_P\, [L]\, V_m}{1 + K_P\, [L]\, V_m} \tag{3.5}$$

with D representing the second or third derivative of the absorbance values of: the initial quantity drug (D_T), quantity of drug in the lipid phase (D_m), and in the aqueous phase (D_w), respectively. *[L]* refers to the lipid molar concentration and V_m to the lipid molar volume. The V_m values for DMPC and DMPC:Chol are 0.663 and 0.623 L mol^{-1}, respectively (Koenig et al., 1997; Koynova et al., 1996).

Predicted octanol/buffer partition coefficients for comparison were determined by the Marvin Sketch Calculator software (Chemaxon™).

3.2.5 Membrane location studies of TMZ and MTIC by fluorescence quenching

Steady-state fluorescence quenching studies were used to assess the preferential location of TMZ and MTIC within the membrane. When a molecule absorbs light, it is excited from the electronic ground state to an excited state. From there it can return to the ground state by releasing the absorbed energy in the form of heat and by radiation in the visible or near-infrared spectral range. The emitted light is called fluorescence. Quenching refers to any process that reduces the florescence intensity of a fluorophore, induced by molecular interactions with a molecule that acts as a quencher. Fluorescence quenching can occur by two main processes, collisional or dynamic quenching and static quenching as shown in figure 3.1. Static quenching occurs when a complex between the probe and the quencher is formed, and dynamic quenching occurs when the probe collides with the quencher. Either way, both quenching processes require close proximity between the quenching and the fluorophore molecules (Neves et al., 2016).

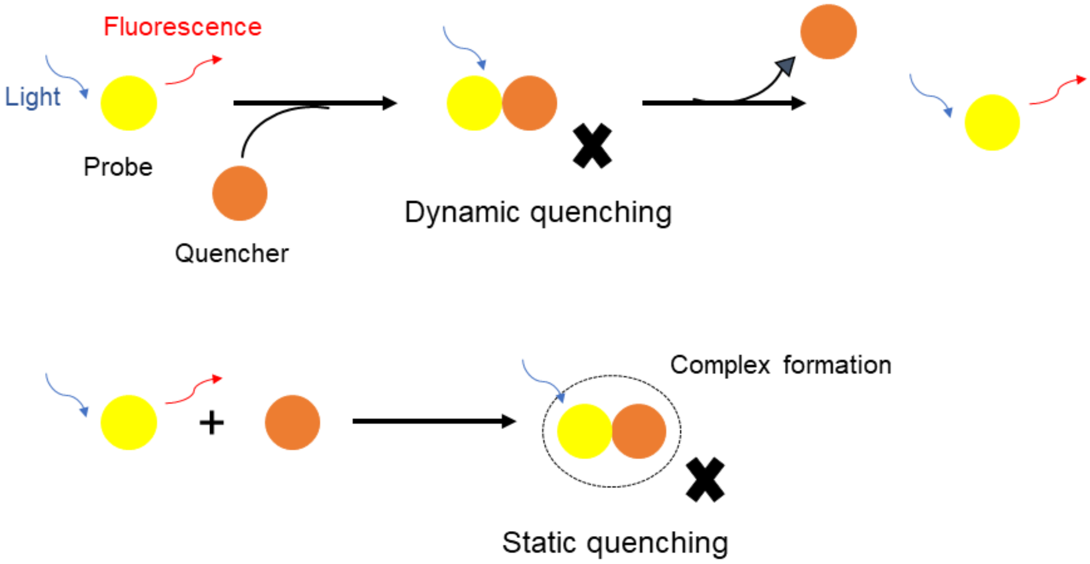

Figure 3. 1 | Schematic representation of dynamic and static quenching processes.

This method evaluates the accessibility of the drug molecules to the chosen probes, providing information on the location of the drug within the membrane. The Stern-Volmer constant (K_{SV}) is an important indicator of the quenching efficiency, since a higher proximity of the drugs to the probes decreases their fluorescence intensity, which yields a higher K_{SV} value (Štěpánek, 2016).

In this study, DMPC and DMPC:chol LUVs labelled with DPH or TMA-DPH fluorescence probes were used. These fluorescence probes have a well-known membrane position and depth allowing to easily identify the positions of drugs in the bilayer. DPH molecules are located deeply in the bilayer parallelly aligned to the phospholipids carbon chains, while TMA-DPH probe possesses a charged group and consequently is at the region of the polar head groups of the phospholipids closer to the lipid/water interface (figure 3.2) (Illinger et al., 1995; Kaiser and London, 1998; Wang et al., 1991).

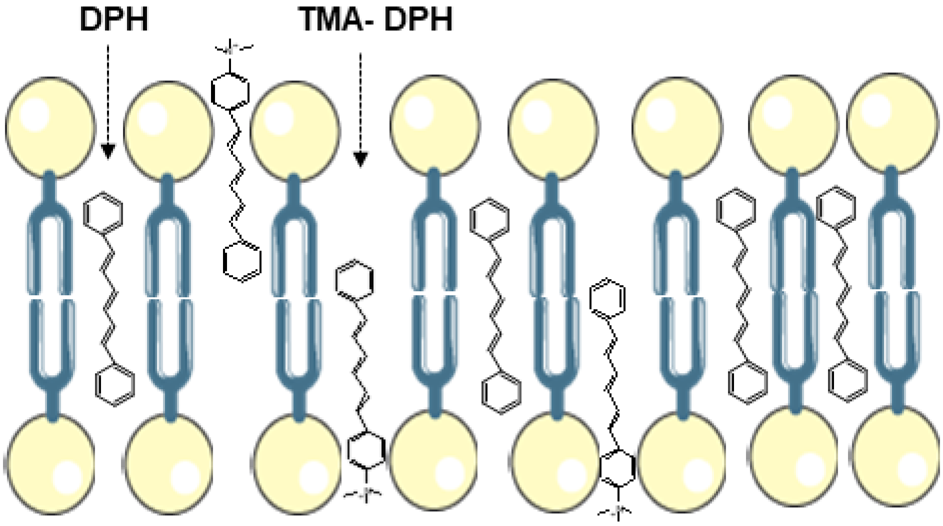

Figure 3. 2 | Schematic representation of the location of DPH and TMA-DPH fluorescent probes within the bilayer.

For the experiments, increasing concentrations of MTIC or TMZ (0 to 150 µM) were added to fluorescent-vesicles at a fixed concentration of 500 µM in PBS. TMZ and MTIC were dissolved in PBS with different pH values, 5.5 and 7.4 respectively. The samples were incubated in the dark at 37 ºC for 30 min with continuous agitation, to allow the drugs to reach the partition equilibrium between the lipid and the water phases. Measurements were then performed at 37 °C (microplate spectrophotometer, Thermo Scientific Varioskan Flash), at excitation/emission wavelengths of 357/427 nm and 361/427 nm for DPH and TMA-DPH, respectively (Lucio et al., 2007; Mosmuller et al., 1994). Attained data was plotted as obtained (I_0/I) versus the quencher concentration ($[Q]_m$), and the quenching ability of the molecules was determined by calculation of the K_{SV} values by fitting a linear regression model to the plot (Lúcio et al., 2009):

$$\frac{I_0}{I} = 1 + K_{SV}\,[\mathrm{Q}]_m \tag{3.6}$$

where, I and I_0 are the fluorescence intensities with and without the drug, respectively. Q_m is the drugs' concentration that is able to partition the membrane and is calculated using the equation below (Pinheiro et al., 2013):

$$[Q]_m = \frac{K_P\,[Q]_T}{(K_P\,\alpha_m) + (1 - \alpha_m)} \tag{3.7}$$

where α_m represents the volume fraction of the membrane phase ($\alpha_m = V_m/V_T$); Q_T is the used drug concentration; V_m and V_T are the volumes of the membrane and aqueous phases, respectively (Pinheiro, et al., 2013).

3.2.6 Determination of phase transition temperature of TMZ and MTIC by dynamic light scattering

DLS technique was also used to evaluate the effect of TMZ and MTIC on the fluidity of the biomembrane models. Interactions between a drug and the phospholipid vesicles can exert an effect on the membrane properties and physical state. The lipid bilayer can exhibit different conformations depending on its physical state. Therefore, the vesicles may present different lateral organization, molecular order, and mobility of the lipid molecules within the bilayer, depending on their phase behaviour. At different temperatures, the lipid bilayer can be in either a liquid–crystalline or a solid-gel phase. In the liquid phase, the phospholipids diffuse more freely due to a more disordered assembly. The lipid transition is influenced by the temperature, hydration, and lipid composition that also influence the arrangement and fluidity of membranes. The main phase transition temperature (T_m) is the temperature at which the phase transition between the solid-gel and the liquid disordered state occur. At this point, besides fluidity, also other biophysical properties of the phospholipid bilayers are drastically changed, as the viscosity, permeability, and mechanical strength (Jing et al., 2014).Since changes in the fluidity of the bilayers usually lead to variations in T_m, the effects of TMZ and MTIC molecules on the membrane fluidity were evaluated by assessment of changes in the T_m and cooperativity (B). The determination of these biophysical parameters was achieved by DLS measurements, by assessing the variation of the mean count rate (average number of photons detected per second) with variation of temperature. Changes in the count rate suggest the occurrence of a macroscopic alteration in the membrane. The measured variations in the scattering intensity occur due to changes in the optical features of the studied sample due to the gel-to-fluid phase transition or *vice versa* (Michel et al., 2006).

Briefly, DMPC or DMPC:chol vesicles (4000 µM) were incubated with TMZ or MTIC (150 µM) for 30 min at 37 ºC with continuous agitation, to allow the drugs to reach the partition equilibrium between the lipid and the water phases. TMZ and MTIC were dissolved in PBS with different pH values, 5.5 and 7.4 respectively. Samples were then analysed at a temperature interval ranging from 10.0 to 55.0 ºC (Zetasizer Nano ZS, Malvern Instruments, UK), and data were plotted as normalized count rate versus temperature and fitted with a non-linear regression using the following equation (Pinheiro et al., 2013):

$$y = A_1 + \frac{A_2 - A_1}{1 + 10^{B\left(\frac{1}{T} - \frac{1}{Tm}\right)}} \tag{3.8}$$

with A_1 representing initial count rate of lipids in phase 1 (y_{initial}); A_2 is the final count rate of lipids in phase 2 (y_{final}) and T is the temperature.

Measurements without addition of drugs were also conducted as control.

3.2.7 Statistical analysis

All results are presented as mean and standard deviation (SD), for at least three independent experiments. Statistical analysis was performed using Student's t-test, with a 95% confidence interval. Data with p-values below 0.05 were considered significant.

3.3 Results and Discussion

3.3.1 Physicochemical properties of the biomembrane models

LUVs were prepared as membrane models. These models may allow to understand the therapeutic efficiency of TMZ dependent on its bioavailability, but also to predict the drug's toxicity towards the cellular membranes. The physicochemical properties of the prepared vesicles were evaluated and are presented in table 3.1 and 3.2. The properties of the prepared vesicles depend on the features of the chosen lipid composition.

Table 3. 1 | Physicochemical features of the prepared LUVs. Results are presented as mean ± SD (n=3).

LUVs	pH	Mean size (nm)	PdI	Zeta Potential (mV)
DMCP	**7.4**	111 ± 10	0.08 ± 0.03	-0.5± 0.2
DMPC:Chol	**7.4**	117 ± 12	0.08 ± 0.01	-1.1± 1.3
DMCP	**5.5**	111 ± 8	0.06 ± 0.01	4.2 ± 1.7
DMPC:Chol	**5.5**	123 ± 7	0.11 ± 0.08	4.2 ± 0.4

DMPC phospholipid was used for the design of the membrane model with or without cholesterol. DMPC possesses two saturated hydrocarbon chains with 14 carbons in length, as shown in figure 3.3. Zwitterionic phospholipids, as DMPC, are characterized by polar but neutral head groups, constituted of one choline and one phosphate group. Choline is a quaternary amine group and it is always positively charged (Liu, 2016). Although the pKa of the phosphate group of DMPC embedded in a bilayer is not well-established, the first pKa of phosphate in water is 2.12 (Teixeira et al., 2014). So, at both studied pH values (5.5 and 7.4) the phosphate group is deprotonated, presenting a negative charge, yielding a neutral net charge of the polar head. However, low positive/negative values of zeta potential were obtained, as expected, due to the reorientation of the phospholipid polar heads (Makino and Shibata, 2006).

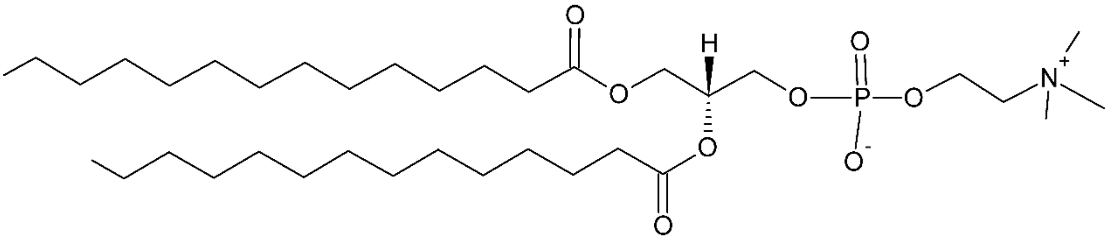

Figure 3. 3 | Schematic representation of DMPC structure (drawn in ACD/ChemSketch).

Although varying the pH from neutral to acidic did not alter the mean size and the PdI values of the LUVs (p>0.05), zeta potential values became less negative and changed sign from negative to positive. This may happened as consequence of the increased ionic strength, causing the phospholipids headgroups rotation due to changes in the direction of the dipoles (Makino and Shibata, 2006).

Changing the buffer pH did not affect the stability of the prepared DMPC and DMPC:chol LUVs, that proved to be stable at both 5.5 and 7.4 pH (table A.1, annex A). Also, cholesterol insertion on the bilayer did not show a significant influence on the studied physicochemical features of the prepared LUVs ($p>0.05$). The obtained PdI values suggest that all the LUVs prepared models are monodisperse (PdI ≤0.01).

3.3.2 Partition coefficient of TMZ and MTIC

Kp value is an important indicator of the lipophilicity of a drug, that is one of the most important parameters that influences drug biodistribution and pharmacokinetics (Loureiro, et al., 2018). Lipophilicity can also be expressed by the logarithm of the partition coefficient (log *P*) or distribution coefficient (log *D*) for ionized molecular species. *Kp* and log *D* values of TMZ and MTIC were determined in a mimetic biomembrane model by derivative spectrophotometry. For that, LUVs were used as model.

Figure 3.4 shows an example of the steps for the determination of *Kp* value for MTIC in DMPC vesicles. Figure 3.4.A shows the absorption spectra of MTIC with increasing concentrations of vesicles. The second- or third-derivative of experimental data was obtained (figure 3.4.B) allowing to eliminate the background of the light scattered by the lipids. The isosbestic points (arrows in figure 3.4.B) indicate that the residual background signal of lipids is eliminated by the use of the second derivative (Magalhães, et al., 2010). Thus, a wavelength corresponding to a maximum of the second derivative between these two points was chosen, in this case 296 nm. Then, the K_P value was obtained by fitting equation 3.4 to the experimental second-derivative spectrophotometric data (figure 3.4.D). The same steps were applied for the other models and for TMZ (figures A.1, A.2 and A.3 in annex A).

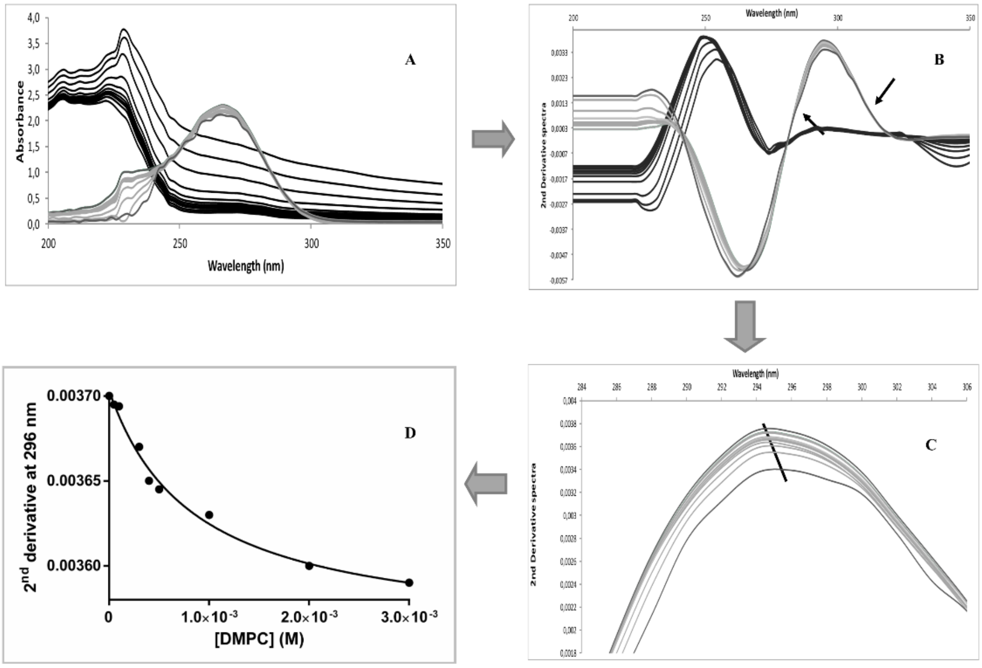

Figure 3. 4 | Illustration of the steps for *Kp* value determination. (A) Absorption spectrum and (B, C) second-derivative spectrum of MTIC at 150 µM incubated in DMPC vesicles at 37 °C (grey lines) and DMPC vesicles without drug (black lines) at increasing lipid concentrations. Black arrows point to isosbestic points, and black line indicates a bathochromic shift. (D) Non-linear regression fitting by equation 3.5 to experimental second-derivative spectrophotometric data at wavelength 296 nm where the scattering is eliminated.

In figure 3.4.C, a change of the spectral band position in the absorption spectrum of the drug with increasing lipid concentrations can be observed. This bathochromic shift occurs due to a decrease on the polarity of medium, which indicates that the drug molecules are partitioning from the polar aqueous phase to the non-polar DMPC vesicles (Loureiro, et al., 2018).

The calculated *Kp* and respective log *D* values are presented in table 3.2. Predicted octanol/buffer log *P* for comparison were determined using the Marvin Sketch Calculator software (Chemaxon™) (table 3.2). Pka values were also calculated using this software.

Table 3. 2| Partition coefficient (*Kp*) and distribution coefficient (log *D*) values of TMZ and MTIC between DMPC and DMPC:chol vesicles and the aqueous medium PBS. The aqueous medium is PBS at pH 5.5 or 7.4 for TMZ and MTIC, respectively. Data represented as mean ± SD (n=3).

Drug	**DMPC**		**DMPC:Chol**		
	K_P	**log *D***	K_P	**log *D***	**Theoretical log *P***
TMZ	3662 ± 127	3.56 ± 0.02	2527 ± 174	3.40 ± 0.03	0.36
MTIC	1772 ± 11	3.25 ± 0.03	890 ± 243	2.95 ± 0.12	-0.65

As observed in table 3.2 predicted log *P* values are significantly different from the calculated experimental log *D* values for both molecules. This occurs because the proposed liposomal models acknowledge the electrostatic interactions between the membrane phospholipids and the drug (Zhang et al., 2015), that the classic two-phase octanol/water system fail to account since it only considers the hydrophobic interactions between the studied compounds and octanol (Hermens Joop et al., 2013). However, other forces such as ion-dipole and electrostatic interactions play a major role in several membrane binding phenomena such as the transport of macromolecules across membranes and barriers (Do et al., 2017), and must be considered. From the calculated pKa value for MTIC (6.55 for nitrogen atom) it was predicted that the majority of the MTIC molecules are negatively charged at physiological pH, which indicates that not only hydrophobic interactions are causing the drug partition, but in fact MTIC-membrane interactions are mainly due to the electrostatic and ion-dipole forces between the negatively charged MTIC species and the polar heads of the phospholipids. While for TMZ neutral species are predominant at pH 5.5, but a small contribution of anionic species still exists (pKa is 10.27 for nitrogen atom) justifying the higher experimental log *D* value. These results show that the ionization state of the molecules regulates their drug distribution between the aqueous solution and the lipids membrane. Both drugs are ionizable molecules and it is well established that ionizable drugs significantly partition into the lipid membrane models due to electrostatic interactions and formation of hydrogen bonds with polar groups of the phospholipids heads (Avdeef et al., 1998). In fact, several studies report different experimental log *D* values from the predicted log *P* values calculated only for the neutral microspecies of the drugs (Alves et al., 2017).

Also, it was observed that drug's partition is dependent on the lipid composition of the biomembrane models, since K*p* and log *D* values significantly decreased for DMPC:chol LUVs for both molecules ($p<0.05$). Cholesterol regulates the phase behaviour of membranes, promoting their ordering and rigidity over the region in which there is contact between the cholesterol and the hydrophobic lipid tails [34]. Therefore, the lipid bilayer presents a more organized and packed structure in DMPC:chol LUVs, slowing the diffusion of the molecules into the biomembrane model (Neves et al., 2015). DMPC:chol LUVs are a more realistic and comparable model for the biological membranes.

As expected *Kp* and log *D* values are significantly higher for TMZ than for MTIC in both LUVs, DMPC and DMPC:chol vesicles ($p<0.05$). TMZ molecules are more lipophilic that MTIC molecules, therefore TMZ is more likely to exhibit a higher partition into the lipid phase. Although TMZ molecules have showed higher affinity to the biomembrane models, after oral administration, TMZ is completely converted to MTIC in within approximately 2 hours (Lopes, et al., 2013). The lower K*p* and log *D* values for MTIC can explain its low bioavailability on the target tissues, since this molecule proved in this experiment to have low affinity to biological membranes. In fact, it has been reported that only negligible amounts of MTIC are detected in tumour tissues (Andrasi et al., 2010).

Hence, drug distribution depends not only on its physicochemical features as its structure and degree of ionization, as also depends on the characteristics of the membrane such as the packing of the lipid molecules (Nunes et al., 2013). Thus, is of the outmost importance to use a suitable the LUVs/water system to obtain a realistic and accurate information about TMZ and MTIC lipophilicity and their *in vivo* membrane partition.

However, *Kp* values do not allow to conclude about the location of the drug molecules within the biomembrane, since the changes in absorbance values can occur due to the drug internalization in the bilayer or to the drug adsorption at the membrane interface (Santos et al., 2003). Thus, location studies to assess this issue were conducted and are discussed in the next section.

3.3.3 Membrane location of TMZ and MTIC

The location of TMZ and MTIC within the two different LUVs, DMPC and DMPC:chol, was assessed by steady-state fluorescence quenching assays. For that, two fluorescent probes with a well-known location, DPH and TMA-DPH, were used. DPH molecules are located deeply in the bilayer, while TMA-DPH is located closer to the lipid/water interface.

Stern-Volmer graphs with increasing concentrations of TMZ were plotted and the attained plots are presented as an example in figure 3.5. Equivalent plots were obtained for MTIC (figure A.4 in annex A). K_{SV} values were calculated from these plots and are presented in table 3.3.

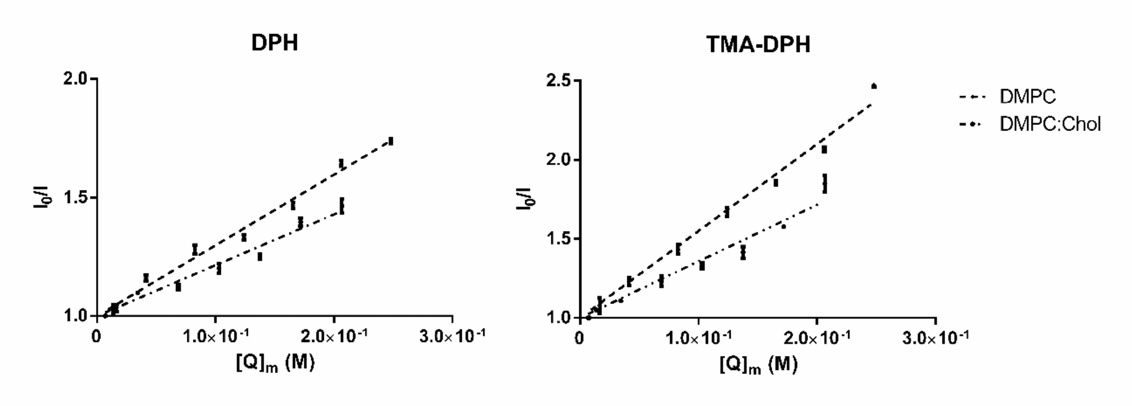

Figure 3. 5 | Stern-Volmer plots for DPH and TMA-DPH probes in LUVs of DMPC and DMPC:chol at pH 5.5 at 37 °C by increasing concentrations of TMZ. Data expressed as mean ± SD (n=3).

Table 3. 3 | Stern-Volmer constants (K_{SV}) values of TMZ and MTIC between DMPC and DMPC:chol vesicles and the aqueous medium PBS. The aqueous medium is PBS at pH 5.5 or 7.4 for TMZ and MTIC, respectively. Data represented as mean ± SD (n=3).

Drug	**DPH**		**TMA-DPH**	
	K_{SV} (M^{-1})		**K_{SV} (M^{-1})**	
	DMPC	**DMPC:Chol**	**DMPC**	**DMPC:Chol**
TMZ	3.5 ± 0.6	2.2 ± 0.2	4.4 ± 0.9	3.5 ± 0.4
MTIC	0.0 ± 0.1	-0.1 ± 0.1	0.0 ± 0.5	-0.1 ± 0.2

As K_{SV} values correspond to the slope of the linear regression, as shown in figure 3.65, the higher the quenching effect, the higher the slope, and consequently the higher the constant value. The obtained K_{SV} values for TMZ show that the quenching effect was more pronounced for TMA-DPH in both DMPC and DMPC:chol, reporting a more superficial location of TMZ near to the phospholipid head groups. However, the attained K_{SV} values for DPH probe suggest that this molecule is also able to penetrate into the bilayer in both used *in vitro* LUVs. These results can be explained by the significant contribution of anionic species of TMZ mentioned in the previous section.

The attained results also suggest that the quenching phenomenon depends on the organization and fluidity of the membrane. In fact, K_{sv} values for DMPC:chol are lower than for DMPC vesicles. As already discussed in the previous section, cholesterol molecules create a more packed and rigid membrane, hampering the diffusion of TMZ molecules into the bilayer, resulting in a decreased fluorescence deactivation of both probes.

K_{SV} values obtained for MTIC indicate that this molecule does not interact with both probes. As both dynamic and static quenching require close proximity between the quenching and the fluorophore molecules (Neves, et al., 2016), these location studies are based in “contact quenching” phenomenon, so it depends on the probe-quencher distance (London and Ladokhin, 2002). The attained K_{SV} results for MTIC may be explained by the insufficient proximity between the MTIC molecules and the probes, since large distances invalidate the measurements. Although MTIC exhibited some affinity for the lipid membrane as shown by its *Kp* and log *D* values, MTIC has been described as an amphipathic molecule, exhibiting high affinity to the water phase (Ramalho et al., 2018). Due to its small size and high affinity to water, free energy regulates MTIC diffusion. It has been reported that for molecules with these characteristics, the free energy increases with their partition from the outer aqueous medium into the lipid membrane, due to the increased density of the lipid bilayer (Bemporad et al., 2004). Therefore, a resistance to the diffusion of MTIC molecules trough the membrane is created. MTIC partition and diffusion are less favourable in the membrane than in the water phase. Thus, the MTIC molecules may be spontaneously driven to diffuse out of the lipid bilayer to minimize the free energy

(Bemporad, et al., 2004). So MTIC molecules may diffuse continually in a cycle from the outer aqueous medium to the lipid bilayer, and then from the membrane back to the external aqueous phase. This cyclic in-out-in diffusion may not allow to achieve enough proximity between the probe and MTIC molecules for the quenching process occur.

Also, the observed linear plotting of I_0/I versus $[Q]_m$ suggests that quenching by TMZ occurs by collisional quenching (Ferreira et al., 2005).

3.3.4 The effect of TMZ and MTIC on membrane fluidity

Before reaching the intracellular environment, drugs face several biological membranes. Since the intracellular environment constitute the pharmacological target in most cases, it is of outmost importance to evaluate the drugs' effects on the biophysical state of the phospholipid membranes. The membrane fluidity plays a major role in several cellular functions, so its study allows the understanding of drug therapeutic and toxic effects. Changes in the T_m from the gel state to the fluid state are suitable indicators for membrane fluidity alterations (Pignatello et al., 2011). So, T_m and B values were determined in a mimetic biomembrane model before and after incubation with TMZ or MTIC by DLS analysis to study the effect of the drugs on the membrane's fluidity.

The effect of temperature on the normalized count rate (number of photons detected per second) of the biomembrane model in the absence and presence of TMZ or MTIC is presented in figure 3.6. Changes in the count rate are verified due to occurrence of a macroscopic alteration in the membrane (Michel, et al., 2006).

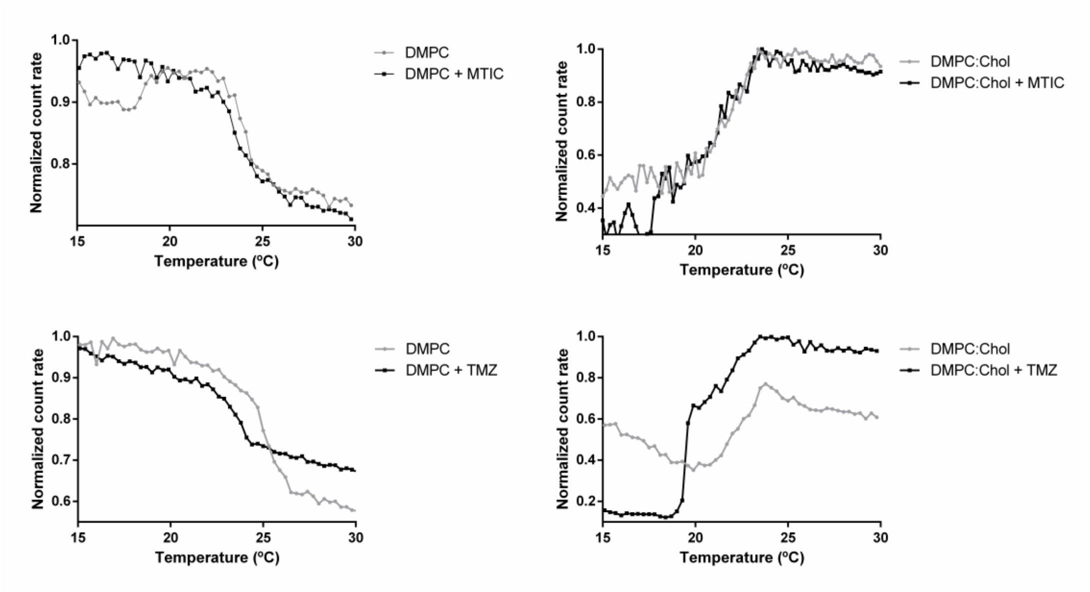

Figure 3. 6 | Normalized count rate of DMPC and DMPC:chol vesicles with and without TMZ and MTIC (150 μM) as a function of temperature. The aqueous medium is PBS at pH 5.5 or 7.4 for TMZ and MTIC, respectively.

T_m and B values were determined by fitting the non-linear regression curve (equation 3.8) to the plotted graphs, and the attained values are presented in table 3.4. The obtained T_m value for DMPC vesicles at pH 7.4, 24.3 ± 0.1 ^{0}C, is accordingly with previously reported (Neves, et al., 2016). It was observed that this value significantly decreased to 21.5 ± 0.2 ^{0}C with the insertion of cholesterol molecules in the model ($p<0.05$). As already mentioned, the cholesterol molecules embedded in the lipid bilayer increase the membrane’s rigidity, therefore decreasing its fluidity altering the T_m value. The same decrease was verified for measurements conducted at pH 5.5 as control. Although no significant changes occurred to the cooperativity.

Table 3. 4 | Phase-transition temperature (T_m) and cooperativity (*B*) values of DMPC and DMPC:chol vesicles with and without TMZ or MTIC. The aqueous medium is PBS at pH 5.5 or 7.4 for TMZ and MTIC, respectively. Data represented as mean ± SD (n=3).

Drug	**pH**	**T_m (°C)**		**Cooperativity (*B*)**	
		DMPC	**DMPC:Chol**	**DMPC**	**DMPC:Chol**
-	**5.5**	25.2 ± 0.2	22.1 ± 0.8	282 ± 45	337 ± 38
TMZ	**5.5**	23.6 ± 0.1	20.6 ± 0.3	109 ± 36	130 ± 39
-	**7.4**	24.3 ± 0.1	21.5 ± 0.2	326 ± 78	333 ± 36
MTIC	**7.4**	23.6 ± 0.1	20.6 ± 0.1	201 ± 18	191 ± 13

The attained lower T_m values indicate that both molecules produce a perturbation in membrane's fluidity, although in a higher extent for TMZ. In fact, TMZ significantly decreased T_m by 1.8 and 1.5 ^{0}C in DMPC and DMPC:chol models, respectively ($p<0.05$), while MTIC only decreased T_m by 1.1 and 0.9 ^{0}C in DMPC and DMPC:chol models, respectively ($p<0.05$). These results are consistent with the determined *Kp* and log *D* values that indicate that TMZ has a higher affinity for the membrane than MTIC, and therefore will penetrate the bilayer in a greater extent, creating a higher perturbation in the fluidity of the membrane. Also, these results support that drug depth diffusion into the membrane is less noticeable when cholesterol molecules are embedded in the membrane, as expected due to the increased rigidity and organization of the bilayer.

In addition, it was observed that TMZ significant decreased the cooperativity of both DMPC and DMPC:chol LUVs ($p<0.05$). Changes in the lipids cooperativity, due to acyl chains undergoing changes simultaneously during phase transition, indicate the presence and interaction of the compounds with the lipid bilayer (Andrushchenko et al., 2007). Charged microspecies of the drug interact with charged groups at the phospholipid polar head, reducing the electrostatic repulsions between DMPC molecules, and consequently modifying the cooperativity of the lipids (Jain and Wu, 1977). Drug molecules reduce the cooperativity of the phase transition because they intercalate into the phospholipid bilayers affecting the number of phospholipid molecules that a single phospholipid molecule can influence (Sarpietro et al., 2015).

Also, these changes in the properties of the membrane corroborate our conclusions on the location of TMZ molecules within the lipid bilayer. It is well-reported that lipid bilayers are characterized by a fluidity gradient with more rigid and ordered outer region near the polar head groups (C1 to C9), and a more fluid and disordered deeper region (C10 to C14 of the acyl chains). Therefore, if the drug induces changes in the fluidity of the bilayer, the drug is more likely to be located in the outer regions of the membrane, near to the polar head groups (Jain and Wu, 1977). The presented T_m and B values suggest that TMZ should be located near the head groups of the phospholipids as also indicated by the calculated K_{SV} values. Besides, due to its ionization state, TMZ and MTIC establish electrostatic and ion-dipole interactions with the phospholipids polar head groups. A more superficial location of TMZ is expected (shown by higher K_{SV} values for TMA-DPH). Thus, changes in the lipid organization of such region occur resulting in alterations on the membrane's fluidity as shown by T_m measurements. Still, TMZ molecules also interact through hydrophobic forces with the acyl chains of the phospholipid (shown by high K_{SV} values for DPH) and alters the fluidity of deeper regions of the membrane as proved by T_m measurements. A schematic representation of the expected location of the drug molecules is shown in figure 3.7.

MTIC also decreased the B values, but in a smaller extent ($p>0.05$). This is agreement with all the previously presented results. As location studies suggested, MTIC molecules may constantly partitioning in and out of the lipid bilayer due to its low affinity to the lipid membranes. Hence, as MTIC has low affinity to the lipid membranes, creating a smaller influence on the lipid cooperativity as expected.

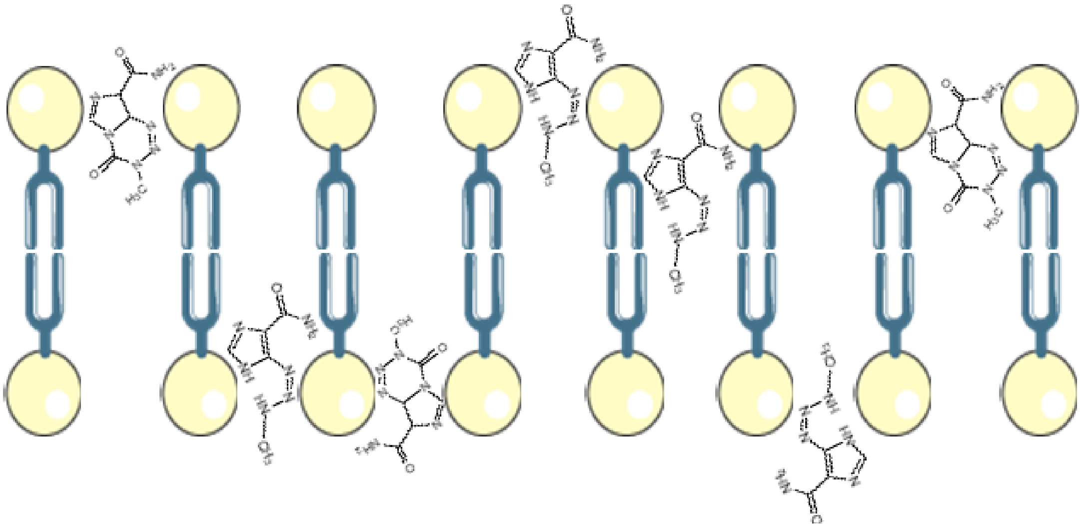

Figure 3. 7 | Schematic representation of the possible interactions of TMZ and MTIC molecules within the phospholipid bilayer.

The use of two different membrane with different lipid composition proved that the membrane compositions influences the drug partition. Hence, drug biodistribution depends not only on its physicochemical features as its structure and degree of ionization, as also depends on the characteristics of the membrane such as the packing of the lipid molecules. DMPC:chol LUVs are a more realistic and comparable model for the biological membranes. The attained results suggest that MTIC low bioavailability on the tumour tissues is due to its low affinity to the biological membranes, hampering its transport across the BBB and its internalization by the GBM cells. Therefore, therapeutic strategies must be envisaged to overcome this issue. In the next chapter, a nanoformulation is presented as a potential answer to TMZ's low bioavailability as other limitations.

References

Akbarzadeh, A., Rezaei-Sadabady, R., Davaran, S., Joo, S.W., Zarghami, N., Hanifehpour, Y., Samiei, M., Kouhi, M., Nejati-Koshki, K. 2013. Liposome: classification, preparation, and applications. Nanoscale research letters. 8 (1), 102-102.

Alves, A.C., Ribeiro, D., Horta, M., Lima, J.L.F.C., Nunes, C., Reis, S. 2017. A biophysical approach to daunorubicin interaction with model membranes: relevance for the drug's biological activity. Journal of The Royal Society Interface. 14 (133).

Andrasi, M., Bustos, R., Gaspar, A., Gomez, F.A., Klekner, A. 2010. Analysis and stability study of temozolomide using capillary electrophoresis. Journal of Chromatography B. 878 (21), 1801-1808.

Andrushchenko, V.V., Vogel, H.J., Prenner, E.J. 2007. Interactions of tryptophan-rich cathelicidin antimicrobial peptides with model membranes studied by differential scanning calorimetry. Biochimica et Biophysica Acta (BBA) - Biomembranes. 1768 (10), 2447-2458.

Avdeef, A., Box, K.J., Comer, J.E.A., Hibbert, C., Tam, K.Y. 1998. pH-Metric logP 10. Determination of Liposomal Membrane-Water Partition Coefficients of lonizable Drugs. Pharmaceutical research. 15 (2), 209-215.

Bannan, C.C., Calabro, G., Kyu, D.Y., Mobley, D.L. 2016. Calculating Partition Coefficients of Small Molecules in Octanol/Water and Cyclohexane/Water. J Chem Theory Comput. 12 (8), 4015-4024.

Bemporad, D., Essex, J.W., Luttmann, C. 2004. Permeation of Small Molecules through a Lipid Bilayer: A Computer Simulation Study. The Journal of Physical Chemistry B. 108 (15), 4875-4884.

Benistant, C., Dehouck, M.P., Fruchart, J.C., Cecchelli, R., Lagarde, M. 1995. Fatty acid composition of brain capillary endothelial cells: effect of the coculture with astrocytes. Journal of lipid research. 36 (11), 2311-2319.

Bhattacharjee, S. 2016. DLS and zeta potential – What they are and what they are not? Journal of Controlled Release. 235 337-351.

Do, T.T.T., Dao, U.P.N., Bui, H.T., Nguyen, T.T. 2017. Effect of electrostatic interaction between fluoxetine and lipid membranes on the partitioning of fluoxetine investigated using second derivative spectrophotometry and FTIR. Chemistry and Physics of Lipids. 207 10-23.

Ferreira, H., Lúcio, M., F. C. Lima, J.L., Cordeiro-da-Silva, A., Tavares, J., Reis, S. 2005. Effect of anti-inflammatory drugs on splenocyte membrane fluidity. Analytical Biochemistry. 339 (1), 144-149.

Hassan, P.A., Rana, S., Verma, G. 2015. Making Sense of Brownian Motion: Colloid Characterization by Dynamic Light Scattering. Langmuir. 31 (1), 3-12.

Hermens Joop, L.M., de Bruijn Jack, H.M., Brooke David, N. 2013. The octanol–water partition coefficient: Strengths and limitations. Environmental Toxicology and Chemistry. 32 (4), 732-733.

Illinger, D., Duportail, G., Mely, Y., Poirel-Morales, N., Gerard, D., Kuhry, J.G. 1995. A comparison of the fluorescence properties of TMA-DPH as a probe for plasma membrane and for endocytic membrane. Biochimica et biophysica acta. 1239 (1), 58-66.

Jain, M.K., Wu, N.M. 1977. Effect of small molecules on the dipalmitoyl lecithin liposomal bilayer: III. Phase transition in lipid bilayer. The Journal of Membrane Biology. 34 (1), 157-201.

Jing, Y., Trefna, H., Persson, M., Kasemo, B., Svedhem, S. 2014. Formation of supported lipid bilayers on silica: relation to lipid phase transition temperature and liposome size. Soft matter. 10 (1), 187-195.

Kaiser, R.D., London, E. 1998. Location of diphenylhexatriene (DPH) and its derivatives within membranes: comparison of different fluorescence quenching analyses of membrane depth. Biochemistry. 37 (22), 8180-8190.

Kaszuba, M., Corbett, J., Watson, F.M., Jones, A. 2010. High-concentration zeta potential measurements using light-scattering techniques. Philos Trans A Math Phys Eng Sci. 368 (1927), 4439-4451.

Koenig, B.W., Strey, H.H., Gawrisch, K. 1997. Membrane lateral compressibility determined by NMR and x-ray diffraction: effect of acyl chain polyunsaturation. Biophysical journal. 73 (4), 1954-1966.

Koynova, R., Caffrey, M. 1998. Phases and phase transitions of the phosphatidylcholines. Biochimica et biophysica acta. 1376 (1), 91-145.

Koynova, R., Koumanov, A., Tenchov, B. 1996. Metastable rippled gel phase in saturated phosphatidylcholines: calorimetric and densitometric characterization. Biochimica et biophysica acta. 1285 (1), 101-108.

Kujawski, J., Bernard, M.K., Janusz, A., Kuźma, W. 2012. Prediction of log P: ALOGPS Application in Medicinal Chemistry Education. Journal of Chemical Education. 89 (1), 64-67.

Langevin, D., Lozano, O., Salvati, A., Kestens, V., Monopoli, M., Raspaud, E., Mariot, S., Salonen, A., Thomas, S., Driessen, M., Haase, A., Nelissen, I., Smisdom, N., Pompa, P.P., Maiorano, G., Puntes, V., Puchowicz, D., Stępnik, M., Suárez, G., Riediker, M., Benetti, F., Mičetić, I., Venturini, M., Kreyling, W.G., van der Zande, M., Bouwmeester, H., Milani, S., Rädler, J.O., Mülhopt, S., Lynch, I., Dawson, K. 2018. Inter-laboratory comparison of nanoparticle size measurements using dynamic light scattering and differential centrifugal sedimentation. NanoImpact. 10 97-107.

Liu, J. 2016. Interfacing Zwitterionic Liposomes with Inorganic Nanomaterials: Surface Forces, Membrane Integrity, and Applications. Langmuir. 32 (18), 4393-4404.

London, E., Ladokhin, A.S. 2002. Measuring the depth of amino acid residues in membrane-inserted peptides by fluorescence quenching, in: Current Topics in Membranes, Academic Press, pp. 89-115.

Lopes, I.C., de Oliveira, S.C.B., Oliveira-Brett, A.M. 2013. Temozolomide chemical degradation to 5-aminoimidazole-4-carboxamide – Electrochemical study. Journal of Electroanalytical Chemistry. 704 183-189.

Lopes, S.G., C.; Rocha, T.; Ferreira, D.; Leite, E.; Oliveira, M. 2013. Liposomes as Carriers of Anticancer Drugs, in: P.L. Rangel (Ed.) Cancer Treatment - Conventional and Innovative Approaches, Intechopen, http://www.intechopen.com/books/cancer-treatment-conventional-and-innovative-approaches/liposomes-as-carriers-of-anticancer-drugs, pp. 85-124.

Loureiro, D.R.P., Soares, J.X., Lopes, D., Macedo, T., Yordanova, D., Jakobtorweihen, S., Nunes, C., Reis, S., Pinto, M.M.M., Afonso, C.M.M. 2018. Accessing lipophilicity of drugs with biomimetic models: A comparative study using liposomes and micelles. European Journal of Pharmaceutical Sciences. 115 369-380.

Lucio, M., Ferreira, H., Lima, J.L., Reis, S. 2007. Use of liposomes to evaluate the role of membrane interactions on antioxidant activity. Analytica chimica acta. 597 (1), 163-170.

Lucio, M., Lima, J.L., Reis, S. 2010. Drug-membrane interactions: significance for medicinal chemistry. Curr Med Chem. 17 (17), 1795-1809.

Lucio, M., Lima, J.L.F.C., Reis, S. 2010. Drug-Membrane Interactions: Significance for Medicinal Chemistry. Current Medicinal Chemistry. 17 (17), 1795-1809.

Lúcio, M., Nunes, C., Gaspar, D., Gołębska, K., Wisniewski, M., Lima, J.L.F.C., Brezesinski, G., Reis, S. 2009. Effect of anti-inflammatory drugs in phosphatidylcholine membranes: A fluorescence and calorimetric study. Chemical Physics Letters. 471 (4–6), 300-309.

Magalhães, L.M., Nunes, C., Lúcio, M., Segundo, M.A., Reis, S., Lima, J.L.F.C. 2010. High-throughput microplate assay for the determination of drug partition coefficients. Nature Protocols. 5 1823.

Makino, K., Shibata, A. 2006. Chapter 2: Surface Properties of Liposomes Depending on Their Composition, in: A.L. Liu (Ed.) Advances in Planar Lipid Bilayers and Liposomes, Academic Press, pp. 49-77.

Michel, N., Fabiano, A.-S., Polidori, A., Jack, R., Pucci, B. 2006. Determination of phase transition temperatures of lipids by light scattering. Chemistry and Physics of Lipids. 139 (1), 11-19.

Mosmuller, E.W., Pap, E.H., Visser, A.J., Engbersen, J.F. 1994. Steady-state fluorescence studies on lipase-vesicle interactions. Biochimica et biophysica acta. 1189 (1), 45-51.

Neves, A.R., Nunes, C., Amenitsch, H., Reis, S. 2016. Effects of resveratrol on the structure and fluidity of lipid bilayers: a membrane biophysical study. Soft Matter. 12 (7), 2118-2126.

Neves, A.R., Nunes, C., Reis, S. 2015. New Insights on the Biophysical Interaction of Resveratrol with Biomembrane Models: Relevance for Its Biological Effects. J Phys Chem B. 119 (35), 11664-11672.

Nunes, C., Brezesinski, G., Lopes, D., Lima, J.L.F.C., Reis, S., Lúcio, M. 2011. Lipid–Drug Interaction: Biophysical Effects of Tolmetin on Membrane Mimetic Systems of Different Dimensionality. The Journal of Physical Chemistry B. 115 (43), 12615-12623.

Nunes, C., Lopes, D., Pinheiro, M., Pereira-Leite, C., Reis, S. 2013. In vitro assessment of NSAIDs-membrane interactions: significance for pharmacological actions. Pharm Res. 30 (8), 2097-2107.

Pignatello, R., Musumeci, T., Basile, L., Carbone, C., Puglisi, G. 2011. Biomembrane models and drug-biomembrane interaction studies: Involvement in drug design and development. Journal of Pharmacy and Bioallied Sciences. 3 (1), 4-14.

Pinheiro, M., Arede, M., Caio, J.M., Moiteiro, C., Lucio, M., Reis, S. 2013. Drug-membrane interaction studies applied to N'-acetyl-rifabutin. European journal of pharmaceutics and biopharmaceutics : official journal of Arbeitsgemeinschaft fur Pharmazeutische Verfahrenstechnik e.V. 85 (3 Pt A), 597-603.

Pinheiro, M., Arede, M., Giner-Casares, J.J., Nunes, C., Caio, J.M., Moiteiro, C., Lucio, M., Camacho, L., Reis, S. 2013. Effects of a novel antimycobacterial compound on the biophysical properties of a pulmonary surfactant model membrane. Int J Pharm. 450 (1-2), 268-277.

Ramalho, M.J., Coelho, M.A.N., Pereira, M.C. 2018. Chapter 18 - Nanocarriers for the delivery of temozolomide in the treatment of glioblastoma: A review, in: A.M.

Grumezescu (Ed.) Design and Development of New Nanocarriers, William Andrew Publishing, pp. 687-722.

Santos, N.C., Prieto, M., Castanho, M.A.R.B. 2003. Quantifying molecular partition into model systems of biomembranes: an emphasis on optical spectroscopic methods. Biochimica et Biophysica Acta (BBA) - Biomembranes. 1612 (2), 123-135.

Sarpietro, M.G., Di Sotto, A., Accolla, M.L., Castelli, F. 2015. Interaction of β-caryophyllene and β-caryophyllene oxide with phospholipid bilayers: Differential scanning calorimetry study. Thermochimica Acta. 600 28-34.

Sezgin, E., Levental, I., Mayor, S., Eggeling, C. 2017. The mystery of membrane organization: composition, regulation and roles of lipid rafts. Nature Reviews Molecular Cell Biology. 18 361.

Siddiqui, M.R., AlOthman, Z.A., Rahman, N. 2017. Analytical techniques in pharmaceutical analysis: A review. Arabian Journal of Chemistry. 10 S1409-S1421.

Štěpánek, M. 2016. Fluorescence Spectroscopy Studies of Amphiphilic Block Copolymer Micelles in Aqueous Solutions, in: K. Procházka (Ed.) Fluorescence Studies of Polymer Containing Systems, Springer International Publishing, Cham, pp. 203-215.

Stetefeld, J., McKenna, S.A., Patel, T.R. 2016. Dynamic light scattering: a practical guide and applications in biomedical sciences. Biophysical Reviews. 8 (4), 409-427.

Teixeira, V.H., Vila-Viçosa, D., Baptista, A.M., Machuqueiro, M. 2014. Protonation of DMPC in a Bilayer Environment Using a Linear Response Approximation. Journal of Chemical Theory and Computation. 10 (5), 2176-2184.

Toda, Y., Takata, K., Nakagawa, Y., Kawakami, H., Fujioka, S., Kobayashi, K., Hattori, Y., Kitamura, Y., Akaji, K., Ashihara, E. 2015. Effective internalization of U251-MG-secreted exosomes into cancer cells and characterization of their lipid components. Biochemical and Biophysical Research Communications. 456 (3), 768-773.

Wang, S., Beechem, J.M., Gratton, E., Glaser, M. 1991. Orientational distribution of 1,6-diphenyl-1,3,5-hexatriene in phospholipid vesicles as determined by global analysis of frequency domain fluorimetry data. Biochemistry. 30 (22), 5565-5572.

Wiersema, P.H., Loeb, A.L., Overbeek, J.T.G. 1966. Calculation of the electrophoretic mobility of a spherical colloid particle. J. Colloid Interface Sci. 22 (1), 78-99.

Zhang, K., Fahr, A., Abraham, M.H., Acree, W.E., Tobin, D.J., Liu, X. 2015. Comparison of lipid membrane–water partitioning with various organic solvent–water partitions of neutral species and ionic species: Uniqueness of cerasome as a model for the stratum corneum in partition processes. International journal of pharmaceutics. 494 (1), 1-8.

Chapter 4 - Design of PLGA nanoparticles for the delivery of temozolomide

4.1 Introduction

TMZ is the first-line treatment for GBM, however is only capable of extending the patients' survival, not being successfully curative (Stupp et al., 2001), due to its low bioavailability due to the already mentioned low biological half-life. Its low ability to interact with biological barriers and membranes as already reported in the previous section, is also a major factor for TMZ low bioavailability in the target tissues. Also, high toxicity is associated with its administration.

Therefore, TMZ delivery by nanocarriers may be a suitable approach to increase its chemotherapeutic efficacy, since it will avoid drug elimination after administration and increasing its accumulation in the target tissues (Coelho et al., 2015). Several types of nanosystems have been extensively studied for drug delivery. In this work, the use of poly(lactic-co-glycolic acid) (PLGA) nanoparticles (NPs) is proposed. Being biodegradable, biocompatible and FDA-approved (Ramalho et al., 2015), the encapsulation of TMZ in PLGA NPs could be a suitable strategy to increase its therapeutic efficacy and to overcome its limitations, as toxicity in healthy tissues by targeting the tumour cells. Also, TMZ encapsulation in PLGA NPs should enhance drug transport across the BBB and avoid drug recognition by p-glycoprotein pump in target cells circumventing drug efflux. Moreover, these NPs exhibit low synthesis complexity (Ramalho and Pereira, 2016) and are able to maintain a controlled drug release for several days, decreasing the need for frequent drug administration and doses, minimizing the side effects in healthy tissues (Makadia and Siegel, 2011). The

PLGA polymer can also be easily functionalized for the design of NPs with different targeting moieties (Danhier et al., 2012).

Active targeting strategies are increasingly used to enhance NPs uptake in the target cell or the transport across biological barriers as BBB. For that, the NPs' surface can be modified using receptors usually overexpressed in target cells or biological barriers (Lockman et al., 2002; Pillai, 2014). In this work, immunocarriers were developed using the mAb type OX26 for the TfR that has proven to efficiently bind cells that overexpress this receptor (Loureiro et al., 2017; Loureiro et al., 2016), as GBM cells (Calzolari et al., 2010) and several other tumour cells types (Frasco et al., 2015). Since mAbs exhibit high specificity for the target receptors, it is possible to achieve high levels of targeting (Loureiro et al., 2014).

Here, the main goal was to develop a suitable nanosystem to encapsulate TMZ and to assess its efficiency in the delivery of the drug into GBM tumour cells. For that, two nanosystems were proposed, non-modified PLGA NPs and NPs with the surface modified with an OX26 mAb, as schematized in figure 4.1. Therefore, this chapter describes the design, synthesis and the properties of OX26 mAb-modified and non-modified PLGA NPs. The internalization and antiproliferative effect of TMZ entrapped in both PLGA nanoformulations was evaluated in GBM cell lines.

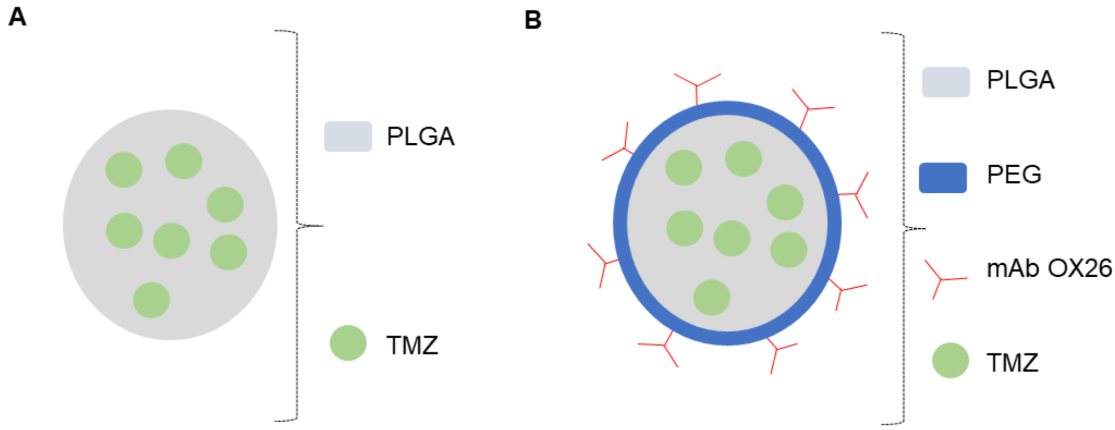

Figure 4. 1 | Schematic representation of the proposed nanosystems. (A) Non-modified TMZ-loaded PLGA NPs and (B) mAb OX26-modified PLGA NPs.

4.2 Materials and Methods

4.2.1 Materials

PLGA Resomer® RG503H (50:50; MW 24,000 – 38,000), poly(vinyl alcohol) (PVA), Coumarin-6 (C6), 1-Ethyl-3-(3-dimethylaminopropyl) carbodiimide (EDC), dichloromethane, ethyl ether, ethylenediaminetetraacetic acid (EDTA), 2-iminothiolane hydrochloride (Traut's reagent), bovine serum albumin (BSA), citric acid, 2,2′-azino-bis(3-ethylbenzothiazoline-6-sulfonic acid) diammonium salt (ABTS), sodium hydroxide, acetic acid, sulforhodamine B (SRB), trypan blue, holo-Transferrin human (purity ≥ 98%), rhodamine B and Triton X™-100 were obtained from Sigma–Aldrich (St. Louis, MO, USA). Uranyl acetate was bought from Electron Microscopy Sciences (Hatfield, UK). Polyethylene glycol functionalized with maleimide (mPEG-Mal, MW 2000) was acquired from Nanocs Inc. (Boston, MA, USA). The OX26 mAb was purchased from Novus Biologicals (Oxfordshire, UK). Transferrin receptor was acquired from Abcam (Cambridge, UK). The secondary antibody Goat anti-Mouse IgG (H+L) Cross Adsorbed Secondary Antibody, HRP conjugate was bought at Thermo Scientific-Pierce Antibodies (Waltham, MA, USA). High-glucose Dulbecco's Modified Eagle medium (DMEM), fetal bovine serum (FBS), SlowFade Gold Antifade Mountant with DAPI (4',6-Diamidino-2-Phenylindole, Dihydrochloride) and Lysotracker DeepRed were acquired from Invitrogen Co. (Scotland, UK). Tricloroacetic acid (TCA) and Tris buffer were purchased from Merck (Darmstadt, Germany). Ringer HEPES (RH) buffer was prepared using 150 mM NaCl, 6 mM $NaHCO_3$, 5.2 mM KCl, 5 mM HEPES, 2.8 mM glucose, 2.2 mM $CaCl_2$ and 0.2 mM $MgCl_2$-$6H_2O$ at pH 7.4). All reagents used for RH buffer composition were acquired from Sigma–Aldrich (St. Louis, MO, USA).

4.2.2 Cell lines

Two human GBM cell lines, U251 and U87, and an immortalized human astrocyte cell line (NHA) were used in this work. All the used lines were cultured in DMEM supplemented with 10% FBS and 1% penicillin-streptomycin. Cells were maintained at 37 °C in a humidified 5% CO_2 incubator. At 80% of confluence, the cells were trypsinized and subcultured. Both U251 and U87 cell lines were chosen since they show significant similarities with the genetic, immunohistochemical and histological and characteristics of human GBM tumour (Jacobs et al., 2011).

4.2.3 Preparation of TMZ-loaded PLGA NPs

TMZ-loaded PLGA NPs were prepared using the single emulsion-solvent evaporation technique. 100 µL of an organic solution of dichloromethane containing 1 mg of TMZ and 10 mg of PLGA was prepared. 200 µL of 2% (w/v) PVA solution was added drop-by-drop to the organic mixture previously prepared. Then, the solution was agitated (Genius 3, ika®vortex, Germany) and emulsified in an ultrasonic bath at an ultrasonic frequency of 45 kHz (Ultrasonic cleaner, VWR™, Malasya). Stirring of the emulsion originates microdroplets. Ultrasound waves induce the reduction of the size of the emulsion droplets through acoustic cavitation, leading to the formation and subsequent collapse of microbubbles. This breaks up the primary droplets of dispersed oil into nanosized droplets (Stepišnik Perdih et al., 2019).

The emulsion was then transferred into 2.5 mL of 0.2% (w/v) PVA solution and maintained in continuous agitation (Colorsquid, ika®, magnetic stirrer), allowing the organic solvent to complete evaporate. Evaporation of the solvent allows the transformation of the droplets of dispersed phase into solid particles.

The suspension was filtered using a membrane with pore size of 200 nm, (polyethersulfone membrane syringe filter, VWR, USA) and stored at 4 ºC overnight to avoid NPs aggregation and increase their stability. After, the samples were centrifuged for 30 minutes at 14100 g (MiniSpin®plus, Eppendorf, Germany), to separate NPs from non-encapsulated drug. The supernatant containing the non-encapsulated drug was saved for analysis.

C6 loaded PLGA NPs were also prepared dissolving 1 mg of C6 in the dichloromethane solution instead of TMZ.

All formulations were prepared in triplicate.

4.2.4 Synthesis of PEGylated PLGA

2 mg of PLGA and 0.04 mg of EDC were dissolved in a 100 µL of dichloromethane. A mixture of ethyl ether: methanol (70:30 ratio) was added to the previously prepared solution to remove the excess of EDC. Then, 0.2 mg of maleimide-PEG-NH_2 were added to the activated PLGA and the solution was maintained

overnight at RT in continuous agitation (Genius 3, ika®vortex, Germany). The mixture was centrifuged for 40 minutes at 14100 g, (MiniSpin®plus, Eppendorf, Germany), and the pellet resuspended in dichloromethane.

4.2.5 Preparation of TMZ-loaded mAb-PLGA NPs

TMZ-loaded PEG-PLGA NPs were prepared using also the single emulsion-solvent evaporation technique. 8 mg of non-modified PLGA was added to the previously prepared PEG-PLGA. Also 1 mg TMZ was added to the PLGA mixture in dichloromethane, and the remaining protocol was performed as described previously in section 4.2.3. C6-loaded PLGA NPs were also prepared dissolving 1 mg of C6 in the dichloromethane solution instead of TMZ.

The prepared NPs were next modified with OX26 mAb by a covalent coupling reaction at a molecular ratio of OX26 mAb: PEG-PLGA of 1:2. The maleimide group on PEG extremity reacts with thiol groups present on mAbs, after mAb activation by Traut's reagent. A drop of EDTA was added to prevent oxidation of the thiol groups (Loureiro, et al., 2016). The activated mAbs were separated from the excess reagents by size exclusion chromatography (PD Minitrap G-25 columns containing Sphadex Medium, GE Healthcare, Sweden). The activated mAbs were then added to the previously prepared PEG-PLGA NPs and incubated 1 h in the dark at RT, followed by overnight incubation at 4 °C. Non-attached antibody was removed by centrifugation for 30 minutes at 14100 g, (MiniSpin®plus, Eppendorf, Germany).

All formulations were prepared in triplicate.

4.2.6 PLGA NPs physicochemical characterization

The size, PdI, zeta potential, morphological appearance and affinity for the TfR were the used parameters to characterize the prepared PLGA NPs.

4.2.6.1 Dynamic light scattering for size determination

The mean diameter and size distribution of the prepared NPs were evaluated by DLS. The measurements were performed in a ZetaSizer Nano ZS (Malvern Instruments, UK). The attained data is given in intensity distribution. At least three independent measurements were performed.

4.2.6.2 Laser doppler velocimetry method for zeta potential determination

The zeta potential values of the prepared NPs were determined by laser doppler velocimetry method. The measurements were also performed in a ZetaSizer Nano ZS (Malvern Instruments, UK) The analysis was performed using the dielectric constant of water. At least three independent measurements were performed.

4.2.6.3 Transmission electron microscopy for morphological analysis

The morphological analysis of the NPs was obtained by transmission electron microscopy (TEM). This is one of the most efficient methods for the characterization of the morphology of NPs. The NPs were prepared on copper grids (Formvar/Carbon-400 mesh Copper, Agar Scientific, UK) and negatively stained. For that, 10 µL of samples were stained with 2% (v/v) uranyl acetate for 45 seconds, and air-dried. This is a heavy metal salt capable of scattering electrons, enhancing the contrast to better visualize the samples (Franken et al., 2017). Then, the NPs were visualized using a Jeol JEM 1400 electron microscope (Japan) at an accelerating voltage of 80kV.

4.2.6.4 ELISA assays for the evaluation of affinity of the immuno-NPs for TfR

The ability of the developed immuno-PLGA NPs to recognize the TfR was evaluated by the enzyme-linked immunosorbent assay (ELISA). This immunoanalytical methodology is useful for antibody detection and it is extensively used for the diagnosis of several diseases. ELISA tests can be classified in different types based on how the analytes and antibodies are bonded and used, such as direct, indirect, "sandwich" and competitive ELISA (González-Martínez et al., 2018).

In this work, indirect ELISA was the chosen methodology. This is a two-step ELISA which involves two binding process of primary antibody and a labelled secondary antibody as shown in figure 4.2. Although indirect ELISA takes more time, it has higher sensitivity than direct ELISA, also known as conventional ELISA (Lin, 2015).

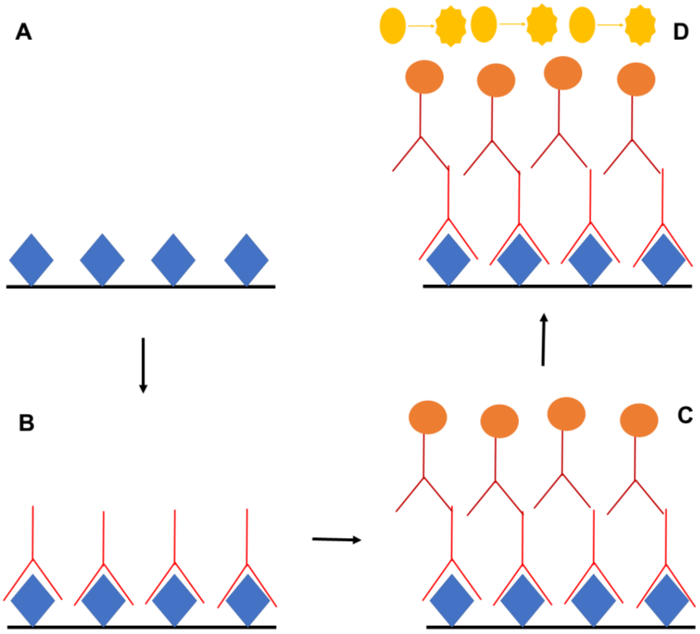

Figure 4. 2 | Schematic representation of the steps of indirect ELISA methodology. (A) The antigen molecules are added to a surface for adhesion to occur. (B) The primary antibody is added to bind to the antigen. (C) A secondary antibody which binds specifically to the primary antibody is added. The secondary antibody is a conjugated with an enzyme. A substrate for the enzyme is added and a change in colour upon reaction with the enzyme occurs.

In this work, indirect ELISA was used to assess the affinity of OX26 mAb-modified PLGA NPs to TfR. For that, the surface of a 96-well plate (Nunc MaxiSorp®) was treated with TfR and incubated overnight at 4 ºC. The plate was then treated with BSA to block any nonspecific binding sites on the surface, and it was then incubated for 2 h at RT, followed by the addition of NPs. After incubation, the wells were subsequently washed to remove unbound NPs. After, the peroxidase-conjugated secondary antibody (goat anti-mouse) was added and incubated for 45 min at RT. After incubation, the wells were subsequently washed to remove unbound secondary antibody. The samples were revealed using a solution of citric acid, ABTS and H_2O_2. The absorbance at the wavelength of 405 nm was measured using a fluorescence microplate reader (HT Microplate Spectrophotometer, BioTek). Non-modified NPs were used as a negative control.

All samples were tested in triplicates and three independent experiments were conducted.

4.2.7 TMZ encapsulation efficiency and drug loading of PLGA NPs

The TMZ encapsulation efficiency (EE) and drug loading (DL) of the prepared PLGA NPs were determined by UV–Vis spectrophotometry using the following equations, respectively:

$$EE = \frac{total\ amount\ of\ TMZ -\ amount\ of\ free\ TMZ}{total\ amount\ of\ TMZ}\ x\ 100 \qquad (4.1)$$

$$DL = \frac{total\ amount\ of\ TMZ -\ amount\ of\ free\ TMZ}{total\ of\ PLGA}\ x\ 100 \qquad (4.2)$$

Non-encapsulated TMZ was obtained from centrifugation of NPs suspension (30 min, 14100 g, MiniSpin®plus, Eppendorf, Germany) and quantified using a UV-1700 PharmaSpec UV-Vis spectrophotometer from Shimadzu (Japan) at λ_{max} 329 nm. The results were correlated to a control sample corresponding to total amount of drug. Three independent experiments were conducted.

4.2.8 PLGA NPs stability studies

The stability of the prepared PLGA NPs was analysed through size and zeta potential variations. PLGA NPs' dispersions in ultrapure water were stored at 4 °C and DLS measurements were performed at different timepoints to evaluate modifications in PLGA NPs size and zeta potential values. These measurements were performed weekly, for 6 weeks. Three independent samples were used.

4.2.9 *In vitro r*elease of TMZ from PLGA NP*s*

In vitro TMZ release studies were performed, over 20 days, using a cellulose dialysis membrane diffusion technique. The membranes were washed in ultrapure water for 24 hours before being used and equilibrated with release buffer 1 hour before the dialysis.

A sufficient amount of TMZ-loaded PLGA NPs was diluted in 2 mL of release buffer and placed into a dialysis device (Float-A-Lyzer G2, CE, 10KDa, SpectrumLabs, USA). The outside space of the dialysis device was filled with 5 mL of release buffer to ensure sink conditions. PBS (pH 7.4, 0.01 M) was used as the release buffer to mimic the salt concentrations and pH of physiological conditions. The dialysis membrane was kept in continuous stirring at 200 rpm at 37 °C simulating the physiological temperature. At predetermined times, samples were collected from the outside medium and, after measurement by UV-Vis spectrophotometry at λmax 329 (UV-1700 PharmaSpec UV-Vis spectrophotometer, Shimadzu, Japan), returned to the release medium. A solution of TMZ in PBS was used as control. Three independent experiments were conducted.

The TMZ release curve, representing the percentage of drug released in function of time, was then plotted by the following equation:

$$\%\,TMZ\ released = \frac{amount\ of\ TMZ\ released\ at\ time\ t}{amount\ of\ encapsulated\ TMZ}\ x\ 100 \qquad (4.3)$$

The cellulose dialysis membrane diffusion technique was also used to evaluate the *in vitro* release of C6. However, here DMEM high glucose was used as the release buffer, to mimic the conditions of the *in vitro* cell experiments.

4.2.10 Confocal microscopy for cellular imaging studies

The NPs *in vitro* uptake in the human cell lines (U251, U87 and NHA) was assessed using laser scanning confocal microscopy (LSCM). This is a well-known imaging technique widely used for the acquisition of high-resolution images of materials.

For fluorescence visualization purpose, C6 was loaded into the NPs. This fluorescent marker is distributed in the NPs matrix, allowing the visualization of the NPs inside the cellular compartments (Holzer et al., 2009). 1000 cells.well^{-1} were seeded in 12-well plates (Ibidi, Germany) and allowed to attach for 24 h (37 °C, in a humidified 5% CO_2 incubator). Cells were then treated with mAb-modified and unmodified C6-loaded NPs for 2 and 72 h. After the incubation period and subsequent wash with PBS, the cells were fixed with 4% (w/v) paraformaldehyde. The acidic cell compartments (as endosomes/lysosomes) were stained with LysoTracker® Red and cell nuclei were marked with DAPI. Samples were visualized using a Leica TCS SP5 II confocal microscope (Leica Microsystems, Germany). At least six images from different areas of each cell lines were acquired in emission mode. Untreated cells were also used control.

4.2.11 Quantification of *in vitro* cellular uptake of mAb-PLGA NPs

Cellular uptake of mAb-modified and unmodified PLGA NPs was quantified by a fluorescence assay using C6 loaded PLGA NPs. U251, U87 and NHA cells were seeded in 96-well plates at a density of 8000 cells per well and allowed to attach for 24 h. NPs samples were diluted in cell culture medium at final polymer concentration of 2.5 mM, and the cells were incubated with these samples for 0.5 h and 2 h. At the end of the incubation period, the cells were washed with cold PBS to remove the non-internalized NPs. The cells were then lysed with 0.1% Triton X-100 in 0.1 N NaOH solution. The fluorescence intensity from C6-loaded NPs was measured using a fluorescence microplate reader (HT Microplate Spectrophotometer, BioTek) with excitation and emission wavelengths set at 430 and 485 nm, respectively.

All samples were tested in triplicates and three independent experiments were conducted.

4.2.12 Transferrin competitive binding assay

Tf blocking assay was used to confirm whether the mAb-PLGA NPs are internalized through TfR-mediated endocytosis. Competitive binding to TfRs was achieved using an excess of Tf, and cellular uptake of PLGA NPs was quantified by fluorescence using C6 as mentioned above. U251, U87 and NHA cells were seeded in 96-well plates at a density of 8000 cells per well and allowed to attach for 24 h. Tf was diluted in cell culture medium and added to the cells at six final different concentrations ranging from 1 to 10 mg.mL^{-1}. The same range of concentrations of folate was used as control. After 1 h, cells were incubated for 2 h with C6-NPs samples at final polymer concentration of 2.5 mM. At the end of the incubation period, the cells were washed and lysed as described in the previous section. The fluorescence intensity from C6-loaded NPs was measured with excitation and emission wavelengths set at 430 and 485 nm, respectively.

All samples were tested in triplicates and three independent experiments were conducted.

4.2.13 Effects of NPs on human brain-like endothelial cells monolayer integrity

In accordance with French legislation, the donors' parents gave their informed consent for the collection of human umbilical cord blood. The protocol was approved by the French Ministry of Higher Education and Research (CODECOH DC2011-1321). All experiments were carried out in accordance with the approved protocol. The *in vitro* human brain-like endothelial cells (HBLECs) model consists of a co-culture of endothelial cells (derived from CD34$^+$-cells) and brain pericytes. Briefly, CD34$^+$-cells were isolated from human umbilical cord blood and then prompted to differentiate into endothelial cells via exposure to endothelial cell medium supplemented with 50 ng/mL vascular endothelial growth factor (PeproTech Inc., Rocky Hill, NJ, USA) (Pedroso et al., 2011). The CD34$^+$-derived endothelial cells thus obtained were seeded onto Matrigel (BD Biosciences, San Jose, CA, USA)-coated filters (Costar Transwell inserts, Corning Inc., Corning, NY, USA, pore size 3 µm, 8x10^{4}cells/cm^2) (Cecchelli et al., 2014). These inserts with cells were maintained with a dry bottom for one week (500 µL of medium in the upper compartment, changed every other day) to avoid the cells crossing the membrane and forming a non-physiological second layer on the lower face of the insert. Next, the inserts were transferred onto pericytes (50,000 cells per well, seeded in 12-well plates two days before the transfer). The resulting co-culture was cultured with endothelial cell medium supplemented with 5% heat inactivated fetal calf serum (GIBCO, Life Technology SAS, Saint Aubin, France) and 50 µg/mL gentamicin. The medium was changed every two days. These culture conditions were maintained for 5 days and enabled the CD34$^+$-derived endothelial cells to acquire a true BBB phenotype (i.e. HBLECs). Under these conditions, the model was stable for 30 days and was then ready for experiments (Cecchelli, et al., 2014; Kuntz et al., 2015).

The effect of non-modified and OX26 mAb-modified PLGA NPs on HBLECs cells was evaluated in Ringer HEPES buffer at 40 µM and 80 µM as previously described (Loureiro, et al., 2017). Culture medium was removed and replaced with NPs and with 1,5KBq/mL of ^{14}C-sucrose, in the luminal compartment. ^{14}C-sucrose was used as an indicator for the integrity of the BBB model. After 120 min, aliquots were taken in abluminal compartments of the cell culture and samples were analysed using Liquid Scintillation Analyser (Tri-carb 2100TR) for ^{14}C-sucrose. The endothelial permeability coefficient (Pe) of ^{14}C-sucrose was determined in cm/min.

4.2.14 *In vitro* cytotoxicity studies

The efficiency of non-modified and OX26 mAb-modified PLGA NPs in enhancing the antiproliferative effect of TMZ on different human cell lines was evaluated by the Sulforhodamine B (SRB) colorimetric method. SBR assay is sensitive, non-destructive, rapid and inexpensive assay that is used for the *in vitro* measurement of cellular protein content. SRB is an anionic bright pink aminoxanthene protein dye with two sulfonic groups. SBR binds to basic amino acids of proteins of TCA-fixed cells. The colorimetric evaluation provides an estimate total protein mass, which is related to cell number and therefore related to cell survival and viability (Voigt, 2005).

U251, U87 and NHA cells were seeded at a density of 1000 cells/well, in 96-well assay plates and incubated for 24 h (37 °C, in a humidified 5% CO_2 incubator) to allow complete cell adhesion. Then, TMZ, TMZ-PLGA NPs and mAb-TMZ-PLGA NPs, diluted in DMEM medium at ten final concentrations of TMZ ranging from 0.1 to 800 µM, were added to the cells. After an incubation period of 72 h, the cells were fixed with 10% (w/v) TCA for 1 h at 4 ºC, and stained with 0.4% (w/v) SRB dye for 30 min. After repeatedly washing the cells with 1% (v/v) acetic acid to remove unbound dye, the cells air-dried, and the protein-bound stain was solubilized with 10 mM Tris solution for UV-VIS absorbance quantification at 560 nm using the (BioTek Synergy HT Microplate Reader, BioTek, UK). Cell growth as a function of drug concentration was plotted using the following equation:

$$\text{Cell growth (\%)} = \frac{(T - T_0)}{(C - T_0)} \text{ x } 100 \qquad (4.4)$$

where T is the absorbance value at the end of the incubation period in the treated wells, T_0 is the absorbance value at the time of test sample administration and C is the absorbance value in the control wells (untreated cells).

Dose-response curves were then obtained using non-linear regression analysis and the GI_{50} value - the concentration inhibiting the net cell growth by 50% - for TMZ was calculated from the dose–response curve.

Unloaded PLGA and mAb-PLGA NPs were added as control to assess if they affect cell growth. Not exposed cells were also included in all assays as no-treatment controls (null controls). All samples were tested in triplicates and three independent experiments were conducted.

4.2.15 Statistical analysis

All results are presented as mean and standard deviation, for at least three independent experiments. Statistical analysis was performed using t-student test, with a 95% confidence interval. p<0.05 values were considered significant.

4.3 Results and Discussion

4.3.1 PLGA NPs physicochemical properties

Different TMZ-loaded PLGA NPs were prepared and in all the prepared formulations, PVA was used as an non-ionic emulsion stabilizer since it has a high affinity to PLGA and forms an uniform layer on the NPs' surface, conferring stability against aggregation (Gelperina et al., 2010). Maleimide-functionalized PEG was also used to allow covalent coupling of OX26 mAb at the PEG terminus with the chemically reactive end-group. The physicochemical properties of the prepared NPs were evaluated and are presented in table 4.1.

Table 4. 1 || Physicochemical features of unloaded PLGA NPs, TMZ-loaded PLGA NPs, mAb-modified PLGA NPs and TMZ-loaded mAb-modified PLGA NPs. Results are presented as mean ± SD (n=3).

PLGA NPs	Mean size (nm)	PdI	Zeta Potential (mV)
Unloaded PLGA NPs	176 ± 3	0.086 ± 0.015	-29 ± 3
TMZ-PLGA NPs	181 ± 2	0.059 ± 0.012	-25 ± 4
mAb-PLGA NPs	193 ± 4	0.067 ± 0.018	-30 ± 1
TMZ-mAb-PLGA NPs	194 ± 1	0.074 ± 0.024	-20 ± 2

The prepared unloaded NPs exhibited a mean diameter of 176 ± 3 nm, and a zeta potential value of -29 ± 3 mV, negative as expected due to the negative charge of the carboxylic groups of PLGA polymer (table 1). The TMZ molecules accommodation in the polymeric matrix caused a significant ($p<0.05$) increase in size for the TMZ-PLGA NPs (181 ± 2 nm). Moreover, NPs mean size was also significantly increased with OX26 mAb modification (194 ± 1 nm) ($p<0.05$), indicating an efficient conjugation since the diameter of the globular antibody is approximately 15 nm (Dammer et al., 1996). The prepared nanocarriers exhibited a small size distribution (PdI ≤ 0.1). Loading of the NPs with TMZ did not significantly affect their zeta potential, however a small decrease was observed due to the adsorption of TMZ molecules on PLGA NPs surface, exerting a masking effect on the superficial net charge (Musumeci et al., 2006). The modification of the NPs' surface with mAb also does not significantly alter their zeta potential, due to the negative nature of this immunoglobulin ($p>0.05$).

NP dimensions and zeta potential are key parameters that affect the efficiency of NP systemic circulation, and uptake by target cells (Wohlfart et al., 2012). Also transport across the BBB will depend on these parameters. Although mAb modification of the NPs' surface is expected to enhance the transport of NPs across the BBB through receptor-mediated transport, these two physiochemical characteristics also are determining factors. Thus, these parameters were considered during the design of this nanosystem. The prepared mAb-modified PLGA NPs exhibit suitable physicochemical characteristics for cancer cell uptake and transport across the BBB. Since neutral and anionic NPs are more easily transported across the BBB and are not associated to BBB toxicity (Wu et al., 2015), most of the NP formulations described in the literature for brain delivery have moderate to high (between −1 to −45 mV) negative zeta potentials, as the one prepared in this work (Saraiva et al., 2016). It has also been proven that NPs with dimensions up to 200 nm are more easily accumulated in brain tissue (Veszelka et al., 2015) since tumour microenvironment exhibits vascular fenestrations in the range of 40–200 nm (Wu, et al., 2015). Also NPs with dimensions up to 200 nm are more efficiently taken up by receptor-mediated endocytosis, as it was intended in this work with the use of TfR (Masserini, 2013).

The colloidal stability of the prepared NPs is a result of electric charge of the carboxylic groups at the NP surfaces, and the PVA layer on the NP's surface causing steric repulsions forming a mechanic barrier prohibiting droplet approaching (Tadros, 2015). In fact, figure 4.3 shows a stabilizer layer surrounding PLGA NPs. TEM analysis also show uniform PLGA NPs with a spherical form (figure 4.3). The mean size of the NPs revealed by TEM are in agreement with those determined by DLS analysis. Therefore, it can be concluded that the method followed for the preparation of PLGA NPs produced well-stabilized monodisperse TMZ-loaded PLGA NPs.

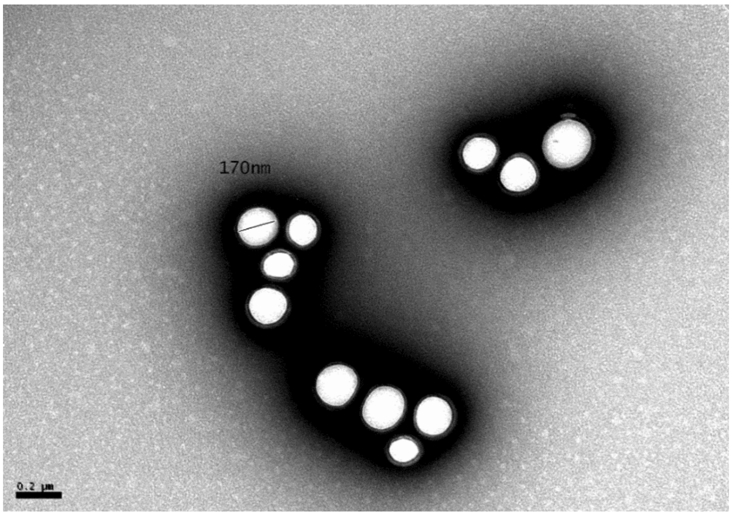

Figure 4. 3 | TEM image of the prepared PLGA NPs. Scale bar is 200 nm.

The binding ability of the mAb-modified NPs to TfR was evaluated by ELISA assays. OX26 mAb-modified NPs showed significantly higher absorbance at 405 nm (0.81 ± 0.05) than non-modified NPs (0.29 ± 0.08) ($p<0.05$). Therefore, OX26 mAb demonstrated that the bioactivity for the TfR is preserved after the mAb conjugation with the NPs.

4.3.2. Stability of PLGA NPs

Mean diameter and zeta potential values measured for the purpose of stability tests are presented in table 4.2. Mean size variation is expressed in terms of ratio St/Si. These data prove that the both mAb-modified and non-modified NPs remained physically stable at storage conditions (4 ^{o}C) for approximately 6 weeks.

Table 4. 2 | | Mean diameter and zeta potential values for both mAb-modified and non-modified TMZ-loaded NPs, over a period 42 days, respectively. Mean size variation is expressed in terms of ratio St/Si, where St is mean diameter after t days of storage and Si is the NPs initial mean size. Data represented as mean ± SD (n=3).

PLGA NPs	Mean diameter (nm)	Ratio S_t/S_i	Zeta potential (mV)
TMZ-NPs			
Day 1	181 ± 2	-	-25 ± 4
Day 7	188 ± 9	1.04	-23 ± 3
Day 14	180 ± 14	0.99	-22 ± 7
Day 21	193 ± 11	1.07	-21 ± 2
Day 28	190 ± 7	1.05	-20 ± 3
Day 35	193 ± 12	1.07	-23 ± 5
Day 42	187 ± 6	1.03	-21 ± 1
mAb-TMZ-NPs			
Day 1	194 ± 1	-	-20 ± 2
Day 7	196 ± 10	1.01	-18 ± 3
Day 14	199 ± 6	1.03	-23 ± 1
Day 21	207 ± 6	1.07	-16 ± 3
Day 28	203 ± 8	1.05	-21 ± 5
Day 35	199 ± 10	1.03	-18 ± 2
Day 42	201 ± 9	1.04	-17 ± 4

Zeta potential values showed a slight increase over time since applying an electric field to the sample may alter it, only values for size were considered for stability evaluation purposes.

4.3.3 TMZ encapsulation efficiency and drug loading of PLGA NPs

PLGA NPs loaded with TMZ showed EE values ranging from 48 ± 10% for mAb-PLGA NPs to 44 ± 3% for non-modified NPs, respectively. DL varied from 10 ± 2% for mAb-PLGA NPs to 9 ± 1% of the polymer weight for non-modified NPs. As expected, OX26 mAb modification did not shown any influence on the EE and DL values.

TMZ exhibits high affinity for the aqueous phase as predicted by its *log P* value of 0.36 (Marvin Sketch Calculator software, Chemaxon™). So, during the preparation of the emulsion, partition of high amounts of TMZ into the aqueous phase may occur, explaining the attained EE values.

4.3.4 TMZ release from the PLGA NPs

The prepared PLGA NPs were evaluated for their ability to sustain the release of TMZ. The *in vitro* release profile of TMZ from PLGA NPs was evaluated at 37 °C in PBS (pH 7.4, 0.01 M) to mimic the physiological pH and salt concentrations. The attained release curve is presented in figure 4.4.

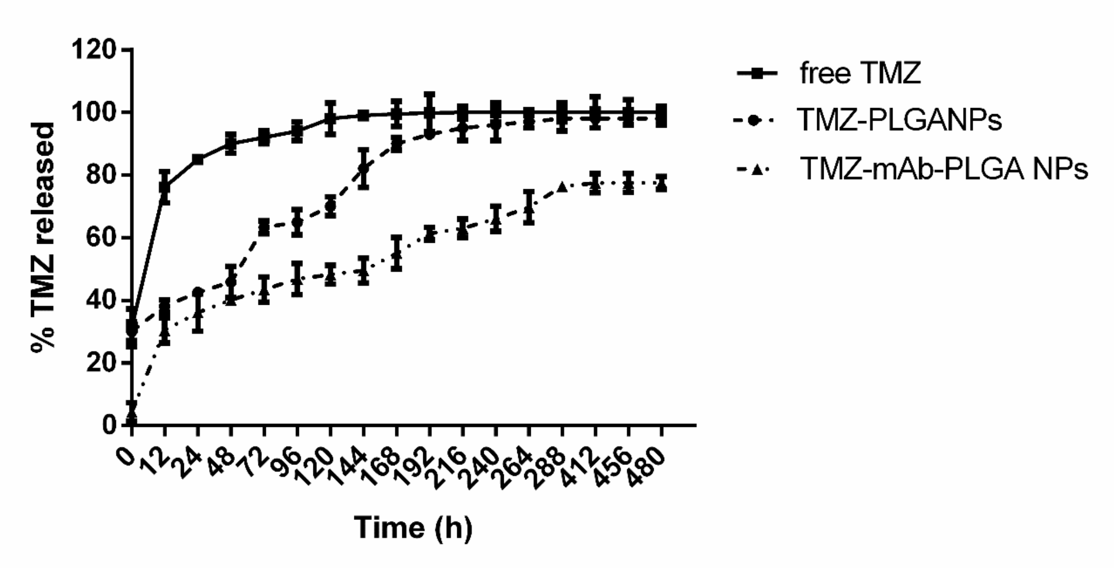

Figure 4. 4 | *In vitro* release of TMZ from mAb-modified and non-modified PLGA NPs in PBS (pH 7.4, 0.01 M) at 37 °C. Free TMZ was used as control. Results are represented as mean ± SD (n=3).

The dialysis method was used to compare the release of encapsulated TMZ with free TMZ. The drug molecules were released in a biphasic pattern, with an initial rapid released followed by a slower and controlled release, characteristic of PLGA NPs. As figure 4.4 shows, 36± 6% of the total TMZ was released at the first 24 h for mAb-modified PLGA NPs and 43 ± 1% for non-modified NPs, respectively. When in aqueous medium, the surface-adsorbed TMZ molecules are rapidly released from the NPs, explaining the verified burst release. The TMZ entrapped in NPs polymeric matrix exhibited a slower and controlled release for several days. This slow release occurs by a combination of three main pathways, the drug diffusion through NP matrix, NP matrix hydrolysis and NP erosion. PLGA polymer suffers hydrolytic cleavage of its ester's bonds into monomers, accumulating its acidic degradation products inside the polymeric matrix that are responsible for reaction auto-catalysis. The hydrolysis process also leads to the formation of pores, resulting in bulk erosion. Thus, the release rate of a drug will depend upon different factors such as drug physicochemical properties and geometry of drug-loaded PLGA NPs (size and shape) (Boimvaser et al., 2016).

The conjugation of mAbs on the surface of the PLGA NPs affected the TMZ release from the PLGA NPs, since it was observed a higher release from non-modified PLGA in comparison to mAb-PLGA NPs. Non-modified PLGA NPs exhibited a total release of TMZ (98 ± 2%) after 9 days, while mAb-modified NPs only released about 78 ± 2% of entrapped TMZ at day 20 (figure 4.4). These results may be explained by the mAb molecules linked to the surface of the NPs that may obstruct water permeation, hindering the diffusion of the drug molecules as previously reported (Loureiro, et al., 2016).

The obtained release profiles allow to conclude that the developed PLGA NPs are an adequate approach for the transport and release of TMZ, due to its biphasic and controlled pattern.

4.3.5 *In vitro* cellular uptake of mAb-PLGA NPs

C6 was used as fluorescence marker to visualize the cellular uptake of the prepared PLGA NPs by confocal microscopy, in malignant glioma cell lines – U87 and U251 - and in immortalized human astrocytes - NHA. This fluorescent dye is distributed in the NPs matrix, allowing their visualization inside the cellular compartments since during the time of the experiment only about 13% of the dye is released from the NPs (figure B.1 – annex B).

The cell nuclei were stained with DAPI and the acidic compartments, as endosomes and lysosomes, with LysoTracker Deep Red. The confocal images of non-treated and mAb-C6-PLGA NPs treated cells are presented in figure 4.5.

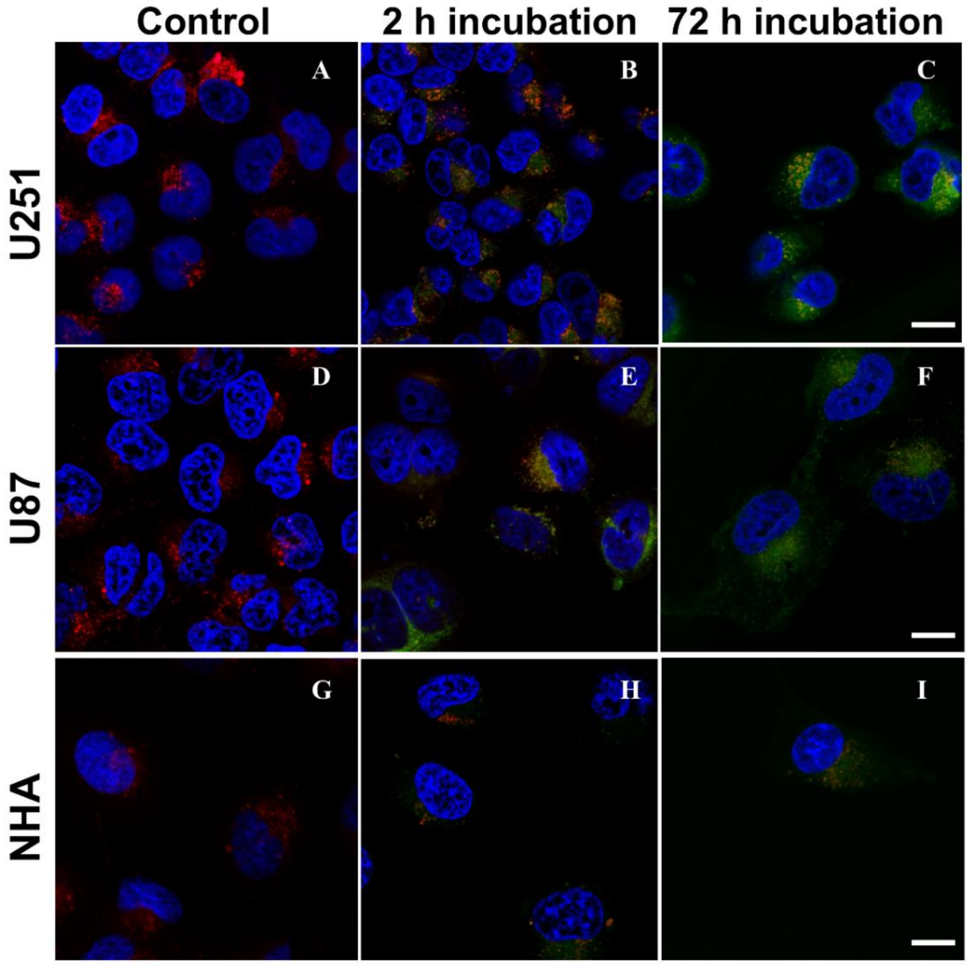

Figure 4. 5 | LSCM images of cells treated with mAb-C6-PLGA NPs. U251 cells: (A) control cells (without NPs treatment); cells after (B) 2 h and (C) 72 h of incubation with mAb-C6–PLGA NPs. U87 cells: (D) control cells (without NPs treatment); cells after (E) 2 h and (F) 72 h of incubation with mAb-C6–PLGA NPs. NHA cells: (G) control cells (without NPs treatment); cells after (H) 2 h and (I) 72 h of incubation with mAb-C6–PLGA NPs. The nuclei are marked in blue, the acidic compartments (late endosomes/lysosomes) in red and the C6-NPs in green. The colocalization of PLGA NPs within the late endosomes/lysosomes is represented by the yellow/orange colour. Scale bar: 25 µm.

After 2 h incubation, the NPs were uptaken by all the treated cells. The colocalization of C6-NPs and lysotracker-stained lysosomes is represented by the yellow/orange dots, due to the combined fluorescence of green and red emission, respectively (Dunn et al., 2011), suggesting that the NPs are internalized by an endocytic mechanism (figures 4.5.B, 4.5.E and 4.5.H). Also, as shown in figures 4.5.C, 4.5.F, 4.5.I, after 72 h incubation it is possible to visualize the NPs in the cytoplasm, suggesting that the NPs can escape the endo-lysosomal compartments. The images after 72 h incubation also show a decrease in the number of cells, due to the antiproliferative activity of the TMZ entrapped in the NPs. All the attained results suggest that these mAb-PLGA NPs are efficient cytoplasmic drug delivery vehicles, avoiding MDR mechanisms such as TMZ efflux from target cells.

4.3.6 Selective cellular uptake of mAb-PLGA NPs

C6 was also used to quantify the cellular internalization of the PLGA NPs in U251, U87 and NHA cell lines. The cellular internalization of mAb-modified and non-modified PLGA NPs was measured after 0.5 and 2 h of incubation, respectively. The results are expressed as the fluorescent intensity of C6 in figure 4.6.

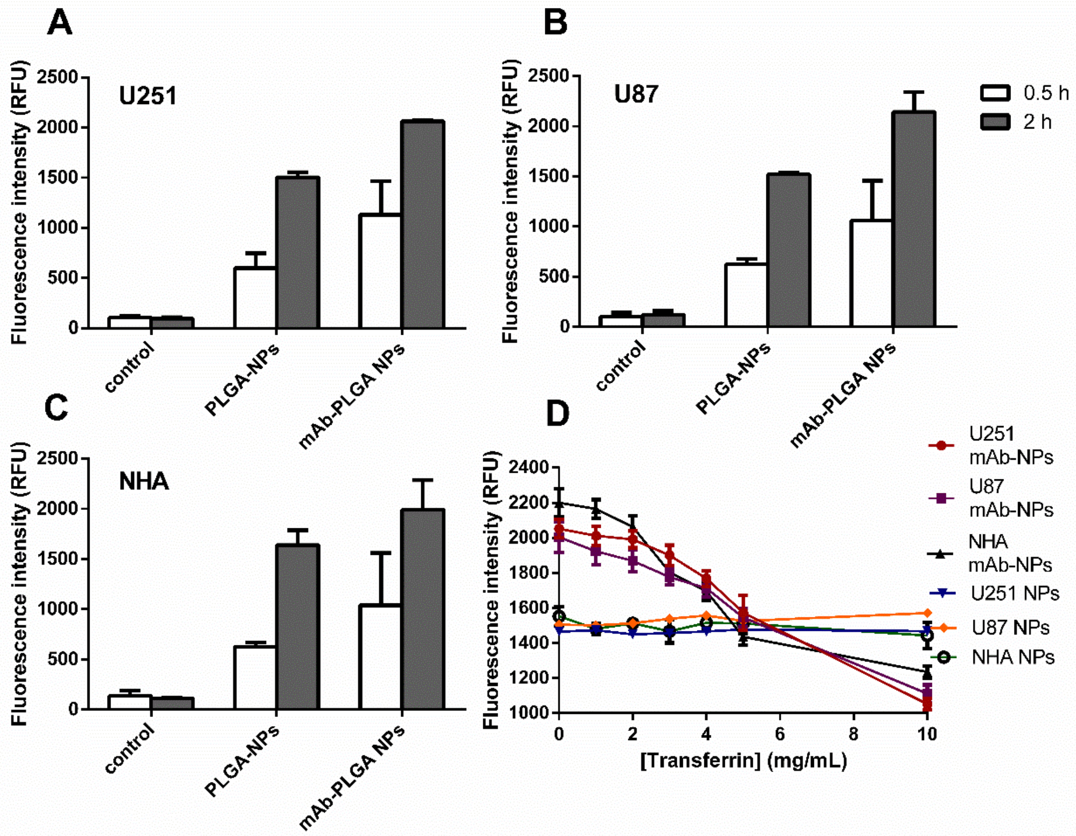

Figure 4. 6 | Quantification of cellular uptake of mAb-modified and non-modified PLGA NPs after 0.5 and 2 h incubation, in three human cell lines: (A) U251 cell line, (B) U87 cell line and (C) NHA cell line. (D) Quantification of cellular uptake of mAb-modified and non-modified PLGA NPs with TfR blocking with increase concentrations of transferrin. The cellular internalization of PLGA NPs is represented as the fluorescent intensity of coumarin-6. Data represented as mean ± SD (n=3).

As the attained results show, the NPs were efficiently internalized by the cells, showing that the longer the incubation time, the higher the cellular uptake ($p<0.05$). Also, modification of the PLGA NPs surface with mAb for TfR significantly increased the cellular internalization in all the studied cell lines for 2 h incubation period ($p<0.05$). Cellular uptake of mAb-NPs by U251 cells after 0.5 h and 2 h of incubation was found to be 1.89 and 1.37-fold higher than unmodified NPs, respectively. For U87 cells, the cellular uptake for mAb-NPs was 1.70 and 1.41-fold higher in 0.5 and 2 h incubation, respectively. Also, in NHA cells the cellular internalization of NPs increased with mAb modification, exhibiting uptake rates 1.67 and 1.21-fold higher in 0.5 h and 2 h incubation, respectively.

Tf competitive binding assay was used to investigate how TfR impacts the mAb-PLGA NPs cell internalization. Cells were pre-treated with increasing doses of Tf to block the TfR before the incubation with NPs. As figure 4.6.D shows, cellular internalization of mAb-NPs significantly decreased with blockage of TfR in a dose-depend manner, in all the studied cell lines ($p<0.05$). It was observed a decrease between 43 and 48% in the internalization of mAb-NPs when using 10 $mg.mL^{-1}$ of Tf. Blockage of the TfR did not affect the internalization of the non-modified NPs (figure 4.6.D). The same blocking experiment, using folate instead of TfR, was used as control, showing that pre-treatment with folate did not exhibit any effects on the mAb-NPs uptake (figure B.2 – annex B). Confocal studies displaying NPs in late endosomes/lysosomes suggest that these NPs are selectively uptaken by TfR-mediated endocytosis.

4.3.7 Effects of NPs on brain-like endothelial cells monolayer integrity

An *in vitro* model for the human BBB was used to assess whether the prepared NPs exhibited harmful effects on the monolayer integrity of the BBB-like cells. The *in vitro model* is composed of endothelial cells derived from hematopoietic umbilical cord blood and brain pericytes and is named Brain-like endothelial cells (HBLECs). Thus, the HBLECs model retains most of the features of the human BBB such as expression of membrane receptors, high transepithelial/transendothelial electrical resistance and low permeability to generally used permeability-markers, like sucrose molecules (Cecchelli, et al., 2014). The obtained results are shown in figure 4.7.

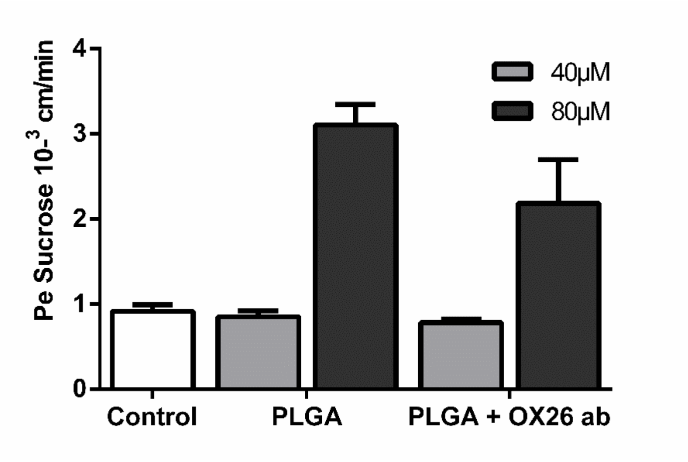

Figure 4. 7 | *In vitro* BBB model monolayer integrity assays. The effects of the studied NPs on the cellular monolayer integrity was assessed in terms of permeability of sucrose (a marker for BBB paracellular integrity). NPs were tested at two different concentrations, 40 and 80 µM, respectively. The results are expressed as mean and standard deviation (n=3).

Using the permeability of sucrose as a marker for integrity of the BBB model (Cecchelli et al., 1999; Deli et al., 2005), the results showed that non-modified and OX26 mAb-modified NPs, at a concentration of 40 µM, exhibited no harmful effects on the integrity of the BBB cellular model. Thus, at 80 µM, HBLEC monolayer integrity to sucrose has been increased, suggesting that in future work is necessary to use concentrations not higher than 40 µM to avoid any dramatic changes in BBB integrity (figure 4.7). These results suggest that is possible to use these NPs for TMZ delivery to GBM cells without causing harmful effects on the BBB integrity.

4.3.8 Cell growth inhibition by TMZ-loaded NPs

The *in vitro* antiproliferative activity of the TMZ-loaded NPs in comparison with free TMZ, was evaluated in two human GBM cells, U251 and U87. NHA cell line was also used as control. Bare PLGA NPS, at a concentration of 2.5 mM, showed no significant antiproliferative effect on the studied cell lines (figure 4.8), proving that the developed nanosystems is biocompatible.

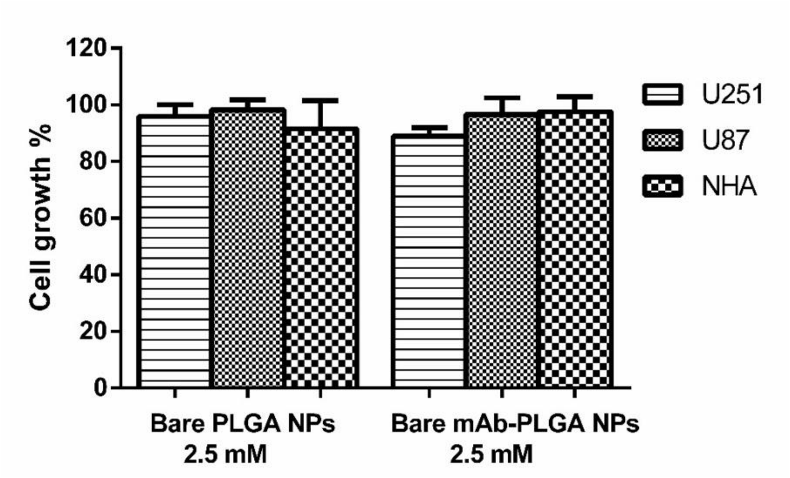

Figure 4. 8 | Cell growth after incubation period in the studied cells. The figures show data for cells treated with 2.5 mM of bare PLGA NPs and bare mAb-PLGA NPs. Growth inhibition is presented as percent [(%)=((T-T_0)/(C-T_0)) x 100]. Data represented as mean ± SD (n=3).

The effect of TMZ at different concentrations, ranging from 0.1 to 800 μM, was tested and the results are presented in figure 4.9 and table 4.3. It was verified that both free and encapsulated TMZ induce a concentration-related decrease in cell growth in all the studied cell lines (figure 4.9). TMZ entrapped in NPs inhibited the cellular growth more efficiently than free TMZ in all the cell lines, resulting in significantly lower GI_{50} values for both mAb-modified and unmodified NPs as shown in table 4.3 ($p<0.05$). Also, these results demonstrated that the TMZ deleterious effect is significantly lower in the non-tumour cell line ($p<0.05$). Although the NPs also potentiate the TMZ effect on NHA cells, these cells show more resistance to TMZ toxicity than U251 and U87 glioma cells, whether encapsulated or not.

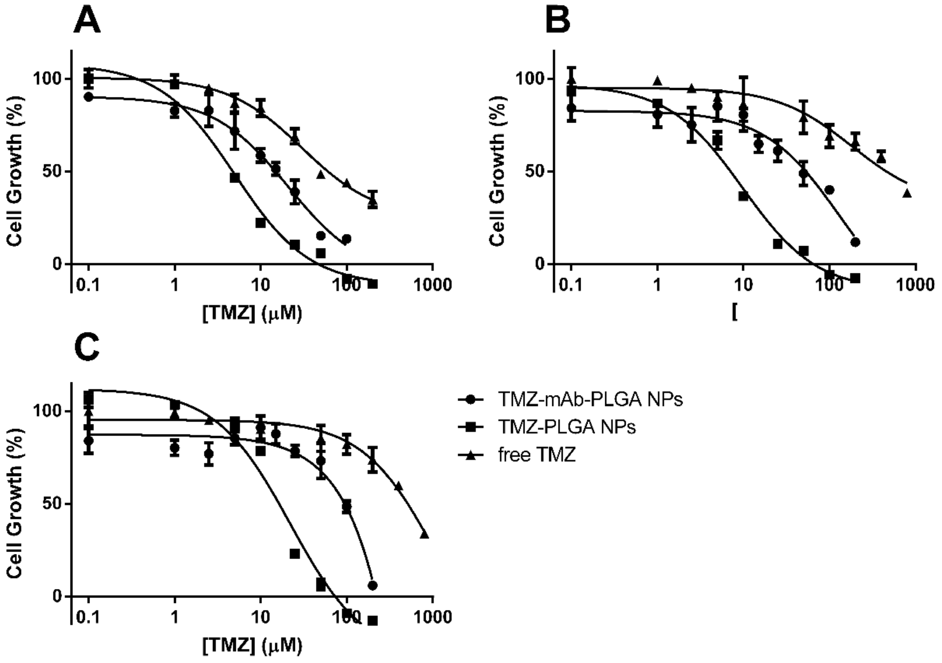

Figure 4. 9 | Cytotoxic effects of TMZ, free or entrapped in mAb-modified and unmodified PLGA NPs, after 72 h treatment on three human cell lines by SRB assay. (A) U251 cell line, (B) U87 cell line and (C) NHA cell line. Growth inhibition is presented as percent [(%)=((T-T_0)/(C-T_0)) x 100]. Data represented as mean ± SD (n=3).

U251 cell line exhibited the highest sensitivity to TMZ. TMZ-mAb-PLGA NPs are significantly more effective than free TMZ, exhibiting a GI_{50} value (15 ± 2 μM) about 4-fold lower than for free TMZ (61 ± 1 μM) in U251 cell line ($p<0.05$).

Table 4. 3 | Cytotoxic effects of TMZ on the growth of U251, U87 and NHA. Results are expressed as GI50 at 72 h of exposure with TMZ, either free or entrapped in mAb-modified and unmodified PLGA NPs, using SRB assay. Data represented as mean ± SD (n=3).

	GI_{50} (μM)		
	U251	**U87**	**NHA**
TMZ-PLGA NPs	4 ± 1	7 ± 1	16 ± 1
TMZ-mAb-PLGA NPs	15 ± 2	50 ± 2	97 ± 3
free TMZ	61 ± 1	493 ± 3	540 ± 7

As the bare NPs did not show any harmful effects, it is possible to conclude that the observed enhanced antiproliferative effect is due to the beneficial effects of encapsulating the TMZ that increase its bioavailability by conferring protection and allowing the transport across the biological barriers. In fact, the entrapment of TMZ in PLGA NPs improves its intracellular delivery, since free TMZ is expected to be transported into cells by a passive diffusion mechanism, suffering a MDR mechanism mediated by the membrane p-glycoprotein pump (Panyam and Labhasetwar, 2003; Vasir and Labhasetwar, 2007). Instead, NPs may be more efficiently transported by receptor-mediated endocytosis. Although internalization of mAb-modified NPs was enhanced, as shown by the *in vitro uptake* studies suggesting that these NPs are transported into the cells through TfR-mediated endocytosis, the cytotoxic effect of TMZ was decreased with the mAb-modification of the NPs' surface (figure 4.9 and table 4.2) ($p<0.05$). In fact, TMZ-PLGA NPs was the formulation that exhibited higher toxicity, with for example a GI_{50} value of 4±1 for the U251 cell line. The decrease in the cytotoxic effect when using mAb-NPs, comparatively with non-modified NPs, is probably due to the lower release rate of the drug, already mentioned in section 4.3.4. Still, both formulations – mAb-modified and unmodified NPs – can improve the *in vitro* therapeutic efficacy of TMZ, indicating that the use of the mAbs should present advantages in *in vivo* conditions, allowing an increased transport of the drug across the BBB.

So, NPs functionalized with an OX26 mAb for TfR could be efficiently used for dual-targeting of both BBB and GBM cells. Therefore, mAb-PLGA NPs was the chosen nanoformulation for the next tasks of this work.

References

Boimvaser, S., Mariano, R.N., Turino, L.N., Vega, J.R. 2016. In vitro bulk/surface erosion pattern of PLGA implant in physiological conditions: a study based on auxiliary microsphere systems. Polymer Bulletin. 73 (1), 209-227.

Calzolari, A., Larocca, L.M., Deaglio, S., Finisguerra, V., Boe, A., Raggi, C., Ricci-Vitani, L., Pierconti, F., Malavasi, F., De Maria, R., Testa, U., Pallini, R. 2010. Transferrin Receptor 2 Is Frequently and Highly Expressed in Glioblastomas. Translational Oncology. 3 (2), 123-134.

Cecchelli, R., Aday, S., Sevin, E., Almeida, C., Culot, M., Dehouck, L., Coisne, C., Engelhardt, B., Dehouck, M.-P., Ferreira, L. 2014. A Stable and Reproducible Human Blood-Brain Barrier Model Derived from Hematopoietic Stem Cells. PLoS ONE. 9 (6), e99733.

Cecchelli, R., Dehouck, B., Descamps, L., Fenart, L., Buée-Scherrer, V., Duhem, C., Lundquist, S., Rentfel, M., Torpier, G., Dehouck, M.P. 1999. In vitro model for evaluating drug transport across the blood–brain barrier. Advanced drug delivery reviews. 36 (2), 165-178.

Coelho, S.C., Pereira, M.C., Juzeniene, A., Juzenas, P., Coelho, M.A.N. 2015. Supramolecular nanoscale assemblies for cancer diagnosis and therapy. Journal of Controlled Release. 213 152-167.

Dammer, U., Hegner, M., Anselmetti, D., Wagner, P., Dreier, M., Huber, W., Güntherodt, H.J. 1996. Specific antigen/antibody interactions measured by force microscopy. Biophysical Journal. 70 (5), 2437-2441.

Danhier, F., Ansorena, E., Silva, J.M., Coco, R., Le Breton, A., Preat, V. 2012. PLGA-based nanoparticles: an overview of biomedical applications. Journal of controlled release : official journal of the Controlled Release Society. 161 (2), 505-522.

Deli, M.A., Ábrahám, C.S., Kataoka, Y., Niwa, M. 2005. Permeability Studies on In Vitro Blood–Brain Barrier Models:Physiology, Pathology, and Pharmacology. Cellular and Molecular Neurobiology. 25 (1), 59-127.

Dunn, K.W., Kamocka, M.M., McDonald, J.H. 2011. A practical guide to evaluating colocalization in biological microscopy. American Journal of Physiology - Cell Physiology. 300 (4), C723-C742.

Franken, L.E., Boekema, E.J., Stuart, M.C.A. 2017. Transmission Electron Microscopy as a Tool for the Characterization of Soft Materials: Application and Interpretation. Advanced Science. 4 (5), 1600476.

Frasco, M.F., Almeida, G.M., Santos-Silva, F., Pereira, M.d.C., Coelho, M.A. 2015. Transferrin surface-modified PLGA nanoparticles-mediated delivery of a proteasome inhibitor to human pancreatic cancer cells. Journal of Biomedical Materials Research Part A. 103 (4), 1476-1484.

Gelperina, S., Maksimenko, O., Khalansky, A., Vanchugova, L., Shipulo, E., Abbasova, K., Berdiev, R., Wohlfart, S., Chepurnova, N., Kreuter, J. 2010. Drug delivery to the brain using surfactant-coated poly(lactide-co-glycolide) nanoparticles: Influence of the formulation parameters. European Journal of Pharmaceutics and Biopharmaceutics. 74 (2), 157-163.

González-Martínez, M.Á., Puchades, R., Maquieira, Á. 2018. Chapter 15 - Immunoanalytical Technique: Enzyme-Linked Immunosorbent Assay (ELISA), in: D.-W. Sun (Ed.) Modern Techniques for Food Authentication (Second Edition), Academic Press, pp. 617-657.

Holzer, M., Vogel, V., Mäntele, W., Schwartz, D., Haase, W., Langer, K. 2009. Physico-chemical characterisation of PLGA nanoparticles after freeze-drying and storage. European Journal of Pharmaceutics and Biopharmaceutics. 72 (2), 428-437.

Jacobs, V.L., Valdes, P.A., Hickey, W.F., De Leo, J.A. 2011. Current review of in vivo GBM rodent models: emphasis on the CNS-1 tumour model. ASN NEURO. 3 (3), e00063.

Kuntz, M., Candela, P., Saint-Pol, J., Lamartiniere, Y., Boucau, M.C., Sevin, E., Fenart, L., Gosselet, F. 2015. Bexarotene Promotes Cholesterol Efflux and Restricts Apical-to-Basolateral Transport of Amyloid-beta Peptides in an In Vitro Model of the Human Blood-Brain Barrier. Journal of Alzheimer's disease : JAD. 48 (3), 849-862.

Lin, A.V. 2015. Indirect ELISA, in: R. Hnasko (Ed.) ELISA: Methods and Protocols, Springer New York, New York, NY, pp. 51-59.

Lockman, P.R., Mumper, R.J., Khan, M.A., Allen, D.D. 2002. Nanoparticle Technology for Drug Delivery Across the Blood-Brain Barrier. Drug Development and Industrial Pharmacy. 28 (1), 1-13.

Loureiro, J., Andrade, S., Duarte, A., Neves, A., Queiroz, J., Nunes, C., Sevin, E., Fenart, L., Gosselet, F., Coelho, M., Pereira, M. 2017. Resveratrol and Grape Extract-loaded Solid Lipid Nanoparticles for the Treatment of Alzheimer's Disease. Molecules. 22 (2), 277.

Loureiro, J.A., Gomes, B., Coelho, M.A., Carmo Pereira, M.d., Rocha, S. 2014. Targeting nanoparticles across the blood-brain barrier with monoclonal antibodies. Nanomedicine. 9 (5), 709-722.

Loureiro, J.A., Gomes, B., Fricker, G., Coelho, M.A.N., Rocha, S., Pereira, M.C. 2016. Cellular uptake of PLGA nanoparticles targeted with anti-amyloid and anti-transferrin receptor antibodies for Alzheimer's disease treatment. Colloids and Surfaces B: Biointerfaces. 145 8-13.

Makadia, H.K., Siegel, S.J. 2011. Poly Lactic-co-Glycolic Acid (PLGA) as Biodegradable Controlled Drug Delivery Carrier. Polymers. 3 (3), 1377-1397.

Masserini, M. 2013. Nanoparticles for Brain Drug Delivery. ISRN Biochemistry. 2013 18.

Musumeci, T., Ventura, C.A., Giannone, I., Ruozi, B., Montenegro, L., Pignatello, R., Puglisi, G. 2006. PLA/PLGA nanoparticles for sustained release of docetaxel. International journal of pharmaceutics. 325 (1-2), 172-179.

Panyam, J., Labhasetwar, V. 2003. Biodegradable nanoparticles for drug and gene delivery to cells and tissue. Advanced drug delivery reviews. 55 (3), 329-347.

Pedroso, D.C.S., Tellechea, A., Moura, L., Fidalgo-Carvalho, I., Duarte, J., Carvalho, E., Ferreira, L. 2011. Improved Survival, Vascular Differentiation and Wound Healing Potential of Stem Cells Co-Cultured with Endothelial Cells. PLoS ONE. 6 (1), e16114.

Pillai, G. 2014. Nanomedicines for Cancer Therapy: An Update of FDA Approved and Those under Various Stages of Development. SOJ Pharm Pharm Sci. 1 (2), 1-13.

Ramalho, M.J., Loureiro, J., Gomes, B., Frasco, M.F., Coelho, M.A.N., Pereira, M.C. 2015. PLGA nanoparticles for calcitriol delivery. Proceedings - 2015 IEEE 4th Portuguese Meeting on Bioengineering, ENBENG 2015.

Ramalho, M.J., Pereira, M.C. 2016. Preparation and Characterization of Polymeric Nanoparticles: An Interdisciplinary Experiment. Journal of Chemical Education. 93 (8), 1446-1451.

Saraiva, C., Praça, C., Ferreira, R., Santos, T., Ferreira, L., Bernardino, L. 2016. Nanoparticle-mediated brain drug delivery: Overcoming blood–brain barrier to treat neurodegenerative diseases. Journal of Controlled Release. 235 34-47.

Stepišnik Perdih, T., Zupanc, M., Dular, M. 2019. Revision of the mechanisms behind oil-water (O/W) emulsion preparation by ultrasound and cavitation. Ultrasonics Sonochemistry. 51 298-304.

Stupp, R., Gander, M., Leyvraz, S., Newlands, E. 2001. Current and future developments in the use of temozolomide for the treatment of brain tumours. The Lancet Oncology. 2 (9), 552-560.

Tadros, T. 2015. Viscoelastic properties of sterically stabilised emulsions and their stability. Advances in Colloid and Interface Science. 222 692-708.

Vasir, J.K., Labhasetwar, V. 2007. Biodegradable nanoparticles for cytosolic delivery of therapeutics. Advanced drug delivery reviews. 59 (8), 718-728.

Veszelka, S., Bocsik, A., Walter, F.R., Hantosi, D., Deli, M.A. 2015. Blood-brain barrier co-culture models to study nanoparticle penetration: Focus on co-culture systems. Acta Biologica Szegediensis. 59 157-168.
Voigt, V. 2005. Sulforhodamine B Assay and Chemosensitivity, in: R.D. Blumenthal (Ed.), Humana Press Inc., Totowa, NJ.
Wohlfart, S., Gelperina, S., Kreuter, J. 2012. Transport of drugs across the blood–brain barrier by nanoparticles. Journal of Controlled Release. 161 (2), 264-273.
Wu, M., Fan, Y., Lv, S., Xiao, B., Ye, M., Zhu, X. 2015. Vincristine and temozolomide combined chemotherapy for the treatment of glioma: a comparison of solid lipid nanoparticles and nanostructured lipid carriers for dual drugs delivery. Drug Delivery. 1-6.

Chapter 5 - PLGA nanoparticles for the co-delivery of temozolomide and O6-benzylguanine

5.1 Introduction

TMZ exhibits a great potential as a chemotherapeutic drug for GBM therapy. However, its clinical use has been questioned due to the ineffective therapeutic effects caused by intrinsic resistance mechanisms. In fact, it is well-reported that MGMT enzyme is one of the major factors limiting the therapeutic efficiency of TMZ by repairing the DNA damage induced by the drug (Lee, 2016). Thus, being a highly aggressive tumour with poor survival outcomes, is urgent to find new approaches for its treatment. A promising strategy is the use of molecules able to revert or inhibit these intrinsic resistance mechanisms.

O6BG has gained attention in the scientific community since it has proved to increase the sensitivity of GBM cells resistant to TMZ, potentiating the drug's cytotoxic effects (Quinn et al., 2009; Warren et al., 2005; Warren et al., 2012). This molecule is a guanine analogue as shown in figure 5.1, that inhibits DNA repair by binding to the MGMT protein, inactivating it (Kaina et al., 2010). Therefore, co-therapy with TMZ and O6BG appears to be a suitable strategic approach for the treatment of resistant GBM, and has shown good outcomes in clinical trials (Quinn, et al., 2009; Warren, et al., 2012).

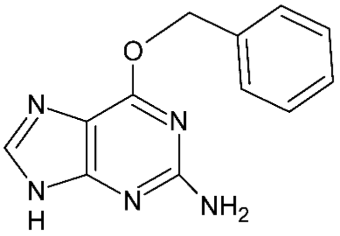

Figure 5. 1 | Schematic representation of the chemical structure of O6BG (drawn in ACD/ChemSketch).

However, the systemic delivery of two free drugs usually leads to an infective pharmacological activity and consequent treatment failure. This occurs mostly due to differences in the pharmacokinetics and biodistribution of each drug (Miao et al., 2014). The delivery of both drugs using a nanocarrier should address this problem. Nanoencapsulation of O6BG also may reduce its toxicity in healthy tissues by targeted delivery. Accumulation of O6BG in healthy tissues is undesirable to avoid inactivation of MGMT protein in these tissues and consequent exacerbated toxicity of the alkylating agents (S. Srivenugopal et al., 2016).

Thus, the aim of this chapter was to prepare a nanocarrier for the co-loading of both drugs and to evaluate its efficiency in the co-delivery into the GBM tumour cells. For that, the nanosystem proposed in the previous chapter was optimized using a factorial experimental design for the entrapment of both drugs. The antiproliferative effect of TMZ and O6BG entrapped in the NPs was evaluated in GBM cell lines. The developed NP is schematized in figure 5.2.

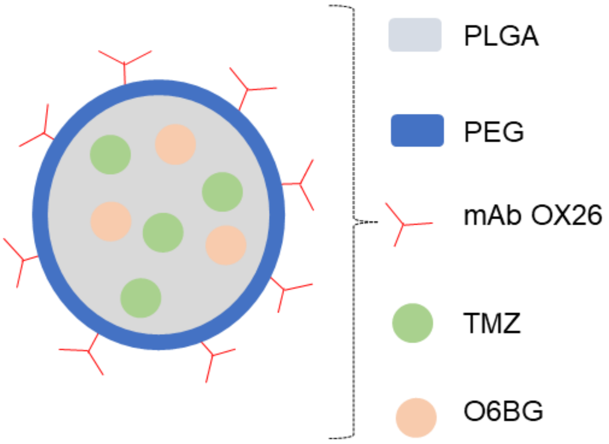

Figure 5. 2 | Schematic representation of the proposed nanosystem.

5.2 Materials and Methods

5.2.1 Materials

O6BG (MW 241.25) was acquired from Abcam (Cambridge, UK). All the other used reagents are already mentioned in section 4.2.1.

5.2.2 Cell lines

Two human GBM cells, U251 and T98G were used. T98G cell line was obtained from ATCC (Virginia,USA) and was chosen due to its well-reported high MGMT expression (Perazzoli et al., 2015). U251 cell line was chosen for comparison due to exhibiting high sensitive to TMZ's activity (Lee, 2016). Both cell lines were cultured in DMEM supplemented with 10% FBS and 1% penicillin-streptomycin. Cells were maintained at 37 °C in a humidified 5% CO_2 incubator. At 80% of confluence, the cells were trypsinized and subcultured.

5.2.3 Preparation of TMZ+O6BG-loaded PLGA NPs

PLGA NPs containing both TMZ and 06BG were prepared using the single emulsion-solvent evaporation technique as described in the previous chapter. For that, TMZ and O6BG were dissolved in a known volume of dichloromethane to prepare the organic phase. PVA solution was also used as the aqueous phase.

5.2.4 Experimental design and data analysis

High and comparable EE of each drug is a prerequisite for the co-loading in the same NP. In preliminary studies, it was verified that the addition of O6BG reduced the encapsulation of TMZ. Thus, it was necessary to optimize the entrapment of both drugs. To obtain an optimized formulation is useful to evaluate the influence of several experimental parameters on the entire production process.

Therefore, a 2^{5-2} fractional factorial design was implemented using the Minitab Statistical Software (Minitab Inc., Pennsylvania, USA) to determine the effect of different experimental parameters on the PLGA NPs features. The studied independent variables were the quantity of used drugs, amount of surfactant and organic solvent, and the amount of polymer. A variation of a full factorial design in which only a subset of the total runs was performed. The chosen factors of interest were varied on two levels (determined in preliminary studies) according to the experimental plan presented in table 5.1. Two replicates were conducted for each combination and for centre levels, and the order of the experiments was randomized to avoid any bias.

Table 5. 1 | Process and formulation parameters of the fractional factorial design.

Parameter	Component	Units	Applied level		
			Low level (-1)	**Centre level (0)**	**High level (+1)**
X_1	m_{TMZ}	mg	0.25	0.5	1
X_2	$m_{O6\text{-}BG}$	mg	0.25	0.5	1
X_3	$\%_{PVA}$	% (w/v)	2	3	4
X_4	V_{DCM}	mL	0.5	0.75	1
X_5	m_{PLGA}	mg	10	15	20

Note: The model was expanded for variables X_1 and X_2, since different increments of levels were used.

The analysed response dependent variables were the NPs size, PdI, zeta potential values and EE of both TMZ and O6-BG. For the experimental design, 18 formulations were prepared and an overview of the experimental plan including the results is given in table 5.2.

Table 5. 2 | Overview of the experimental design and results. The two experimental levels (low, centre and high) are represented by the normalized values of −1, 0 and +1, respectively.

Run order	Coded independent variables					Measured dependent variables				
									EE (%)	
	X_1	X_2	X_3	X_4	X_5	mean size (nm)	PdI	zeta potential (mV)	TMZ	O6-BG
1	+1	+1	-1	+1	-1	183	0.148	-26.2	55.1	78.5
2	-1	+1	+1	-1	-1	202	0.110	-26.7	38.7	74.1
3	0	0	0	0	0	171	0.106	-26.0	43.7	70.9
4	+1	+1	-1	+1	-1	179	0.165	-24.1	56.7	80.8
5	-1	-1	-1	+1	+1	178	0.132	-24.4	53.5	94.0
6	-1	+1	-1	-1	+1	193	0.158	-22.4	52.3	91.6
7	+1	-1	-1	-1	-1	162	0.158	-27.5	31.8	99.0
8	0	0	0	0	0	180	0.156	-24.8	46.2	76.4
9	-1	-1	+1	+1	-1	192	0.190	-27.0	42.6	79.7
10	+1	+1	+1	+1	+1	171	0.142	-20.3	27.2	78.5
11	+1	-1	+1	-1	+1	200	0.137	-22.7	40.3	99.8
12	+1	-1	+1	-1	+1	205	0.109	-22.5	46.3	99.6
13	+1	+1	+1	+1	+1	180	0.118	-22.3	28.9	82.6
14	+1	-1	-1	-1	-1	176	0.125	-28.0	36.6	99.5
15	-1	+1	-1	-1	+1	189	0.130	-21.7	50.9	95.5
16	-1	-1	-1	+1	+1	172	0.158	-23.4	54.5	98.0
17	-1	-1	+1	+1	-1	184	0.146	-26.2	46.7	78.1
18	-1	+1	+1	-1	-1	205	0.141	-27.5	36.5	76.9

The applied experimental design accounts for main terms and two-factor interactions terms. The later refers to two different variables that interact with each other creating a combined effect on the response, that independently would not occur. Therefore, the main effects and the two-factor interactions are included in the used statistical model. Thus, regression equations were obtained for each studied dependent variable to quantify the relationship between these and all the experimental independent variables. The experimental data was then fitted to the following polynomial regression model (Cun et al., 2011):

$$Y = \beta_0 + \sum_{i=1}^{5} \beta_i X_i + \sum \beta_{ij} X_i X_j \tag{5.1}$$

in which Y is the predicted response; β_0 is the intercept term and the remaining term; $X_{i,j}$ are the levels of the independent variables; and $\beta_{j,i}$ are the fitted coefficients for $X_{i,j}$.

The statistical models for the different dependent variables were fitted independently. And, the polynomial equations were statistically validated using ANOVA by statistical significance of coefficients, r^2 values and normal distribution of the residues. Minitab Statistical Software was also used for the statistical analysis of the data.

5.2.5 Preparation of TMZ+O6BG-loaded mAb-PLGA NPs

TMZ+O6BG-loaded PEG-PLGA NPs were prepared using also the single emulsion-solvent evaporation technique. For that, PLGA was pegylated as previously described in section 4.2.4. A known amount of non-modified PLGA was then added to the prepared PEG-PLGA, and the remaining protocol was performed using the chosen optimal experimental conditions in the experimental design.

All formulations were prepared in triplicate.

5.2.6 PLGA NPs physicochemical characterization

The size, PdI and zeta potential were the used parameters to characterize the prepared PLGA NPs. The measurements were performed in a ZetaSizer Nano ZS, Malvern Instruments, UK. At least three independent measurements were performed.

Size and zeta potential variations over time were also evaluated to assess NPs' stability. PLGA NPs' dispersions in ultrapure water were stored at 4 °C and DLS and ELS measurements were performed at different timepoints.

Efficiency of OX26 mAb conjugation was evaluated by ELISA assay as previously described in section 4.2.6.4.

5.2.7 Drug encapsulation efficiency and drug loading of PLGA NPs

The EE and DL values of the prepared PLGA NPs were determined by UV–Vis spectrophotometry. Non-encapsulated TMZ and O6BG were obtained from centrifugation of NPs suspension and quantified using a UV-1700 PharmaSpec UV-Vis spectrophotometer from Shimadzu (Japan). The results were correlated to control samples corresponding to total amount of drug. Three independent experiments were conducted.

5.2.8 *In vitro r*elease of TMZ from PLGA NP*s*

In vitro drug release studies were performed using a cellulose dialysis membrane diffusion technique for 20 days at 37°C. PBS (pH 7.4, 0.01 M) was used as the release buffer. The amount of drug release ate predetermined timepoints was quantified by UV-Vis spectrophotometry. A solution of TMZ and O6BG in PBS was used as control. Three independent experiments were conducted.

5.2.9 *In vitro* cytotoxic effect of TMZ and O6BG combination

The antiproliferative effects of TMZ alone and in combination with O6BG were compared in two human glioblastoma cell lines, U251 and T98G, by the SRB assay.

U251 and T98G cells were seeded at a density of 1000 cells/well, in 96-well assay plates and incubated for 24 h (37 °C, in a humidified 5% CO_2 incubator). Then, TMZ alone and combination of TMZ and O6BG diluted in DMEM medium at eight final concentrations of TMZ ranging from 0.1 to 3000 μM, were added to the cells. Four different TMZ/O6BG ratios were tested, 1:1, 1:1.2, 1:2 and 2:1. After an incubation period of 72 h, the SRB protocol was conducted as previously described in section 4.2.14. Cell growth as a function of TMZ concentration was plotted, and the GI_{50} value was determined by non-linear regression analysis.

O6BG alone at different concentrations was added as control to assess if it affects cell growth. Not exposed cells were also included in all assays as no-treatment controls (null controls). All samples were tested in triplicates and three independent experiments were conducted.

5.2.10 *In vitro* cytotoxicity of the PLGA NPs

The efficiency of OX26 mAb-PLGA NPs in enhancing the antiproliferative effect of both drugs was also evaluated using the SRB assay. For that, 100 µL of U251 and T98G cells at a concentration of 10000 cells.mL^{-1} were seeded in a 96-well plate. After an incubation period of 24 h (37 °C, in a humidified 5% CO_2 incubator), the cells were treated with O6BG+TMZ-mAb-PLGA NPs diluted in DMEM medium at six final concentrations of TMZ ranging from 0.1 to 200 µM. The TMZ/O6BG ratio in the NPs was 1:1.2. After an incubation period of 72 h, the SRB protocol was conducted as already described. Cell growth as a function of TMZ concentration was plotted, and the GI_{50} value was determined by non-linear regression analysis.

Unloaded mAb-PLGA NPs were added as control to assess if they affect cell growth. Not treated cells were also used as controls (null controls). All samples were tested in triplicates and three independent experiments were conducted.

5.2.11 Statistical analysis

All results are presented as mean and standard deviation, for at least three independent experiments. Statistical analysis was performed using t-student test and ANOVA, and p-values ≤ 0.05 were considered significant.

5.3 Results and Discussion

5.3.1 Optimization of the TMZ+O6BG PLGA NPs

The experimental design allowed to identify the experimental factors influencing the physicochemical properties of the NPs, as their size, polydispersity and zeta potential, as also the efficiency of incorporation of both drugs on the polymeric matrix. Based on the previously nanoformulation studies, five major variables affecting the PLGA NPs properties and drug EE were identified: amount of TMZ, amount of O6BG, amount of surfactant, amount of organic solvent and amount of polymer. All other parameters, as time of sonication, type of surfactant and organic solvent, temperature, emulsification process, evaporation process, aqueous to organic phase ratio, were kept constant to minimize fluctuations.

Statistical analysis and calculated *p*-values were determined together with the fitting mathematical model (equation 5.1) involving the individual main effects and interaction factors and are presented in table 5.3. The regression coefficient (RC) describes the size and direction of the relationship between a predictor and the variable response. The positive sign before a factor reveals that this response increases whereas the negative sign indicates that the response decreases with the factor. Interaction terms are represented by more than one factor in the regression equations. The size of the coefficient is usually a good way to assess the practical significance of the effect that a term has on the response variable. However, the size of the coefficient does not indicate whether a term is statistically significant since the calculations for significance also consider the variation in the response data. To determine statistical significance, it is important to evaluate the p-value for the term (Cun, et al., 2011). p-values lower than 0.05 were considered significant, at a 95% confidence interval.

Table 5. 3 | Summary of the results of regression analysis for the studied responses.

Parameter	**Size (Y_1)**		**PdI (Y_2)**		**Zeta potential (Y_3)**		**EE % TMZ (Y_4)**		**EE % O6-BG (Y_5)**	
	RC	***p*-value**	**RC**	***p*-value**	**RC**	***p*-value**	**RC**	***p*-value**	**RC**	***p*-value**
X_1	431	0.026	0.504	0.492	-21.3	0.424	-11.3	0.875	623.6	0.001
X_2	525	0.01	0.523	0.479	-24.7	0.358	70.4	0.341	602.7	0.001
X_3	15.05	0.001	0.0051	0.661	-0.928	0.049	-3.4	0.014	-4.12	0.005
X_4	373	0.031	0.496	0.455	-19.6	0.415	5.7	0.93	540.2	0.001
X_5	1.644	0.011	-0.00266	0.269	-0.3726	0.001	1.461	0.008	0.854	0.004
X_1X_2	-705	0.024	-0.82	0.485	32.6	0.445	4	0.972	-990	0.001
X_2X_3	-13.41	0.004	-0.0163	0.32	1.242	0.054	-13.87	0.004	-0.17	0.915
X_2X_5	-2.541	0.006	0.00227	0.483	-0.074	0.527	-2.153	0.007	0.093	0.767
R^2	**0.907**		**n.a.**		**0.931**		**0.967**		**0.975**	

The high R^2 values obtained showed that all responses, excepted PdI, are well fitted and predicted by the used model, indicating a good and valid model with good predictive power.

For all the studied dependent variables, standardized Pareto charts are given presenting the results of the statistical significance analysis. Also, polynomial equations were determined showing the relationship between the independent variables, and each of the dependent variables measured as well as the corresponding RC values. Response surface analysis and contour graphs were plotted based on the determined model polynomial function in a three or two-dimensional model, respectively, depicting the effect of the chosen significant independent factors on each observed response. The effect of all the independent variables on each dependent variable was studied and the effects of the most significant variables are discussed in detail below.

5.3.1.1 Effect on NPs' size

The size of the NPs is a critical property, influencing its half-life, biodistribution and cellular internalization, as already mentioned. The size of the NPs ranged from 162 nm (sample 7) to 205 nm (sample 12), with the selected levels of variables. All the studied variables affected significantly the size of the NPs ($p<0.05$) as shown in table 5.3 and in Pareto chart (figure 5.3).

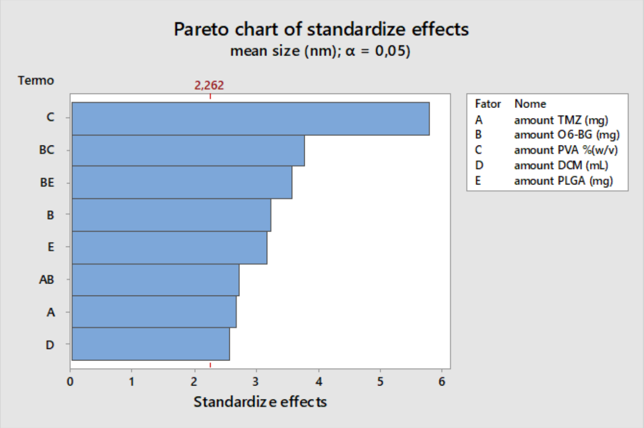

Figure 5. 3 | Standardized Pareto chart of the experimental factors influencing the size of the PLGA NPs. The length of each bar is proportional to the standardized effect, which corresponds to the estimated effect divided by its standard error. Effects which pass the line (α = 0.05) are considered as statistically significant at a confidence level of 95%.

The most significant factor affecting NP size was the amount of surfactant, that exhibited a positive effect on the size of the NPs. Thus, an increase in PVA concentration led to an increase in NP size. Although, higher amounts of surfactant may promote formation and stabilization of smaller NPs due to the decrease in interfacial tension between the polymer and the external aqueous phase (Liu et al., 2010), the opposite effect was verified. This may be explained by the increased viscosity of the aqueous phase, when increasing the PVA concentration. A higher viscosity decreases the shear stress, originating emulsion droplets with larger sizes. Also higher amounts of surfactant can promote the coalescence of the NPs, yielding NPs with larger diameters (Tefas et al., 2015). As well, some studies report that residual PVA remains at the surface, contributing to the size increase (Narayanan et al., 2014).

Additionally, the amount of PLGA also exhibited a significantly positive effect on the size of the NP ($p<0.05$). Increasing the polymer concentration, increases the viscosity of the organic phase, decreasing the shear stress as mentioned above. Also, the increased viscosity, hampers the diffusion of the organic solvent into the aqueous phase, leading to the formation of larger emulsion droplets, originating larger NPs after solvent evaporation (dos Santos et al., 2012).

Also, as expected, higher initial loading of both drugs positively affected the NPs size ($p<0.05$), since will result in higher drug loading. Although, the less significant factor ($p<0.05$), the volume of organic solvent also positively affected the NPs size, as proved by the positive RC value (table 5.3). This effect was not expected, since the aqueous-to-organic ratio was kept constant in all experiments.

The statistical analysis of the obtained values yielded the following polynomial regression equation, which quantified the relationship between each of the studied experimental variables and the size of the NPs:

$$\begin{aligned} Size = {} & -437 + 431\, amount\ TMZ\ (mg) + 525\, amount\ O6BG\ (mg) \\ & + 15.05\, amount\ PVA\ (\%) + 373\, amount\ DCM\ (mL) \\ & + 1.644\, amount\ PLGA\ (mg) \\ & - 705\, amount\ TMZ\ (mg)\ x\ amount\ O6BG\ (mg) \\ & - 13.41\, amount\ O6BG\ (mg)\ x\ amount\ PVA\ (\%) \\ & - 2.541\, amount\ O6BG\ (mg)\ x\ amount\ PLGA\ (mg) \end{aligned}$$

Response surface analysis and contour graphs were plotted (figure 5.4) based on this model polynomial function illustrating the effect of two of the most significant independent factors, amount of PVA and PLGA, on the observed response.

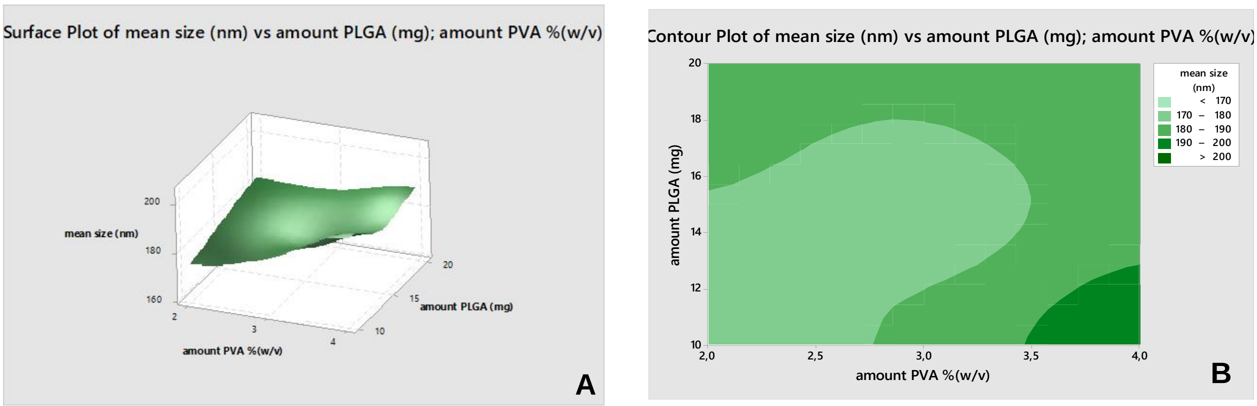

Figure 5. 4 | (A) Response surface plot and (B) contour plot showing the influence of two factors (amount of PVA and PLGA) on the resulting NP size.

Contour and surface response plots allow to visually identify the optimal levels of each factor, to choose the most suitable values for the development of an optimal formulation. Both response surface and contour plots (figure 5.4 A and B) showed that the higher the amount of PVA and PLGA, the higher is the NPs size, as already predicted by the calculated positive RC values (table 5.3). Thus, optimal nanoformulation with small dimensions would fall into the low and central levels of both factors.

In addition to all the five factors significantly affecting the NPs size, also significant two-factor interaction were observed (BC, BE and AB bars in figure 5.3). Interaction plots on figure 5.5 show high interaction between two factors. Each point in the interaction plot shows the mean size values at different combinations of factor levels. As the lines are not parallel, with different slopes, the plot indicates that there is an interaction between the two factors (Calignano et al., 2013). The same is verified in the all the attained interaction plots.

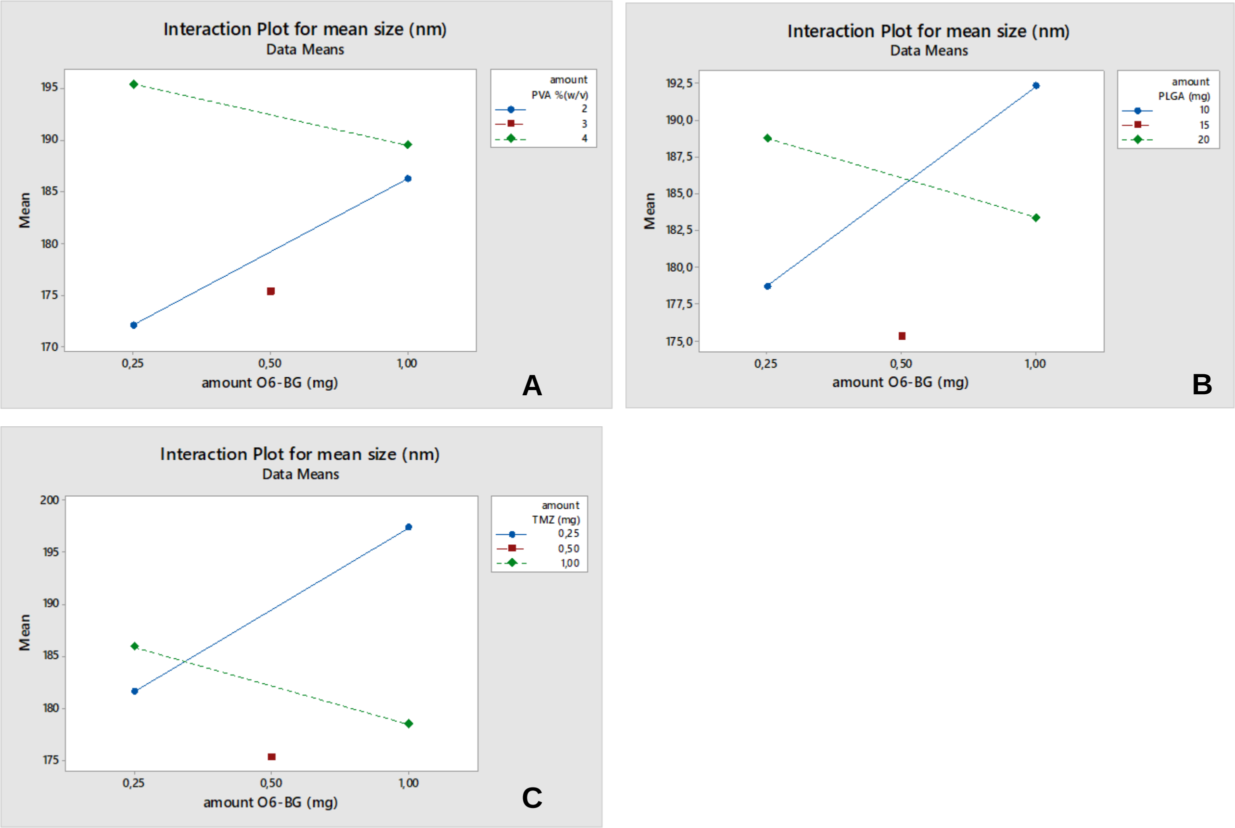

Figure 5. 5 | Interaction plots showing significant two-way interaction terms for the independent variables. Solid blue lines display factor at low level, whereas dashed green lines are the high level of the factors. (A) interaction term X_2X_3 – amount of O6-BG/amount of surfactant. (B) X_2X_5 – amount of O6-BG/amount of PLGA. (C) interaction term X_1X_2 – amount of TMZ/amount of O6BG.

5.3.1.2 Effect on NPs' zeta potential

The surface charge of a NP influences its interaction with biological barriers and membranes, affecting its bioaccumulation in the target cells, as already mentioned. Also, zeta potential values are a key indicator of the NPs' stability. The zeta potential values of the prepared NPs ranged from -20.3 mV (sample 10) to – 28.0 mV (sample 14), with the selected levels of variables. Only the concentration of PVA and PLGA significantly affected the net charge of the NPs ($p<0.05$), as shown in table 5.3 and in Pareto chart (figure 5.6).

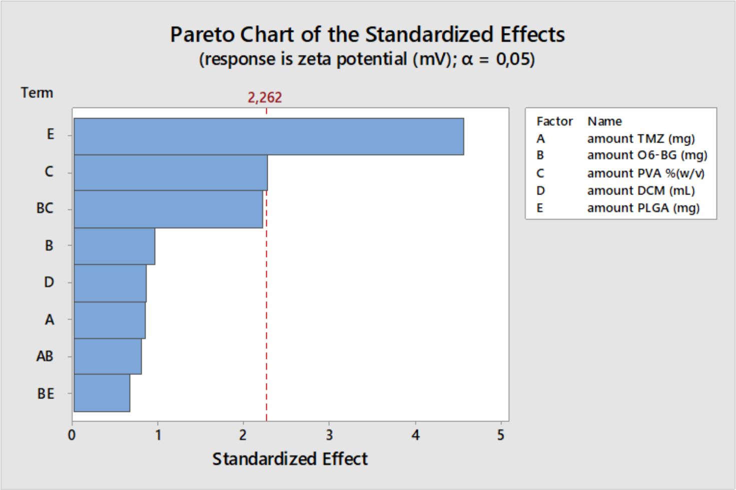

Figure 5. 6 | Standardized Pareto chart of the experimental factors influencing the zeta potential values of the PLGA NPs. The length of each bar is proportional to the standardized effect, which corresponds to the estimated effect divided by its standard error. Effects which pass the line (α = 0.05) are considered as statistically significant at a confidence level of 95%.

As expected, the absolute zeta potential values decreased with increasing surfactant concentration due to increased adsorption of PVA at the NP's surface, exerting a shielding effect on the superficial charge (Sahoo et al., 2002). Thus, despite slightly decreasing zeta potential values, the NPs maintain the stability. In fact, all the prepared nanoformulations proved to be stable for at least one month at storage conditions (4 ºC) (data not shown).

Additionally, the amount of PLGA also exhibited a significantly negative effect on the NP's superficial charge, which was not expected due to the negatively charged carboxylic groups of the polymer.

The statistical analysis of the obtained values yielded the following polynomial regression equation, which quantified the relationship between each of the studied experimental variables and the zeta potential values of the NPs:

$$\begin{aligned} Zeta\ pot. = {} & 62.0 - 21.3\ amount\ TMZ\ (mg) - 24.7\ amount\ O6BG\ (mg) \\ & - 0.928\ amount\ PVA\ (\%) - 19.6\ amount\ DCM\ (mL) \\ & - 0.3726\ amount\ PLGA\ (mg) \\ & + 32.6\ amount\ TMZ\ (mg)\ x\ amount\ O6BG\ (mg) \\ & + 1.242\ amount\ O6BG\ (mg)\ x\ amount\ PVA\ (\%) \\ & - 0.074\ amount\ O6BG\ (mg)\ x\ amount\ PLGA\ (mg) \end{aligned}$$

Response surface analysis and contour graphs were plotted (figure 5.7) based on this model polynomial function illustrating the effect of the two only significant independent factors, amount of PVA and PLGA, on the observed response.

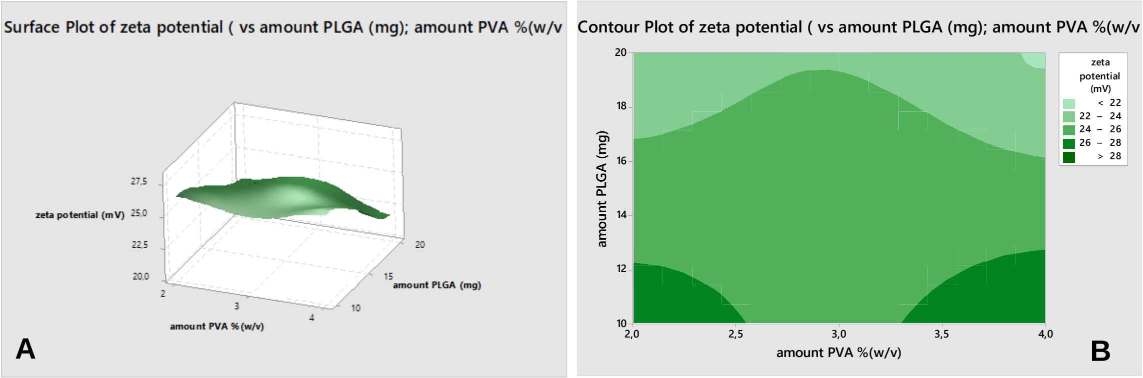

Figure 5. 7 | (A) Response surface plot and (B) contour plot showing the influence of two factors (amount of PVA and PLGA, respectively) on the resulting zeta potential values.

Both response surface and contour plots (figure 5.7 A and B) showed that the lower the amount of PLGA and PVA, the more negative is the zeta potential value, as already predicted by the calculated RC values (table 5.3). Thus, optimal nanoformulation with high absolute zeta potential values would fall into the low levels of PLGA and PVA concentrations.

No significant two-factor interactions were observed on the zeta potential response (p>0.05).

5.3.1.3 Effect on the encapsulation efficiency of TMZ

High encapsulation of the drug is desirable to increase the nanosystem efficiency and to reduce the amount of administered polymer. The EE values for TMZ in the prepared NPs ranged from 27.2 (sample 10) to 56.7% (sample 4). EE values were significantly influenced by the amount of PVA surfactant and PLGA polymer, as shown in the standardized Pareto chart (figure 5.8) and by the calculated p-values on table 5.3. PLGA had a positive effect on the EE of TMZ. As already mentioned, higher amount of PLGA polymer, results in larger NPs and consequent higher encapsulation of the drug. Also, the increased viscosity caused by higher PLGA concentration mentioned above, could difficult the diffusion of TMZ molecules into the aqueous phase, enhancing the drugs entrapment into the NPs' polymeric matrix (Song et al., 2008).

Also, the encapsulation of TMZ decreased with PVA concentration, due to a higher partition of TMZ molecules into the aqueous phase during emulsification, decreasing the EE values. It is reported that drug molecules can diffuse out from the oil nanodroplets and solubilize in PVA micelles at the aqueous phase (Sharma et al., 2016).

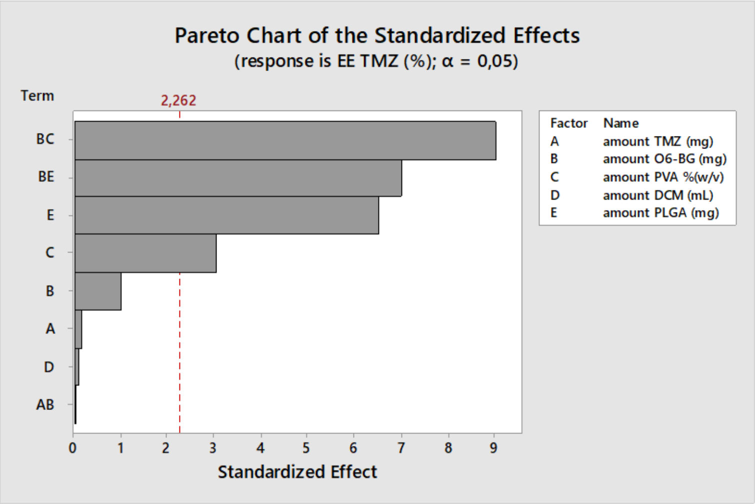

Figure 5. 8 | Standardized Pareto chart of the experimental factors influencing the EE of TMZ in the PLGA NPs. The length of each bar is proportional to the standardized effect, which corresponds to the estimated effect divided by its standard error. Effects which pass the line (α = 0.05) are considered as statistically significant at a confidence level of 95%.

The statistical analysis of the obtained values yielded the following polynomial regression equation, which quantified the relationship between each of the studied experimental variables and the encapsulation efficiency of TMZ:

$$
\begin{aligned}
EE\%\ TMZ = {} & 14.9 - 11.3\ amount\ TMZ\ (mg) + 70.4\ amount\ O6BG\ (mg) \\
& - 3.40\ amount\ PVA\ (\%) + 5.7\ amount\ DCM\ (mL) \\
& + 1.461\ amount\ PLGA\ (mg) \\
& + 4\ amount\ TMZ\ (mg)\ x\ amount\ O6BG\ (mg) \\
& - 13.87\ amount\ O6BG (mg)\ x\ amount\ PVA\ (\%) \\
& - 2.153\ amount\ O6BG\ (mg)\ x\ amount\ PLGA\ (mg)
\end{aligned}
$$

Response surface analysis and contour graphs were plotted (5.9) based on this model polynomial function illustrating the effect of the two most significant independent factors, amount of PVA and PLGA, on the observed response.

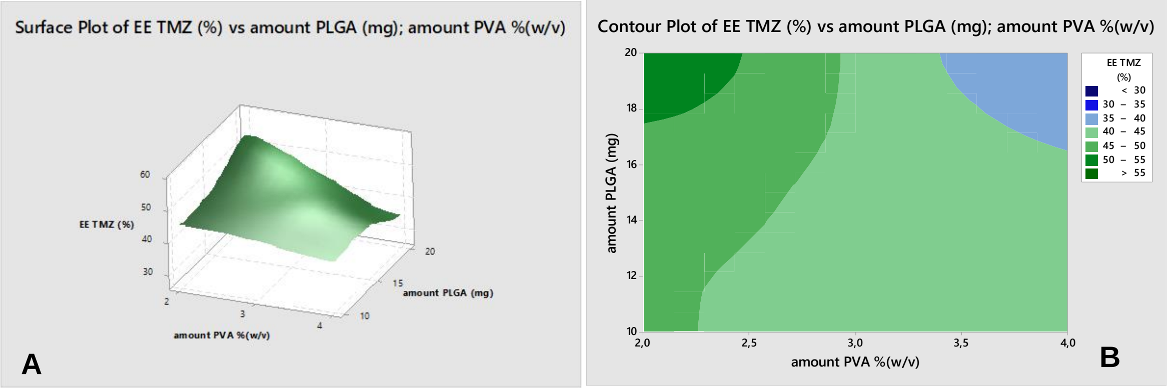

Figure 5. 9 | (A) Response surface plot and (B) contour plot showing the influence of two factors (amount of PVA and PLGA, respectively) on the resulting EE values.

Both response surface and contour plots (figure 5.9 A and B) are in agreement with the calculated RC values (table 5.3). Therefore, optimal formulation would be prepared with low amounts of PVA and high amounts of PLGA.

The amount of PVA and PLGA were the only statistically significant main factors affecting the TMZ EE values. However, all five studied variables were part of as extensive interaction system. A significant two-factor interaction of O6BG amount with both PLGA and PVA amounts (BC and BE bars in Pareto chart, figure 5.8) was verified ($p<0.05$), as shown in figure 5.10.

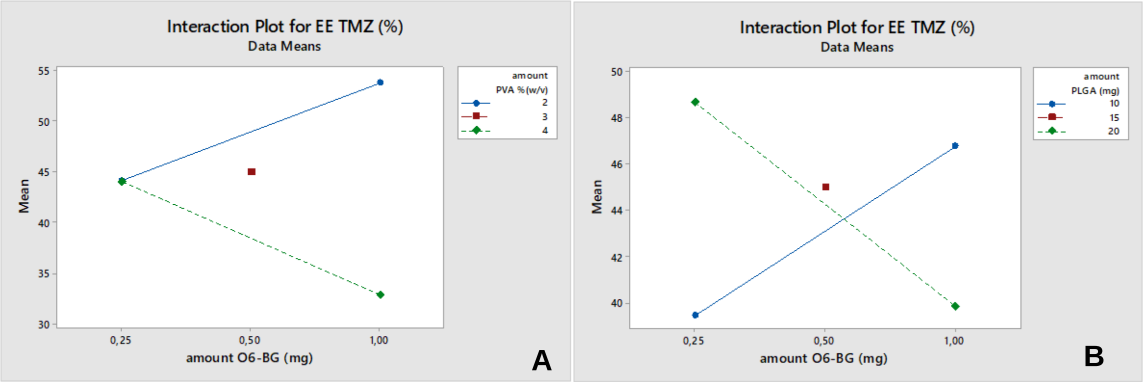

Figure 5. 10 | Interaction plots showing significant two-way interaction terms for the dependent variables. Solid blue lines display factor at low level, whereas green dashed lines are the high level of the factors. (A) interaction term X_2X_3 – amount of O6BG/amount of surfactant. (B) X_2X_5 – amount of O6BG/amount of PLGA.

The described two-factor interaction between the PVA and O6BG amounts, shows a significant PVA concentration effect and interaction term. In this case, the slopes are unequal and thus there is an interaction term. There is a difference among the means of the two PVA levels, but not a difference in the means among O6BG amount. This proves that although the amount of O6BG did not show a significant direct effect on the EE values, the interaction term exists. The amount of O6BG affected the nanoformulation at both low and high PVA amounts. At low PVA levels, O6BG amount shown a positive effect in the TMZ encapsulation. The contrary, was observed at high PVA amounts.

The same is verified in the two-factor interaction between the PLGA and O6BG amounts.

5.3.1.4 Effect on the encapsulation efficiency of O6BG

The EE values of O6BG in the prepared NPs ranged from 70.9 (sample 3) to 99.8% (sample 11). EE values were significantly influenced by all the studied independent variables as shown in the standardized Pareto chart (figure 5.11) and by the calculated p-values on table 5.3. All the experimental variables shown a positive effect on the EE of O6BG, except PVA concentration. In fact, increasing PVA concentration, hampered the encapsulation of the drug, since enhanced the partition of O6BG molecules into the aqueous phase during emulsification, decreasing the encapsulation efficiencies values (Sharma, et al., 2016). On the other hand, increased volumes of organic solvent, increased drug solubility and therefore increasing drug entrapment. Also, as already mentioned, higher amount of PLGA polymer, results in larger NPs and consequent higher encapsulation of the drug. Also, the increased viscosity caused by higher PLGA concentration mentioned above, could difficult the diffusion of O6BG molecules into the aqueous phase, enhancing the drugs entrapment into the NPs' polymeric matrix (Song, et al., 2008).

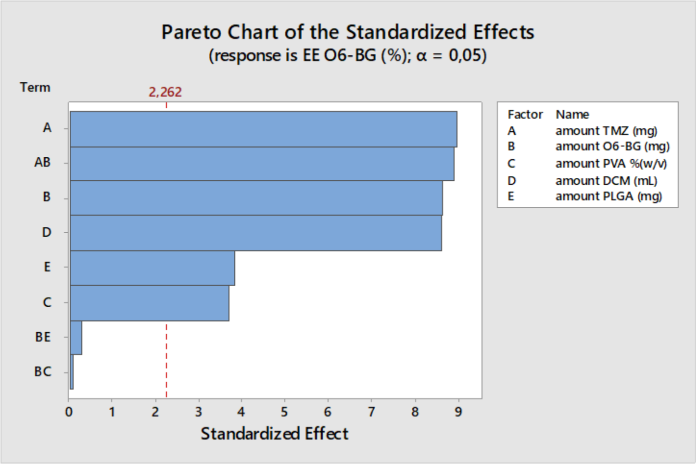

Figure 5. 11 | Standardized Pareto chart of the experimental factors influencing the EE values of O6BG in the PLGA NPs. The length of each bar is proportional to the standardized effect, which corresponds to the estimated effect divided by its standard error. Effects which pass the line (α = 0.05) are considered as statistically significant at a confidence level of 95%.

The statistical analysis of the obtained values yielded the following polynomial regression equation, which quantified the relationship between each of the studied experimental variables and the EE values for O6BG:

$$
\begin{aligned}
EE\%\ O6BG = {} & -698.1 + 623.6\ amount\ TMZ\ (mg) + 602.7\ amount\ O6BG\ (mg) \\
& - 4.12\ amount\ PVA\ (\%) + 540.2\ amount\ DCM\ (mL) \\
& + 0.854\ amount\ PLGA\ (mg) \\
& - 990\ amount\ TMZ\ (mg)\ x\ amount\ O6BG\ (mg) \\
& - 0.17\ amount\ O6BG\ (mg)\ x\ amount\ PVA\ (\%) \\
& + 0.093\ amount\ O6BG\ (mg)\ x\ amount\ PLGA\ (mg)
\end{aligned}
$$

Response surface analysis and contour graphs were plotted (figure 5.12 A and B) based on this model polynomial function illustrating the effect of two of the most significant independent factors on the observed response.

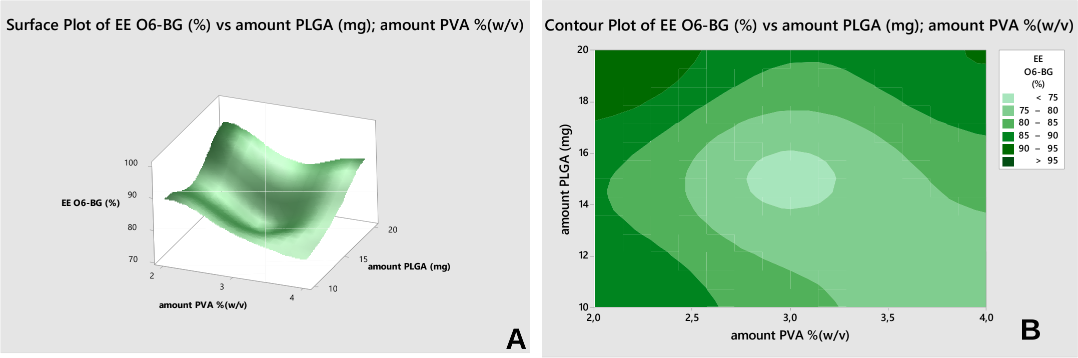

Figure 5. 12 | (A) Response surface plots and (B) contour plot showing the influence of two factors (amount of PLGA and PVA, respectively) on the resulting EE values.

Predicted optimal nanoformulation with high O6BG molecules entrapment would fall into the high levels of PLGA and low levels of surfactant concentration.

In addition to all the five factors significantly affecting the encapsulation of the drug, also a significant two-factor interaction was noticed (AB bar in the Pareto chart, figure 5.11). Interaction plot on figure 5.13, show high interaction between the two studied factors, amount of TMZ and O6BG, respectively.

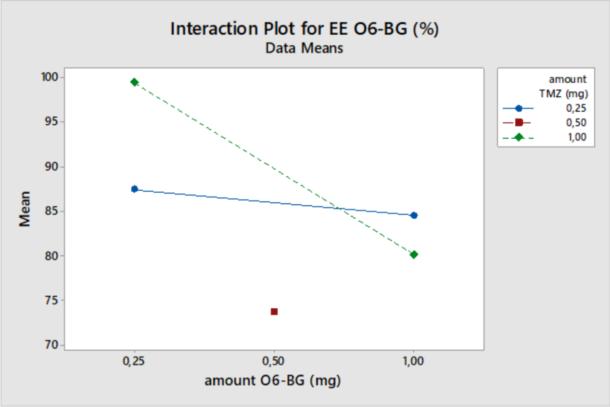

Figure 5. 13| Interaction plots showing significant two-way interaction term between the amount of TMZ and the amount of O6BG (X_1X_2).

5.3.1.5 Effect on the polydispersity

The PdI values of the PLGA NPs ranged from 0.106 (sample 3) to 0.190 (sample 9). No significant main effects neither two-factor interactions were observed on the studied response as shown in table 5.3 and in the Pareto chart presented below (figure 5.14). Therefore, the software was not able to determine the R^2 value.

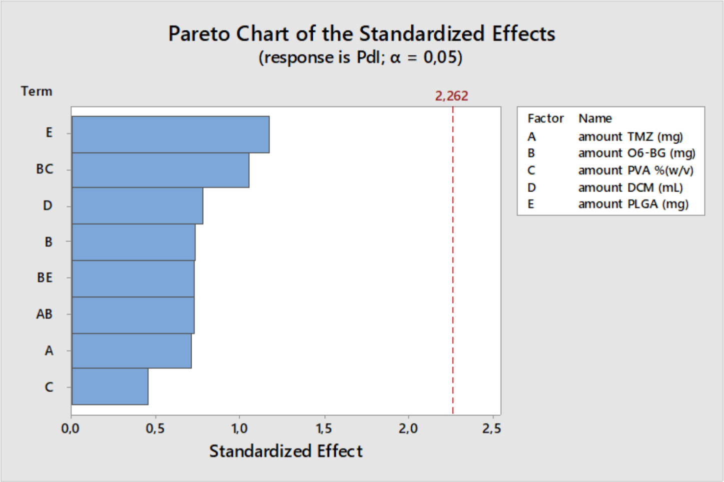

Figure 5. 14 | Standardized Pareto chart of the experimental factors influencing the PdI values of the PLGA NPs. The length of each bar is proportional to the standardized effect, which corresponds to the estimated effect divided by its standard error. As none of the observed effects passed the line (α = 0.05), no effect was considered statistically significant at a confidence level of 95%.

The statistical analysis of the obtained values yielded the following polynomial regression equation, which quantified the relationship between each of the studied experimental variables and the PdI values of the NPs:

$$\begin{aligned} PdI = {} & -0.517 + 0.504\, amount\ TMZ\ (mg) + 0.523\, amount\ O6BG\ (mg) \\ & + 0.0051\, amount\ PVA\ (\%) + 0.496\, amount\ DCM\ (mL) \\ & - 0.00266\, amount\ PLGA\ (mg) \\ & - 0.82\, amount\ TMZ\ (mg)\ x\ amount\ O6BG\ (mg) \\ & - 0.0163\, amount\ O6BG\ (mg)\ x\ amount\ PVA\ (\%) \\ & + 0.00227\, amount\ O6BG\ (mg)\ x\ amount\ PLGA\ (mg) \end{aligned}$$

5.3.1.6 Optimal parameters for the nanoformulation

After establishing the polynomial equations that describe the relationship between the formulation factors and the responses, the optimization process was carried out. Of the five studied dependent variables, size and EE of both drugs were the most critical properties of the NPs. Since zeta potential and PdI values were always inside the desired interval values, the following criteria were adopted: the particle size (Y_1) was minimized, the EE values were maximized (Y_4 and Y_5), while PdI (Y_2) and zeta potential (Y_3) were excluded. The optimum levels of the formulation factors were: 1 mg of both drugs, 0.5% (w/v) of PVA, 1 mL of dichloromethane and 15 mg of PLGA.

A formulation checkpoint was prepared according to the predicted model to validate the reliability of the factorial design, using these optimal experimental conditions. The checkpoint formulation was prepared in triplicates and the properties of the attained NPs were in agreement with the predicted values as shown in table 5.4.

Table 5. 4 | Validation of the predicted optimal results with experimental values. The experimental data is presented as the mean ± SD (n = 3).

	Size (Y_1) (nm)	**PdI (Y_2)**	**Zeta potential (Y_3) (mV)**	**EE TMZ (Y_4) (%)**	**EE O6-BG (Y_5) (%)**
Predicted values	174 (162-187)	0.171 (0,118-0,225)	-22 (21-24)	68 (63-73)	91 (86-96)
Experimental values	177 ± 4	0.186 ± 0.013	-22 ± 1	63 ± 4	90 ± 4

The developed NPs exhibit mean dimensions and surface charge suitable for brain delivery. The high absolute zeta potential values also suggest that the NPs are stable. Also, PdI values suggest that the colloidal suspension is monodisperse. Higher encapsulation verified for O6BG can be explained by its greater affinity for the organic phase, comparatively with TMZ. While TMZ exhibits a log P value of 0.36, for O6BG log P is 1.66 (values obtained from Marvin Sketch Calculator software, Chemaxon™).

5.3.2 Physicochemical properties of TMZ+O6BG mAb-PLGA NPs

The NPs modified with mAb were further prepared also using the optimal experimental parameters. The obtained PLGA NPs exhibited a mean diameter of 187 ± 7 nm (n=3), and the increase in size, comparatively with non-modified NPs (177 ± 4 nm), suggest an efficient mAb conjugation that was also confirmed by ELISA (data not shown). The developed nanocarriers exhibited zeta potential values of -15 ± 9 mV (n=3), lower than for non-modified NPs (-22 ± 1 mV), maybe due to the charge masking effect exerted by the PEG molecules ($p<0.05$). These NPs also exhibit mean sizes and superficial charge suitable for brain delivery. PdI values of 0.15 ± 0.03 (n=3) indicate that the attained colloidal suspension is monodisperse.

No significant changes were verified on the EE values for mAb-modified NPs, when comparing to non-modified ones, as expected ($p>0.05$). In fact, NPs showed EE values of 62 ± 8% for TMZ and 92 ± 7% for O6BG, respectively. DL varied from 14 ± 3% for TMZ to 19 ± 1% for O6BG.

5.3.3 Stability of PLGA NPs

Although the mAb-modified NPs exhibited lower zeta potential values of (–15 ± 9 mV), nevertheless the NPs proved be stable at storage conditions (4 °C) for approximately 6 weeks (table 5.5). No mean diameter and zeta potential significant changes were verified in this time period as shown in table 5.5. ($p>0.05$). Mean size variation is expressed in terms of ratio St/Si.

Table 5. 5 | Mean diameter and zeta potential values for both mAb-modified O6BG+TMZ-loaded NPs, over a period 42 days, respectively. Mean size variation is expressed in terms of ratio St/Si, where St is mean diameter after t days of storage and Si is the NPs initial mean size. Data represented as mean ± SD (n=3).

mAb-O6BG+TMZ-NPs	Mean diameter (nm)	Ratio S_t/S_i	Zeta potential (mV)
Day 1	187 ± 7	-	-15 ± 9
Day 7	185 ± 9	0.99	-12 ± 3
Day 14	194 ± 7	1.04	-13 ± 1
Day 21	192 ± 3	1.03	-11 ± 2
Day 28	190 ± 5	1.02	-12 ± 1
Day 35	192 ± 1	1.03	-14 ± 2
Day 42	193 ± 7	1.03	-13 ± 3

5.3.4 Drug release from the PLGA NPs

The release profile of the developed O6BG+TMZ mAb-PLGA NPs was evaluated *in vitro* at 37 °C in PBS (pH 7.4, 0.01 M) to mimic the physiological pH and salt concentrations. The attained release curve is presented in figure 5.15.

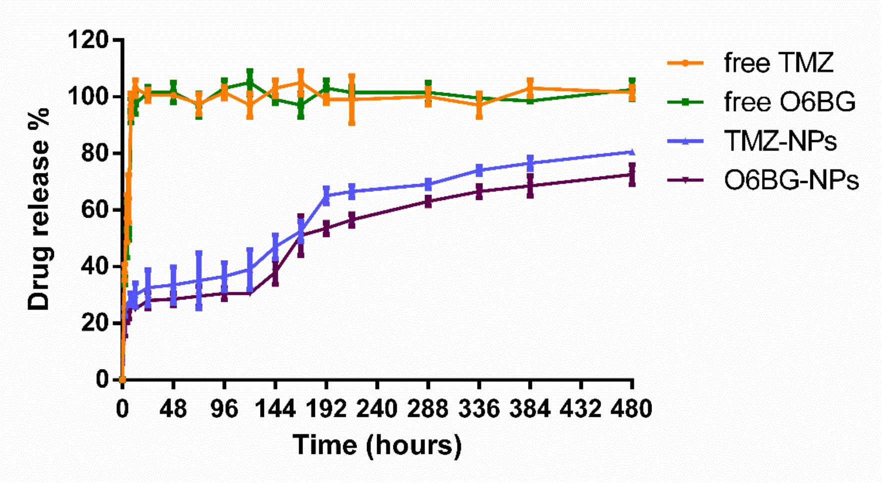

Figure 5. 15 | *In vitro* release of TMZ and O6BG from mAb-PLGA NPs in PBS (pH 7.4, 0.01 M) at 37 °C. Free TMZ and O6BG were used as control. Results are represented as mean ± SD (n=3).

Both drug molecules exhibited an initial rapid release followed by a slower and controlled release. At the first 24 h, 33 ± 6% of the total TMZ and 28 ± 3% of the total O6BG were released, as shown in figure 5.15. This burst occurs due to the release of the surface-adsorbed drug molecules. The TMZ and O6BG entrapped in NPs polymeric matrix exhibited a slower and controlled release that was maintained for 20 days.

A faster release for TMZ was verified in comparison to O6BG. The mAb-PLGA NPs exhibited a total release of TMZ of 81 ± 1% after 20 days, while for O6BG only about 73 ± 4% of entrapped drug was released at day 20 (figure 5.15). These results may be explained by the higher affinity of TMZ to the aqueous buffer, as already mentioned.

The obtained release profile proved that the developed mAb-modified PLGA NPs are suitable nanovehicle for the co-delivery of TMZ and 6BG.

5.3.5 Efficiency of O6BG in decreasing resistance to TMZ's activity

The *in vitro* ability of O6BG in increasing the sensitivity of GBM resistant cells to TMZ activity was evaluated. For that two human GBM cell lines were used, U251 and T98G. In the previous experiments described in chapter 4, we determined that

U251 was more sensitive to TMZ's activity than U87 cell line. Therefore, this line was chosen for comparison with the T98G cell line.

The effect of TMZ alone and in combination with O6BG was evaluated and the results are presented in figure 5.16 and table 5.6. In both treatment regimes, a concentration-related decrease in cell growth was observed in all the studied cell lines (figure 5.16). The combination therapy of TMZ with O6BG did not enhanced the antiproliferative effects of TMZ in the sensitive U251 cell line ($p>0.05$), but the cell growth of T98G cells was significantly reduced when comparing to treatment with TMZ alone ($p<0.05$). This yielded significantly lower GI_{50} values using combination therapy for T98G cells ($p<0.05$), but no different GI_{50} values for the U251 cell line ($p>0.05$), as shown in table 5.6. This suggests that combination therapy enhances the sensitivity to TMZ, by inhibition of the MGMT protein since this protein is reported to be overexpressed in T98G cells but not in the U251 cells (Lee, 2016).

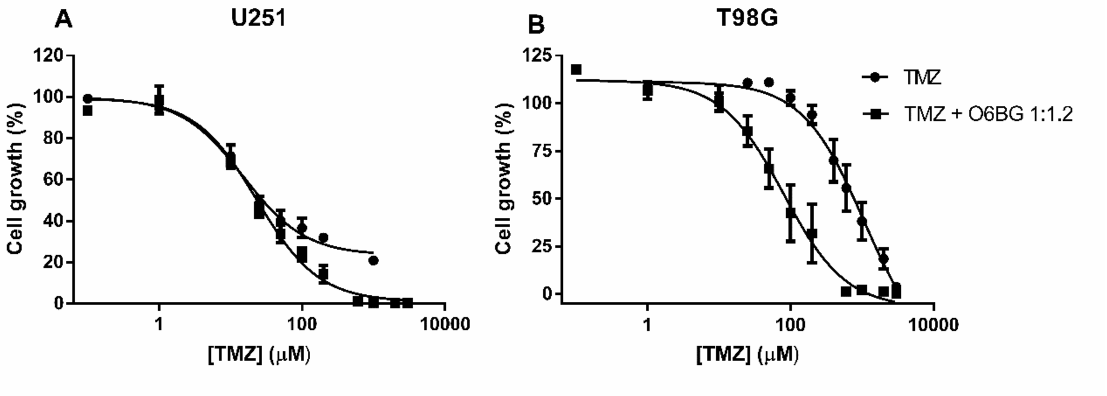

Figure 5. 16 | Cytotoxic effects of TMZ, alone or plus O6BG (at a molar ratio of 1:1.2), after 72 h treatment on two human cell lines by SRB assay. (A) U251 cell line, (B) T98G cell line. Growth inhibition is presented as percent$[(\%)=((T-T_0)/(C-T_0)) \times 100]$. Data presented as mean ± SD (n = 3).

Table 5. 6 | Cytotoxic effects of alone TMZ or in combination with O6BG, at different molar ratios, on the growth of U251 and T98G cells. Results are expressed as GI_{50} at 72 h of exposure with TMZ. Data presented as mean ± SD (n = 3).

GI_{50} (μM)									
U251					T98G				
TMZ:O6BG ratios					TMZ:O6BG ratios				
1:0	1:1	1:1.2	1:2	2:1	1:0	1:1	1:1.2	1:2	2:1
29 ± 8	22 ± 1	23 ± 1	21 ± 1	29 ± 6	799 ± 170	79 ± 17	77 ± 27	76 ± 23	78 ± 27

The first tested ratio (TMZ/O6BG at 1:1.2) was chosen since it is the ratio that naturally occurs in the developed NPs due to the difference in the encapsulation of both drugs. Three other ratios were evaluated, to choose the most suitable ratio for further experiments with NPs. Since no significant differences were verified between all the studied ratios (table 5.6 and figure 5.17) ($p>0.05$), TMZ/O6BG at 1:1.2 ratio was maintained.

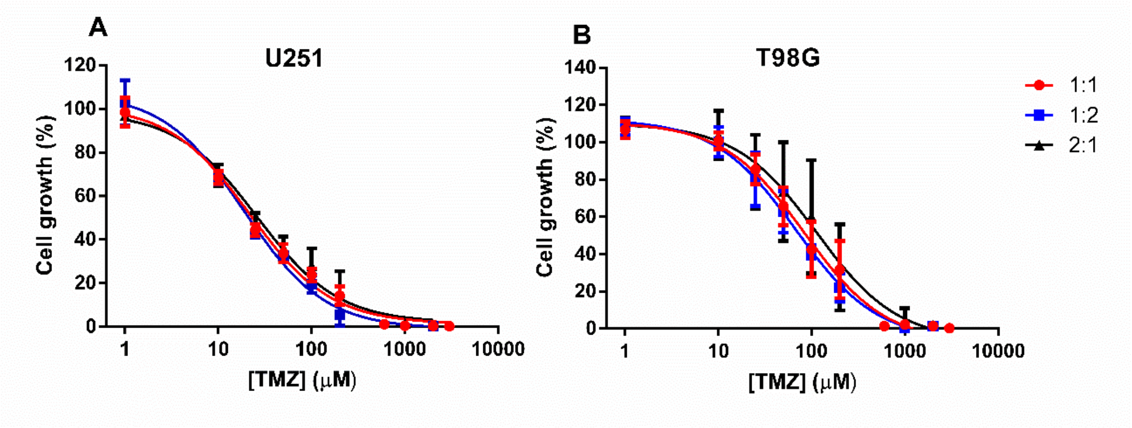

Figure 5. 17 | Cytotoxic effects of TMZ plus O6BG at different molar ratio, after 72 h treatment on two human cell lines by SRB assay. (A) U251 cell line, (B) T98G cell line. Growth inhibition is presented as percent[(%)=((T-T_0)/(C-T_0)) x 100]. Data presented as mean ± SD (n = 3).

Treatment with O6BG alone did not inhibit cell growth in both cell lines as shown in figure 5.18, proving that this drug doesn't exert antiproliferative effects *per se*, but increases the efficiency of TMZ by inhibiting DNA repair as already reported (Kanzawa et al., 2003; Quinn, et al., 2009). Since the major mechanism described for the resistance in TMZ's treatment is the DNA repair by the MGMT protein, co-therapy with both drugs presents a very promising approach for GBM.

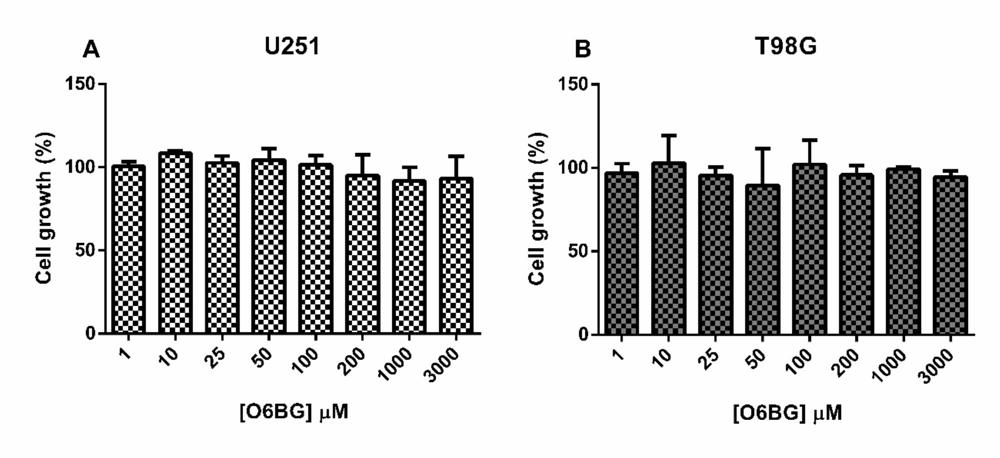

Figure 5. 18 | Cell growth after incubation period in (A) U251 and (B) T98G cells. The figures show data for cells treated with different concentrations of O6BG. Growth inhibition is presented as percent [(%)=((T-T_0)/(C-T_0)) x 100]. Data represented as mean ± SD (n=3).

The use of nanocarriers will allow an increased bioaccumulation in the target tissues of both molecules, promoting an effective therapeutic strategy.

5.3.6 Cell growth inhibition by O6BG+TMZ-loaded mAb-NPs

The *in vitro* antiproliferative effects of the O6BG+TMZ-loaded NPs in comparison with the combination of free drugs, was also evaluated in the same two GBM cell lines. Bare OX26 mAb-modified PLGA NPS, at a concentration of 1.5 mM, proved to be biocompatible, since no significant cytotoxicity on the treated cells was observed (figure 5.19).

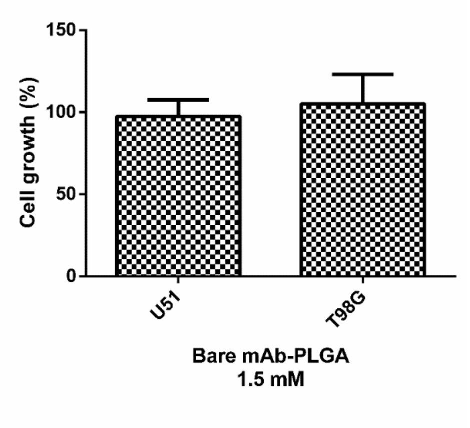

Figure 5. 19 | Cell growth after incubation period in U251 and T98G cells. The figures show data for cells treated with 1.5 mM of bare mAb-PLGA NPs. Growth inhibition is presented as percent [(%)=((T-T_0)/(C-T_0)) x 100]. Data represented as mean ± SD (n=3).

As shown in figure 5.20, co-loading of TMZ and O6BG in the NPs inhibited the cellular growth more efficiently than the combination of free drugs in both cell lines, resulting in significantly lower GI_{50} values ($p<0.05$). The determined GI_{50} value was 7 ± 1 µM for the sensitive U251 cell line, and 16 ± 8 µM for the resistant T98 cells.

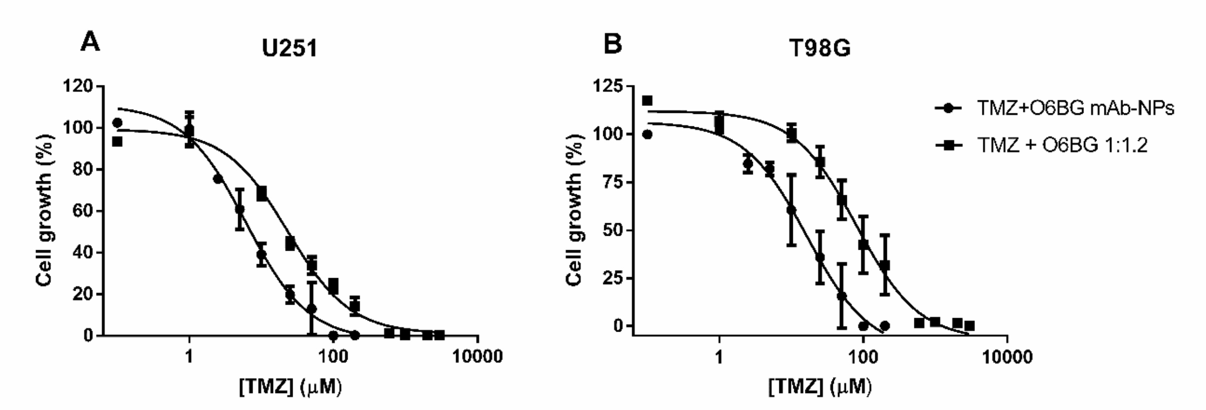

Figure 5. 20 | Cytotoxic effects of TMZ plus O6BG, free or entrapped in mAb-modified PLGA NPs, after 72 h treatment on two human cell lines by SRB assay. (A) U251 cell line, (B) T98G. Survival inhibition is presented as percent [(%)=((T-T_0)/(C-T_0)) x 100]. Data presented as mean ± SD (n = 3).

The attained results proved that the developed nanoformulation is an efficient approach for GBM treatment with TMZ, overcoming the resistance to this drug due to the intrinsic DNA repair mechanisms by the MGMT enzyme. This combination therapy allows to maximize the therapeutic efficiency of TMZ, and potentially will improve the *in vivo* therapeutic outcomes by overcoming the issue related with the differences in the biodistribution of each drug, allowing an accumulation of both drugs in the target cells.

References

Calignano, F., Manfredi, D., Ambrosio, E.P., Iuliano, L., Fino, P. 2013. Influence of process parameters on surface roughness of aluminum parts produced by DMLS. The International Journal of Advanced Manufacturing Technology. 67 (9), 2743-2751.

Cun, D., Jensen, D.K., Maltesen, M.J., Bunker, M., Whiteside, P., Scurr, D., Foged, C., Nielsen, H.M. 2011. High loading efficiency and sustained release of siRNA encapsulated in PLGA nanoparticles: Quality by design optimization and characterization. European Journal of Pharmaceutics and Biopharmaceutics. 77 (1), 26-35.

dos Santos, K.C., da Silva, M.F.G.F., Pereira-Filho, E.R., Fernandes, J.B., Polikarpov, I., Forim, M.R. 2012. Polymeric nanoparticles loaded with the 3,5,3′-triiodothyroacetic acid (Triac), a thyroid hormone: factorial design, characterization, and release kinetics. Nanotechnology, Science and Applications. 5 37-48.

Kaina, B., Margison, G.P., Christmann, M. 2010. Targeting O6-methylguanine-DNA methyltransferase with specific inhibitors as a strategy in cancer therapy. Cellular and Molecular Life Sciences. 67 (21), 3663-3681.

Kanzawa, T., Bedwell, J., Kondo, Y., Kondo, S., Germano, I.M. 2003. Inhibition of DNA repair for sensitizing resistant glioma cells to temozolomide. Journal of neurosurgery. 99 (6), 1047-1052.

Lee, S.Y. 2016. Temozolomide resistance in glioblastoma multiforme. Genes & Diseases. 3 (3), 198-210.

Liu, Y., Pan, J., Feng, S.-S. 2010. Nanoparticles of lipid monolayer shell and biodegradable polymer core for controlled release of paclitaxel: Effects of surfactants on particles size, characteristics and in vitro performance. International Journal of Pharmaceutics. 395 (1), 243-250.

Miao, L., Guo, S., Zhang, J., Kim, W.Y., Huang, L. 2014. Nanoparticles with Precise Ratiometric Co-Loading and Co-Delivery of Gemcitabine Monophosphate and Cisplatin for Treatment of Bladder Cancer. Advanced Functional Materials. 24 (42), 6601-6611.

Narayanan, K., Subrahmanyam, V.M., Venkata Rao, J. 2014. A Fractional Factorial Design to Study the Effect of Process Variables on the Preparation of Hyaluronidase Loaded PLGA Nanoparticles. Enzyme Research. 2014 162962.

Perazzoli, G., Prados, J., Ortiz, R., Caba, O., Cabeza, L., Berdasco, M., Gónzalez, B., Melguizo, C. 2015. Temozolomide Resistance in Glioblastoma Cell Lines: Implication of MGMT, MMR, P-Glycoprotein and CD133 Expression. PloS one. 10 (10), e0140131-e0140131.

Quinn, J.A., Jiang, S.X., Reardon, D.A., Desjardins, A., Vredenburgh, J.J., Rich, J.N., Gururangan, S., Friedman, A.H., Bigner, D.D., Sampson, J.H., McLendon, R.E., Herndon, J.E., 2nd, Walker, A., Friedman, H.S. 2009. Phase II trial of temozolomide plus o6-benzylguanine in adults with recurrent, temozolomide-resistant malignant glioma. Journal of clinical oncology : official journal of the American Society of Clinical Oncology. 27 (8), 1262-1267.

S. Srivenugopal, K., Rawat, A., K. Niture, S., Paranjpe, A., Velu, C., N. Venugopal, S., Rao Madala, H., Basak, D., R. Punganuru, S. 2016. Posttranslational Regulation of O6-Methylguanine-DNA Methyltransferase (MGMT) and New Opportunities for Treatment of Brain Cancers. Mini Reviews in Medicinal Chemistry. 16 (6), 455-464.

Sahoo, S.K., Panyam, J., Prabha, S., Labhasetwar, V. 2002. Residual polyvinyl alcohol associated with poly (d,l-lactide-co-glycolide) nanoparticles affects their physical properties and cellular uptake. Journal of Controlled Release. 82 (1), 105-114.

Sharma, N., Madan, P., Lin, S. 2016. Effect of process and formulation variables on the preparation of parenteral paclitaxel-loaded biodegradable polymeric nanoparticles: A co-surfactant study. Asian Journal of Pharmaceutical Sciences. 11 (3), 404-416.

Song, X., Zhao, Y., Hou, S., Xu, F., Zhao, R., He, J., Cai, Z., Li, Y., Chen, Q. 2008. Dual agents loaded PLGA nanoparticles: Systematic study of particle size and drug entrapment efficiency. European Journal of Pharmaceutics and Biopharmaceutics. 69 (2), 445-453.

Tefas, L.R., TomuŢĂ, I., Achim, M., Vlase, L. 2015. Development and optimization of quercetin-loaded PLGA nanoparticles by experimental design. Clujul Medical. 88 (2), 214-223.

Warren, K.E., Aikin, A.A., Libucha, M., Widemann, B.C., Fox, E., Packer, R.J., Balis, F.M. 2005. Phase I Study of O6-Benzylguanine and Temozolomide Administered Daily for 5 Days to Pediatric Patients With Solid Tumors. Journal of Clinical Oncology. 23 (30), 7646-7653.

Warren, K.E., Gururangan, S., Geyer, J.R., McLendon, R.E., Poussaint, T.Y., Wallace, D., Balis, F.M., Berg, S.L., Packer, R.J., Goldman, S., Minturn, J.E., Pollack, I.F., Boyett, J.M., Kun, L.E. 2012. A phase II study of O6-benzylguanine and temozolomide in pediatric patients with recurrent or progressive high-grade gliomas and brainstem gliomas: a Pediatric Brain Tumor Consortium study. Journal of Neuro-Oncology. 106 (3), 643-649.

Chapter 6 - Conclusions and future perspectives

TMZ is the main used drug for GBM treatment, and although its therapeutics effects are well-established, the drug fails to efficiently treat GBM tumours. It is reported that MTIC, the active form of this drug, is not able to reach the target cells at effective concentrations.

In a first approach, a biomimetic model to study the drug-membrane interactions at physiological conditions was used to evaluate the penetration of TMZ and its active metabolite into biological membranes and their ability to reach the intracellular targets to efficiently exert the pharmacological activity. This membrane model proved to be an efficient approach to study the molecular interactions between the drug with biological barriers and membranes, to understand their role in the low bioavailability of the drug. In this context, different studies were conducted to evaluate the drugs' partition coefficient, their preferential location within the membrane and their effects on membrane properties such as fluidity. TMZ molecules have shown higher affinity to membranes, however this pro-drug is rapidly converted into the active form MTIC after administration. Since TMZ conversion into MTIC is irreversible, it was also crucial to evaluate the interactions with membranes of the active metabolite. The partition, location and fluidity studies suggested that MTIC have low affinity to biological membranes, explaining its low bioavailability on the target cells. These studies give a more realistic prediction about the active metabolite' lipophilicity and its *in vivo* membrane partition and interactions. These predictions were helpful for the design of new strategies to improve drug's bioavailability to enhance its efficacy.

Thus, NPs appear as promising candidates for TMZ delivery, being able to increase the bioavailability of the drug. Several other advantages are related with the use of NPs as providing drug protection against external and physiological factors and providing an increased and controlled release into the specific final target. Therefore, the use of PLGA NPs were proposed to improve the brain delivery of TMZ. For that, NPs functionalized with OX26 mAb for TfR were developed for GBM tumour cells targeting, since these cells are known for overexpressing this receptor. Stable NPs were prepared with suitable physicochemical features for brain delivery, such as mean dimensions smaller than 200 nm and negative net charge. The developed nanocarriers exhibited acceptable TMZ encapsulation efficiency and were able to maintain a controlled and sustained release of the drug for up to 20 days. Cytotoxicity studies showed that the entrapment of the drug in PLGA NPs significantly improves the antiproliferative activity of TMZ. The use of the mAb for the TfR proved to be advantageous in enhancing the cellular internalization of the NPs in the target cells, suggesting that these are selectively uptaken by a TfR-mediated endocytosis mechanism. Although the modification of the NPs with OX26 mAb apparently decreased the cytotoxic potential in GBM cells, the use of this antibody could enhance the permeability across the BBB during *in vivo* conditions, since BBB cells are also known for overexpressing this receptor. As such, the NPs functionalized with OX26 mAb for TfR were chosen for the last task of this work.

The developed NPs were optimized for the co-loading of TMZ with O6BG. This molecule is guanine analogue able to inhibit the activity of the MGMT protein, hampering the DNA repair. Thus, O6BG can decrease the resistance to TMZ's therapy, that is one of the major obstacles for GBM treatment. In fact, cellular studies proved that co-therapy with both molecules enhanced the antiproliferative effects of TMZ in the used GBM resistant cell line. However, differences in the pharmacokinetics and biodistribution of each drug are a major drawback in the systemic delivery of the drugs. The entrapment of both drugs in NPs offers a suitable solution to this issue.

For the optimization of the nanoformulation, a fractional factorial design was used. After determining the optimal experimental parameters, mAb-modified NPs were prepared and characterized. The developed NPs exhibited high encapsulation efficiencies for both drugs and showed a sustained drug release. Thus, it is expected that these nanocarriers will provide an effective brain delivery allowing the drug to reach the brain at desirable doses, leading to a significantly improvement on the GBM treatment. The efficiency of the proposed nanosystem in enhancing *in vitro* cytotoxicity was then evaluated, and the attained results proved that it was able to increase the efficiency of the drugs. Therefore, the developed nanocarrier could be efficiently used for the co-delivery of TMZ and O6BG targeting the GBM cells. Nanoencapsulation in PLGA NPs offer a new and potentially effective strategy for the co-administration of TMZ and O6BG, presenting a potential solution for the intrinsic resistance mechanisms to TMZ due to MGMT high expression.

Though these NPs could potentially overcome the limitations of the currently available therapies, future *in vivo* tests using animal models, as pharmacokinetics and biodistribution studies are necessary to better assess the nanosystem efficacy.

Annexes

Annex A

Table A. 1 | Mean diameter and zeta potential values for DMPC vesicles, over a period 10 days. Mean size variation is expressed in terms of ratio St/Si, where St is mean diameter after t days of storage and Si is the LUVs initial mean size. Data represented as mean ± SD (n=3).

LUVs	Mean diameter (nm)	Ratio S_t/S_i	Zeta potential (mV)
DMPC (pH 7.4)			
Day 1	111 ± 10		- 0.5 ± 0.2
Day 10	115 ± 6	1.04	- 1.0 ± 0.3
DMPC:Chol (pH 7.4)			
Day 1	117 ± 12		- 1.1 ± 1.3
Day 10	125 ± 10	1.07	- 0.7 ± 1.0
DMPC (pH 5.5)			
Day 1	111 ± 8		4 ± 2
Day 10	113 ± 6	1.02	6 ± 2
DMPC:Chol (pH 5.5)			
Day 1	123 ± 7		4.2 ± 0.4
Day 10	130 ± 10	1.06	4 ± 1

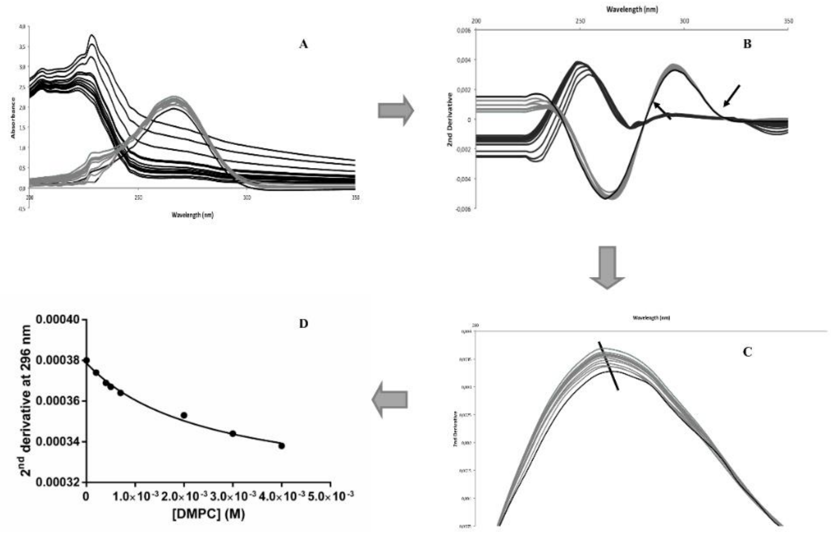

Figure A. 1 | Illustration of the steps for *Kp* value determination. (A) Absorption spectrum and (B, C) second-derivative spectrum of MTIC at 150 µM incubated in DMPC:chol vesicles at 37 °C (grey lines) and DMPC vesicles without drug (black lines) at increasing lipid concentrations. Black arrows point to isosbestic points, and black line indicates a bathochromic shift. (D) Non-linear regression fitting by equation 3.5 to experimental second-derivative spectrophotometric data at wavelength 296 nm where the scattering is eliminated.

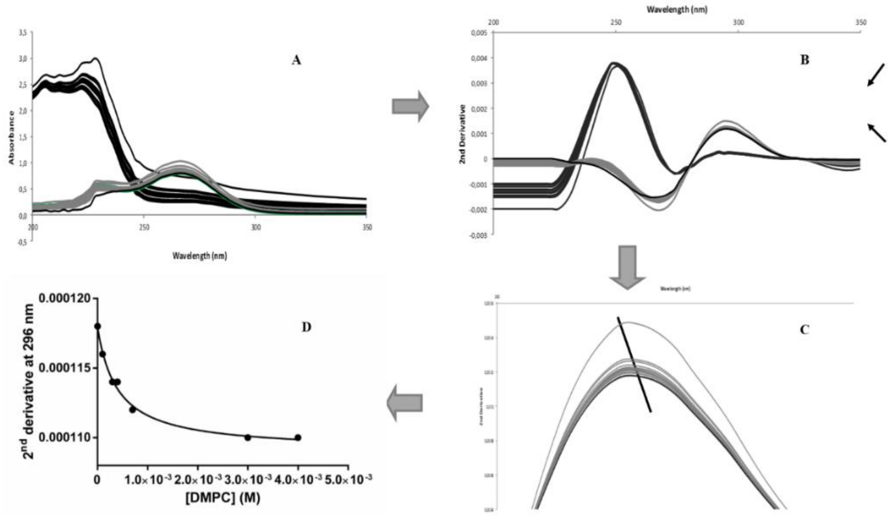

Figure A. 2 | Illustration of the steps for *Kp* value determination. (A) Absorption spectrum and (B, C) second-derivative spectrum of TMZ at 150 µM incubated in DMPC vesicles at 37 °C (grey lines) and DMPC vesicles without drug (black lines) at increasing lipid concentrations. Black arrows point to isosbestic points, and black line indicates a bathochromic shift. (D) Non-linear regression fitting by equation 3.5 to experimental second-derivative spectrophotometric data at wavelength 296 nm where the scattering is eliminated.

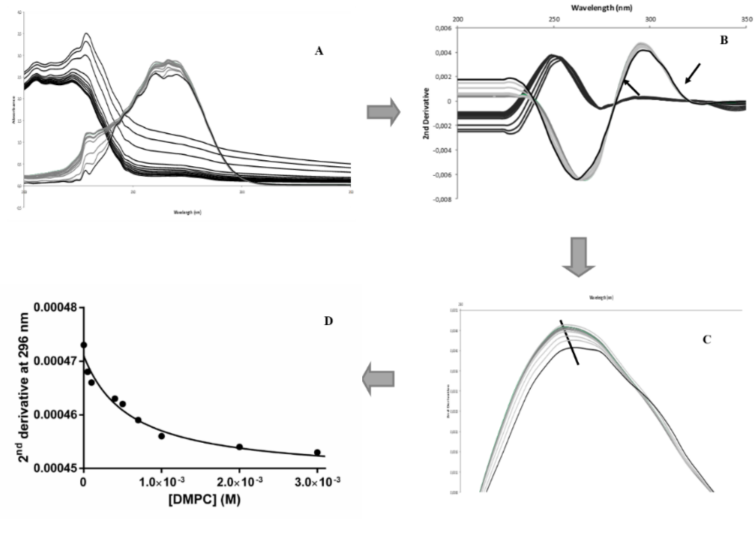

Figure A. 3 | Illustration of the steps for *Kp* value determination. (A) Absorption spectrum and (B, C) second-derivative spectrum of TMZ at 150 µM incubated in DMPC:chol vesicles at 37 °C (grey lines) and DMPC vesicles without drug (black lines) at increasing lipid concentrations. Black arrows point to isosbestic points, and black line indicates a bathochromic shift. (D) Non-linear regression fitting by equation 3.5 to experimental second-derivative spectrophotometric data at wavelength 296 nm where the scattering is eliminated.

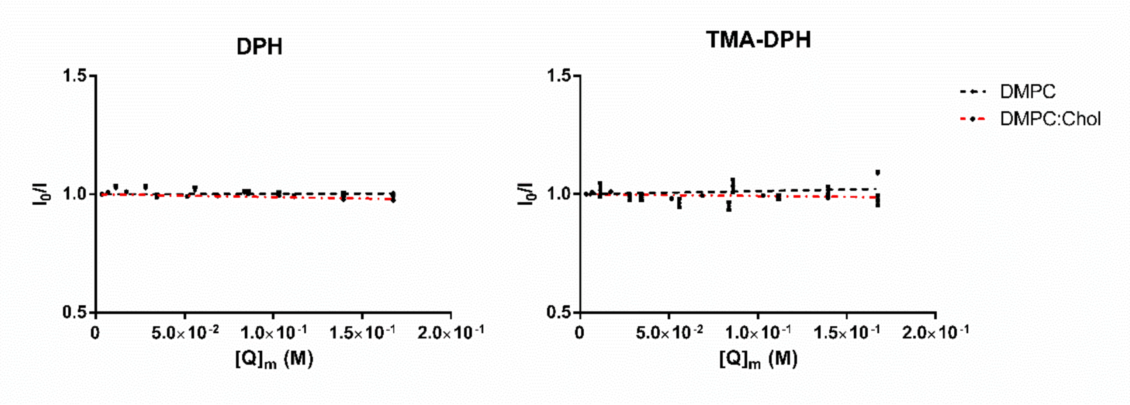

Figure A. 4 | Stern-Volmer plots for DPH and TMA-DPH probes in LUVs of DMPC and DMPC:chol at pH 7.4 at 37 °C by increasing concentrations of MTIC. Data expressed as mean ± SD (n=3).

Annex B

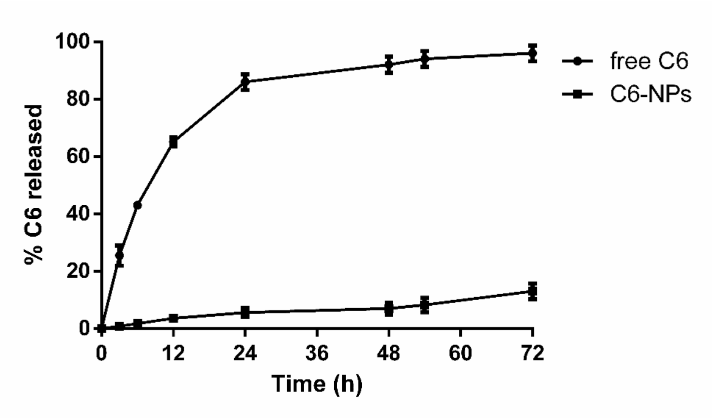

Figure B. 1 | *In vitro* release of C6 from PLGA NPs in DMEM high glucose medium at 37 °C. Free C6 was used as control. Results are represented as mean ± SD (n=3). To ensure that the C6 is inside the NPs and not free without NPs, release studies in cell culture medium were performed to quantify the amount of C6 released for 72 hours (the duration of the internalization assays). As the assay was performed in cell culture medium at 37ºC, it mimics the conditions of the cell experiments. As only about 13% of C6 was released during the duration of the assay, it is possible to conclude that the green dots in the images are C6-NPs and not free C6.

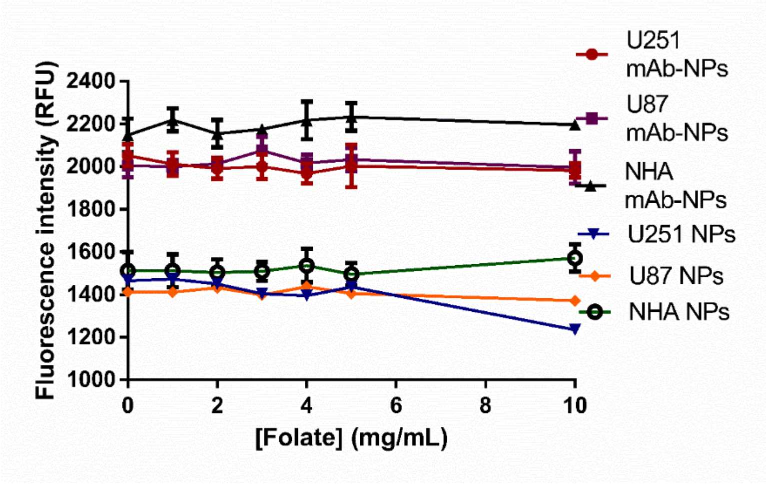

Figure B. 2 | Quantification of cellular uptake of mAb-modified and non-modified PLGA NPs with blockage of the folate receptor, with increase concentrations of folate. Experiments were conducted in three human cell lines: U251, U87 and NHA. The cellular internalization of PLGA NPs is represented as the fluorescent intensity of coumarin-6. Data represented as mean ± SD (n=3).